Progress in Quantum Electronics 89 (2023) 100469

Contents lists available at ScienceDirect

Progress in Quantum Electronics

journal homepage: www.elsevier.com/locate/pqe

Software-defined nanophotonic devices and systems empowered by machine learning

Yihao Xu [a,1], Bo Xiong [b,1], Wei Ma [b,**], Yongmin Liu [a,c,*]

[a] Department of Mechanical and Industrial Engineering, Northeastern University, Boston, MA, USA
[b] State Key Laboratory of Modern Optical Instrumentation, College of Information Science and Electronic Engineering, Zhejiang University, Hangzhou, 310027, China
[c] Department of Electrical and Computer Engineering, Northeastern University, Boston, MA, USA

A B S T R A C T

Nanophotonic devices, such as metasurfaces and silicon photonic components, have been progressively demonstrated to be efficient and versatile alternatives to their bulky counterparts, enabling compact and light-weight systems for the application of imaging, sensing, communication and computing. The tremendous advances in machine learning provide new design methods, metrology and functionalities for nanophotonic devices and systems. Specifically, machine learning has fundamentally changed automatic design, measurement and result processing of highly application-specific nanophotonic systems without the need of extensive expert experience. This trend can be well described by the popular concept of "software-defined" infrastructure in information technology, which can decouple specific hardware from end users by virtualizing physical components using software interfaces, making the entire system faster, more flexible and more scalable. In this review, we introduce the concept of software-defined nanophotonics and summarize the interdisciplinary research that bridges nanophotonics and intelligence algorithms, especially machine learning algorithms, in the device design, measurement and system setup. The review is organized in an application-oriented manner, showing how the software-defined scheme is utilized in solving both forward and inverse problems for various nanophotonic devices and systems.

1. Introduction and background

Nanophotonic structures and devices offer powerful means to manipulate light-matter interaction at nanoscale with extreme flexibility [1]. According to the material composites and structural properties, nanophotonics research can be categorized into several major domains including photonic crystals (PC) [2], plasmonics [3], metamaterials/metasurfaces [4,5], and silicon photonics [6]. After decades of endeavor, the performance, manufacturability and stability of these nanophotonic structures and devices have been continuously improving to scale up to the system level, which find a vast range of applications in communication [7], computing [8], imaging [9], signal processing [10], biochemical sensing [11], as well as quantum information processing [12]. The success of nanophotonics largely benefits from the advances in powerful simulation tools and precise nano-fabrication facilities. Unlike macroscopic optical components designed according to geometric optics principles, nanophotonic structures and devices usually require a deep understanding of the material properties and physical mechanisms to guide the design. For example, split-ring resonators, widely used to produce effective magnetism, utilize the physical effect that varying external magnetic fields can induce a current loop and thus a magnetic dipole in a ring-like structure [13]. Knowing that a single cross resonator behaves like an electrical dipole antenna with polarization-independent response, a multi-band or broadband device can be configured by multiplexing

* Corresponding author. Department of Mechanical and Industrial Engineering, Northeastern University, Boston, MA, USA.
** Corresponding author.
E-mail addresses: ma_wei@zju.edu.cn (W. Ma), y.liu@northeastern.edu (Y. Liu).
[1] These authors contributed equally to this work: Yihao Xu, Bo Xiong.

https://doi.org/10.1016/j.pquantelec.2023.100469
Received 31 December 2022; Received in revised form 20 March 2023; Accepted 2 April 2023
Available online 4 April 2023

different-sized cross resonator within a single unit cell [14]. The expertise required in nanophotonic design sometimes hinders its scalability and system-level applications, defying demand-driven applications from end users without much professional background.

On the other hand, "software-defined" becomes a growingly popular term in information technology, which usually appears as a prefix in many scenarios like software-defined networking, software-defined storage, software-defined data center, and even the general condition of software-defined everything [15]. The essence of software-defined infrastructure is to decouple specific hardware from end users by virtualizing physical components using software interfaces. For example, software-defined networking, different from conventional hardware-centric networking, has an architecture with network control decoupled from the forwarding mechanism and it is directly programmable [16]. Treating information technology in a software-defined manner overcomes the shortcomings of conventional solutions, such as manageability, flexibility, and extensibility. Users only need to take advantage of software interfaces rather than physical implementations to realize their ideas.

More recently, with the aid of intelligent algorithms, the nanophotonic community has witnessed tremendous development in the design, measurement and application of nanophotonic devices and systems. The core impetus is the prevalence of inverse design methods, which convert a design problem into an optimization problem, and solve it with various algorithms automatically [17]. This revolution in the design scheme unleashes the designers from the complex underlying physical mechanisms and enables more focus on device functionalities. Therefore, similar to other software-defined IT infrastructures, flexible algorithmic interfaces appear in the design, measurement and application of nanophotonic systems. The interplay of algorithmic software and nanophotonic hardware not only boosts the design capability, but also broadens the application scenarios of nanophotonic systems. In this review, we adopt the term "software-defined" from the information technology community and introduce the concept of software-defined nanophotonics. To help the readers better understand the potency of the "software-defined" scheme, we organize this review in an application-oriented manner, highlighting the rich applications in real-world scenarios to demonstrate the benefit of transitioning from hardware-centric nanophotonics to software-defined nanophotonics. For information focused on the inverse design algorithms, photonic measurement using intelligent algorithms and photonic hardware to perform intelligent computing, the readers are recommended to refer to some recent review papers [18–31].

As shown in Fig. 1, the architecture of software-defined nanophotonic systems is composed of three interconnected layers, namely, data layer, control layer and application layer. At the very bottom is the data layer, or infrastructure layer, which stores the physical realization of different functional nanophotonic components and devices, including the unit cell of metamaterials or PCs, various

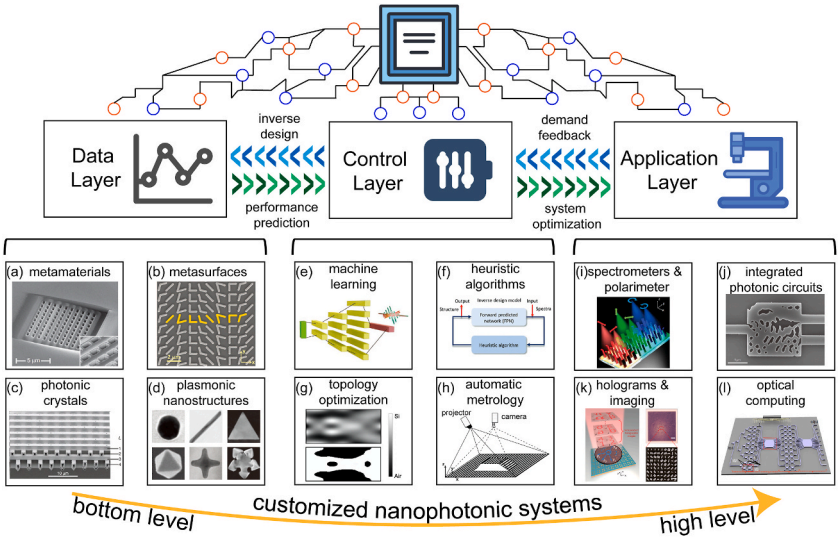

Fig. 1. Architecture of software-defined nanophotonic systems. (a) A metamaterial with a negative refractive index. Reproduced with permission from Ref. [32] copyright 2008 Nature Publishing Group. (b) A metasurface antenna array with phase gradient. Reproduced with permission from Ref. [33] copyright 2011 American Association for the Advancement of Science. (c) A three-dimensional tungsten photonic crystal with a large infrared bandgap. Reproduced with permission from Ref. [34], copyright 2002 Nature Publishing Group. (d) Plasmonic nanoparticles with different geometries. Reproduced with permission from Ref. [35], copyright 2011 Nature Publishing Group. (e) Statistical machine learning model for spectrum prediction of meta-atoms. Reproduced with permission from Ref. [36], copyright 2022 WILEY-VCH Verlag GmbH & Co. KGaA, Weinheim. (f) Inverse metasurface design based on forward model and a heuristic algorithm. Reproduced with permission from Ref. [37], copyright 2022 WILEY-VCH Verlag GmbH & Co. KGaA, Weinheim. (g) Topology-optimized lightsail designs. Reproduced with permission from Ref. [38], copyright 2021 American Chemical Society. (h) Automatic metrology in structured light profilometry. Reproduced with permission from Ref. [39], copyright 2019 Optical Society of America. (i) Schematic of a metasurface for polarimetry. Reproduced with permission from Ref. [40], copyright 2018 American Chemical Society. (j) Wavelength demultiplexer for integrated circuit. Reproduced with permission from Ref. [41], copyright 2015 Nature Publishing Group. (k) Polarization-multiplexed holograms using metasurfaces. Reproduced with permission from Ref. [42], copyright 2023 American Association for the Advancement of Science. (l) Schematic of the optical integrated diffractive neural networks. Reproduced with permission from Ref. [43], copyright 2019 Nature Publishing Group.

plasmonic nanostructures, and silicon photonic components. These are the basic building blocks for more complex nanophotonic systems, whose properties are characterized by transmission/reflection/absorption spectra, polarization response, near field distribution and so on. On the top is the application layer, which is directly visible to end users with a demand-driven interface. For example, a nanophotonic spectrometer design focuses on the spectral response of the constituent components, while in imaging applications, the phase response and the associate wavefront control ability are the major concerns. In between the data layer and application layer is the control layer, the pivot layer that bridges software frontend and hardware backend. In the control layer, various algorithms play an important role to automatically link the target application with physical implementations, including automatic design of the nanophotonic devices and automatic data processing in the measurement process.

The ability to design is crucial for the physical realization of software-defined nanophotonic systems. Conventionally, nanophotonic devices are designed in a rule-based routine. Empirical designs are first proposed by experienced designers, and then a parameter sweep process are usually carried out to optimize the initial design. Such design methods highly require the designers' physical understanding of the device, and the corresponding manual optimization is often inefficient. In software-defined scheme, the design and optimization of nanophotonic devices become an automatic process, namely inverse design, with little need for human intervention. According to the mechanism, the inverse design algorithms can be classified into three major categories, namely, gradient-based algorithm, heuristic algorithms and data-driven algorithms. Gradient-based algorithms first calculate the gradient of the target function with respect to the design parameters, and then perform the optimization using gradient-descent algorithm and its variants like Newton Methods. To accurately capture the gradient information, the most popular approach is the adjoint methods [44]. In a reciprocal electromagnetic system, the gradient of a function of field distribution with respect to permittivity can be conveniently calculated by applying two electromagnetic simulations, so-called a forward simulation and an adjoint simulation [45]. The gradient-based algorithm is very efficient in the inverse design process, since all the gradients are calculated in parallel with only two simulations. However, it is a local optimization method, which can be easily trapped in non-ideal local optimal points. On the other hand, heuristic algorithms explore the design space following certain empirical rules, such as direct binary search algorithm that simply uses random modification of the design parameters [46], genetic algorithm (GA) inspired by the evolution process in nature [47,48], particle swarm algorithm that mimics the foraging behavior of birds [49], and so on. These algorithms introduce certain stochasticity in the searching process with no need for gradient information and thus can optimize the target globally. Nevertheless, heuristic algorithms require very frequent evaluations of the target function relying on intensive numerical simulations, and hence can hardly scale up as the design parameters increase. Data-driven methods, typically statistical machine learning algorithms, solve the design problem by discovering the relationship of design parameters and optical responses from a vast number of training data [19]. Different from iterative optimization algorithms, data-driven methods require a pre-collected data set to train the model. Once fully trained, these models can tackle forward prediction or inverse design tasks much faster, often by orders of magnitude compared to conventional optimization methods. The most popular data-driven models are various deep neural networks (DNNs), also known as deep learning models, including multilayer perceptron, convolutional neural network (CNN), recurrent neural network (RNN), graph neural network (GNN), and so on. By automatically learning multilevel abstraction of data using hierarchically structured layers, deep learning models benefit from empirical design data and can generalize to similar design tasks. With various intelligent algorithms, especially data-driven methods, the control layer in software-defined nanophotonic systems offers flexible and programmable software interface for the underlying data layer containing specific physical implementation of photonic devices.

Apart from design ability, control layer in the software-defined scheme is also supportive to the application layer, where artificial intelligence contributes to the measurement, result processing and demand feedback of the nanophotonic system to enhance its functionality. The most straightforward case is the application of intelligent algorithms in the processing of images generated in various optical measurement scenarios. In particular, deep learning and other data-driven models are vastly applied in solving inverse optical metrology problems, such as image deblurring, single-frame phase retrieval, depth extraction, and holographic reconstruction [29]. Spectral data is another type of important data usually generated in the measurement. Deep learning models are able to analyze the scattering spectra of plasmonic nanostructures to push the information storage limit [50]. In nanophotonic systems for biochemical applications, machine learning models are also frequently employed to process the raw data from direct microscopic measurement to enhance the system functionalities, like principal component analysis (PCA) that extracts features from noisy measurements [51], or linear least-squares regression that can resolve molecule-specific information in a metasurface-based mid-infrared biosensor [52]. It should be noted that besides being a separate design method or signal processing approach, artificial intelligence algorithms in software-defined nanophotonic systems are more than add-ons but the hub that is seamlessly embedded in the entire design and application flow. Taking the idea of computational imaging as an example, a full color metasurface imager is constructed to simultaneously benefit from the high design flexibility of metasurface and the powerful image post-processing of deep learning models [53]. Therefore, as depicted in Fig. 1, the connection of data layer, control layer and application layer in the software-defined nanophotonic system is not a one-way process but are interconnected in both directions. The software interface enables simultaneous nanophotonic design and result processing to realize system-level optimization for specific applications.

To better guide the readers to understand the principle of software-defined nanophotonics as a holistic methodology, we organize the review in an application-oriented manner instead of dividing the techniques into pieces of algorithms for design, measurement, results processing and others. In the preceding part, we have introduced the overall picture and formalized the concept of software-defined nanophotonics, which includes all efforts to facilitate the design and application of nanophotonic systems. In the rest of the review, we will discuss several typical application scenarios where the software-defined scheme show its potency, including (1) nanophotonic design with multiple functions and extreme functions beyond manual labor, (2) intelligent nanophotonic systems for spectrometry, polarimetry and imaging, (3) ultra-compact silicon photonic devices and integrated photonic circuits with ultra-high integration density, (4) nanophotonic systems for optical neural networks and optical computing, and (5) physics informed

machine learning models for quantum optics and materials. We provide concrete examples to demonstrate the application, even often implicit, of software-defined methodology in nanophotonics. While some optimization methods are not directly related to machine learning, we still include them in this review. The reason is that optimization methods have been long utilized in photonic design, and machine learning can further enhance their effectiveness. We will highlight the research on both traditional optimization methods and hybrid models that combine optimization methods with machine learning. By examining these different approaches, we aim to provide a comprehensive understanding of how software-defined methodology is applied in nanophotonics. In the end, we will summarize current research results, and provide perspectives on future research directions such as co-design of software and hardware in nanophotonic systems.

2. Nanophotonic devices with multiple or extreme functions

2.1. Inverse design of metalenses

It is widely known that the properties of natural materials are essentially determined by atoms and their spatial arrangement (i.e., lattices). Using artificial meta-atoms, people have demonstrated metamaterials with exotic properties difficult to achieve or even unavailable in natural materials [54–59]. The meta-atoms are precisely engineered nanostructures with adjustable characteristics and responses. The size of the meta-atoms is significantly smaller than the wavelength of electromagnetic or light waves. Therefore, we can apply the effective medium theory to homogenize metamaterials and define effective material properties. Very importantly, the effective properties of metamaterials are primarily determined by the geometries rather than the chemical constituents of meta-atoms. One recent focus in the field of metamaterials is metasurfaces [5,60–65], which comprise just a single layer of meta-atoms. Meamaterials and metasurface can produce novel properties and phenomena that are distinctly different from those found in natural materials. For instance, natural materials typically have positive refractive indices. However, by making electric permittivity and magnetic permeability simulatatnely negative, metamaterials can achieve negative refractive indices and reverse Snell law to bend refracted light to the negative direction [66,67]. People have also shown that metamaterials can manipulate the flow of electromagnetic waves around an object and produce an invisibility cloak to hide the object [68–70], which used to exist only in science fiction. On the other hand, altering the spatial arrangement of various meta-atoms is helpful in controlling the optical response, enabling complex functionalities even with a single layer of metasurfaces. Some representative examples include flat metalenses [9, 71–73], chiral metamaterials [74–79], color routers [80–83], and meta-holograms [42,84–86]. The design of the metamaterials and metasurfaces, however, typically necessitates time-consuming full-wave simulation and iterative meta-atom optimization. In recent years, researchers have developed flexible inverse design methodologies to accelerate the design of meta-devices and thereby enable

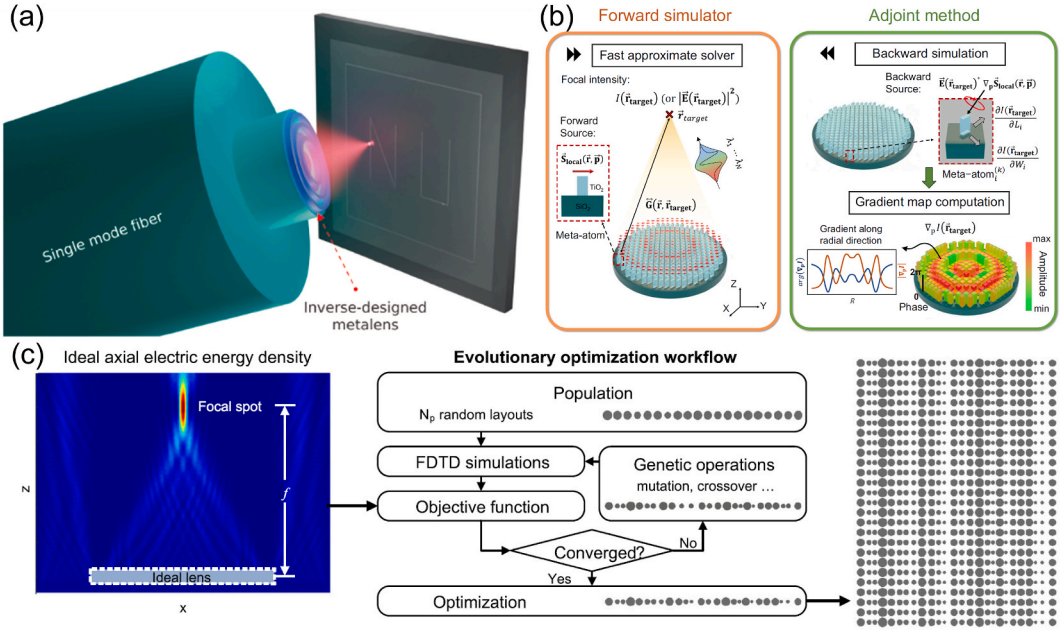

Fig. 2. (a) Schematic of the metalens integrated on top of a single mode fiber (SMF), which can be used for direct laser lithography. Reproduced with permission from Ref. [87], copyright 2021 American Chemical Society. (b) Left: Fast approximate forward simulator that calculates the field intensity at the target via the convolution of the equivalent current and the appropriate Green's function. Right: Adjoint method that calculates the gradient with respect to all the metasurface design parameters. Reproduced with permission from Ref. [88], copyright 2022 Nature Publishing Group. (c) The target electric energy distribution, the evolutionary optimization workflow, and the metalens layout designed by the optimization. Reproduced with permission from Ref. [89], copyright 2020 Nature Publishing Group.

more complex and intriguing functionalities.

In 2021, Hadibrata and co-workers designed and demonstrated an infrared metalens that can be integrated to an optical fiber tip for direct laser lithography [87]. The requirements of the metalensinclude small size, light weight, and a high numerical aperture (NA). The authors applied an objective-first inverse method, which considered the material permittivity and the field distribution, and substituted them into a minimization problem. In each iteration, two subproblems were solved where either permittivity or field was fixed while alternatively solving the other. The authors realized a grating-liked metalens with focal length of 7.8 μm, NA of about 0.85, and a focusing efficiency of 73% at the wavelength of 980 nm. To validate the usefulness of the metalens, the authors integrated it on a fiber top and performed direct laser lithography, as shown in Fig. 2(a). Surprisingly, a feature size of about 200 nm with a high accuracy and precision was realized.

Novel inverse design methods have also been explored in visual systems, such as virtual reality and augmented reality. As a representative work, Li et al. developed a large-scale high-performance metalens by combining a fast approximate solver and an adjoint method [88]. The conventional optimization relies on time-consuming parameter sweeping and full-wave simulations, which can be mitigated with the proposed methods. On one hand, the faster solver is achieved by the convolution of local fields and Green's function, and the local periodic approximation is applied to predict the local field. On the other hand, a forward and adjoint simulation

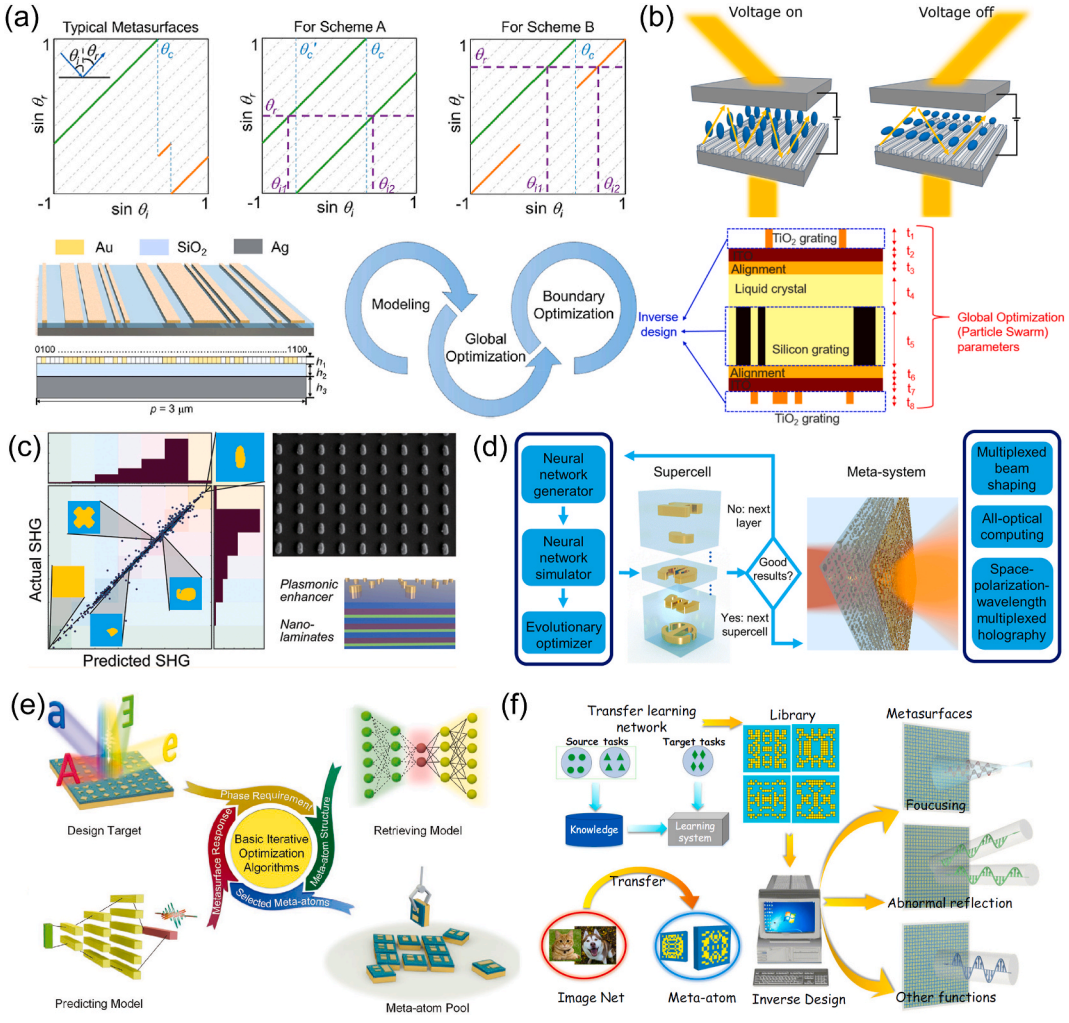

Fig. 3. (a) Design scheme and workflow for the optical merging meta-grating. Reproduced with permission from Ref. [90], copyright 2020 American Chemical Society. (b) Top: Tunable metasurfaces with liquid crystal sandwiched between meta-gratings. Bottom: Design framework combining global search and local inverse design. Reproduced with permission from Ref. [91], copyright 2020 American Chemical Society. (c) Inverse design of plasmonic structures to maximize the efficiency of send harmonic generation. Reproduced with permission from Ref. [93], copyright 2022 American Chemical Society. (d) Hybrid model that combines evolutional strategy and neural networks for multilayer metasurface design. Reproduced with permission from Ref. [94], copyright 2021 American Chemical Society. (e) End-to-end design pipeline for multifunctional metasurfaces. Reproduced with permission from Ref. [101], Copyright 2022, WILEY-VCH Verlag GmbH & Co. KGaA, Weinheim. (f) Transfer learning architecture to transfer the knowledge of image classification to meta-atom design. Reproduced with permission from Ref. [104], copyright 2021 Nature Publishing Group.

are performed in each optimization loop to calculate the gradient of the objective function with respect to the geometric parameters, and the designs are updated, which is also visualized in Fig. 2(b). As a result, metalenses with diameter of 2 mm and 1 cm were designed and fabricated, showing an achromatic and polarization insensitive properties as expected. The authors also demonstrated that with the cm-scale meta-optic device, a virtual reality system can be built with greatly reduced size and weight compared to the conventional counterparts.

The design and implementation of meta-atoms typically has the trade off in terms of performance and feasibility in fabrication. This is caused by the locally periodic approximation (LPA) in the metasurface design, which assumes that every meta-atom is electromagnetically independent from its neighbors, allowing us to use the periodic boundary conditions when evaluating the response of individual meta-atoms. However, in dielectric meta-atom design, the nanostructures need to be thick (~hundreds of nanometers) and high-aspect-ratio to have a good electromagnetic isolation with neighbors, resulting difficulties in fabrication due to issues like shadowing effect. On the other hand, the ultrathin meta-atoms are easy to fabricate, but there exists strong evanescent field coupling among the meta-atoms. Therefore, the LPA may not hold anymore and the response of meta-atoms can deviate from the simulations based on LPA. To address this issue, Cai et al. proposed a global evolutionary optimization approach to consider the non-local interactions and inversely design metasurfaces [89]. In the inverse design for a one-dimensional metalens, first a population of metasurface structures was randomly generated. As depicted in Fig. 2(c), for each member in the population, the target properties, such as the phase profile, transmittance, and focusing intensity, were evaluated by numerically solving Maxwell's equations for the entire device. Different from the conventional GA approach, such evolutionary procedure also took advantage of clustering the populations into different classes; this classification was completed based on the performance of individual populations and the resultant grouping improved the diversity of the pool. Such a process allows winning classes (representing a better set of individuals) to expand their sizes. It translates into a more expanded search of the phase space, enabling us to explore solutions near the possible global minimum. As a demonstration, the authors designed and evaluated the thinnest ($\sim\lambda/5$) metalenses with the highest efficiencies at the visible wavelength.

2.2. Design of meta-systems with complicated functionalities

The applications of meta-devices can go beyond metalenses. For example, Wang et al. designed a meta-grating that can merge free-space beam with a much higher efficiency [90]. In conventional themes, the free-space optical merging (FSOM) requires bulky components like beam splitters, which inevitably introduce additional stray beam and reduce the efficiency. In this work, the authors used an alternative design approach, aiming to manipulate the diffraction orders of the incident beam with meta-gratings. To be specific, the FSOM requires a single reflection angle for two different incident angles. The authors designed two different schemes for such FSOM, as shown in Fig. 3(a). For example, in the first proposed scheme, the meta-grating was designed to provide only 3rd and -2nd order manipulation. As a result, the light beam incident from these two directions can be coupled out to the normal direction with minimized stray beams. However, such abnormal phenomenon is hard to achieve with conventional gratings. To solve the problem, the authors used a two-step optimization: First, a global optimization was performed using non-dominated sorting genetic algorithm-II (NSGA-II), a multi-objective optimization algorithm based on GA, to optimize the geometric parameters of the meta-gratings. GA is a class of non-gradient-based optimization algorithms that emulate the process of natural evolution. Due to their probabilistic transition rules, GA is well-suited for complex and noisy parameter spaces, and can effectively search from a population of potential solutions, enabling multi-objective optimization of the Pareto front. Nevertheless, GA is often computationally expensive and does not guarantee improvement after each iteration, making convergence to the optimal solution slower compared to other optimization algorithms. After applying global optimization, a boundary optimization was performed to randomly vary the design from the global optimization. The entire optimization loop ended when the current design surpasses all its variants. The authors proved the performance of the meta-grating via experimentation. The total merging efficiency was around 60–90% in the visible regime from 665 nm to 705 nm.

Due to their potential for extraordinarily diverse functionality and temporal turnability, tunable and reconfigurable metasurfaces have recently attracted wide attention. The responses of these metasurfaces can be adjusted by external inputs such as voltage, heat, and surrounding media. However, the capability of such designs heavily depends on and is constrained by physical intuition. To overcome these limitations, Chung et al. developed the inverse design for tunable metasurfaces in 2020. They demonstrated high switching efficiency (80%) and large angular deflection (144°) simultaneously [91]. A liquid crystal (LC) layer was included in the design, which was placed on top of a periodic meta-grating array and encased between two contact layers. The LC director was oriented perpendicular or parallel to the TE-mode electric field when the voltage was turned on or off, enabling the meta-grating to exhibit completely different deflection behavior. The schematic of the tunable system is shown in the top panel of Fig. 3(b). The effectiveness of the switching is greatly influenced by the meta-grating design. In this work, each grating has been pixelated to a size of 77.5 nm, and the permittivity of each pixel acts as the design parameter. The inverse design combines the local optimization of the grating and the global search of the layer thicknesses as shown in the bottom panel of Fig. 3(b). The gradient of switching efficiency with respect to the parameters is rapidly computed by topology optimization (TO). Backpropagation of the gradient is carried out throughout each iteration to update the design of the gratings. On the other hand, the particle swarm optimization (PSO) is utilized to globally optimize the layer thicknesses because they are also key components of the design. This technique first creates a large number of "particles" with arbitrary structural properties. Then inverse design is executed within each "particle" to improve the fine-scale properties of the devices. New parameters are then chosen in accordance with the evaluation function of standard particle swarm optimization [92]. The global search for the ideal thickness encompasses the grating optimization process. The highest deflection-angle design, which uses a triple-grating structure to achieve deflection from $-72°$ to $72°$, is obtained using the proposed inverse design method. This study

utilizes both TO and PSO algorithms, leveraging their respective strengths while mitigating their shortcomings. To be more specific, TO as a gradient-based approach, exhibits proficiency in tackling problems with high-dimensional parameter space by updating all variables in a single iteration step, and works best for optimizing material morphology or spatial distribution. However, it is highly reliant on complex mathematical models, lacks the ability to account for real-world fabrication constraints, and may be susceptible to local optima. In contrast, PSO, with its stochastic nature, is more adaptable to global search, easy to implement, and computationally efficient. Nevertheless, the convergence of PSO is not guaranteed especially in complicated parameter space.

The nonlinear effect is also one important phenomenon in photonics. For instance, we can achieve second harmonic generation (SHG) by breaking the inversion symmetry of structures. However, the nonlinearity of natural materials is usually very weak. Therefore, it is important to design photonic materials and structures with high nonlinearity. With this aim, Raju et al. proposed an inverse design scheme to implement nonlinear metamaterials with maximized SHG efficiency [93], as illustrated in Fig. 3(c). In this paper, the contribution of SHG comes from two parts. On one hand, the design platform is based on a nanolaminate, in which three kinds of materials (i.e., TiO_2–Al_2O_3-HfO_2) are alternatively stacked to form the substrate. This configuration readily breaks the centrosymmetry at each interface and the second order nonlinear effects can emerge. On the other hand, a periodic array of gold nanostructure is deposited on top of the substrate. Thanks to the large field enhancement from such plasmonic naonstructures, the SHG can also be amplified since it is proportional to the field intensity. However, the plasmonic modes are sensitive to the structure design and its boundary, which need to be optimized to achieve maximized efficiency. To facilitate the design process, the authors first trained a simulator that can predict the SHG efficiency from structure image, described by a 64×64 binary image, to replace the time-consuming numerical simulation. Then, the simulator was directly inserted to an optimization loop based on evolution strategy (ES). However, the image input might not be ideal given the extremely large number of parameters in the design space. Therefore, an encoder-decoder network was built to map between the image and a latent vector: The encoder can encode the structure to a latent distribution. And the decoder can decode the latent vector, which was randomly sampled from the latent distribution, back to the structure image. With these two trained neural networks, the optimization can be run much more efficiently. Based on this method, an optimal design was generated, with the maximized SHG among all the designs and was verified in both numerical simulation and experimentation.

Recently, Zhu et al. have reported that combines neural networks with an ES-based optimizer to design cascading layers of metasurfaces with multifunctional capabilities [94]. As shown in Fig. 3(d), the entire design loop involves a generator based on generative adversarial networks (GANs), a forward simulator, and an ES-based optimizer. First, random structures are generated and denoted as binary images, the GANs try to generate fake images based on latent vectors that look like the real images from the dataset. This function of the GANs is similar to the variational auto-encoder (VAE) [95–97]. Both of them attempt to build a generator that can generate the structures based on a random variable. In parallel, a forward simulator is also trained to predict the spectra of the structure. Then, the optical response of the multi-layer supercell is calculated by the matrix-chain multiplication of the wave matrix. Finally, the ES optimizer connects both networks in an end-to-end manner and optimizes the latent space for generating the structure at each layer. As a proof of effectiveness, a polarization-multiplexed dual-functional beam generator, a second-order differentiator for optical computing, as well as a space-polarization-wavelength multiplexed hologram have been designed and verified with numerical simulation.

The GANs are frequently used a generative model. The work by An et al. proposes the use of the GAN to design a multifunctional all-dielectric metasurface [98]. In order to solve the one-to-many mapping problem. The training process comprises the improvement of both generator and discriminator; the generator will produce high-quality designs that are quite close to the real meta-atoms, while the discriminator is very sensitive to the distinction between fake designs and real designs. The generator can then be employed for the inverse design of new meta-atoms under the predefined condition of target EM response after training. The conditional GAN and the Wasserstein generative adversarial networks (WGAN) are specifically combined by the authors [99,100]. As another popular GAN alternative, WGAN incorporates the earth-mover distance as a loss evaluation approach, stabilizing the training procedure and enabling the network to solve complex metasurface design problems. Additionally, the proposed method processes several inputs simultaneously, hence the complexity is unaffected by the size of the inputs. This trait further establishes the GAN-based method as the ideal strategy for dealing with complicated and multifunctional inverse design issues. In order to demonstrate the adaptability and scalability of the suggested technology, the authors have constructed and verified a number of multifunctional metasurfaces based on this highly efficient network, including a bifocal lens, a polarization-multiplexed beam deflector, and two multipurpose metalenses. The usefulness, power, and simplicity of this strategy have been confirmed by the ability of the proposed network to perfectly meet the multifunctional design goals as well as by the performances of the assembled metasurface devices.

It is always favorable to integrate multiple functions in a single metasurface. Due to the interdependence between channels (e.g., different wavelengths or polarizations), it is very challenging to achieve fully independent information channels. Aiming to further push the multiplexing capability in metasurface design, Ma et al. proposed an end-to-end inverse design technique based on DNNs [101]. The design framework of this work is illustrated in Fig. 3(e). It consists of one retrieving model based on a VAE that can generate individual meta-atom designs, and a predicting model that evaluates the response of the meta-atoms. The authors first perform statistical analysis based on the training dataset, and select the information channels that have minimized crosstalk according to the mutual information analysis. Then, for a given task (e.g., metalens or meta-hologram design), the required phase response of individual meta-atoms are calculated. The trained retrieving model can retrieve meta-atoms that fit the requirements and build a meta-atom pool. Next, the predictive model is utilized as a rapid evaluation tool to obtain responses from the meta-atom candidates, enabling the assessment of the current design's performance. Finally, the designs can be further optimized depending on the discrepancy between the target and the current performance. It is worth noting that this method can be integrated with gradient-based methods including diffraction integral or non-gradient-based methods like Gerchberg-Saxton algorithm, providing significant generality in different

design scenarios. The authors have successfully demonstrated a single metasurface with up to 8 information channels (4 wavelengths and 2 polarizations), and each channel can function as a meta-hologram with user-defined images. The authors verified their metasurface designs via experimentation and the results agreed very well with the design target.

As shown in the previous papers, the most time-consuming part in a deep-learning-based inverse design is the data generation. Usually, the required data number is from 10^3 to 10^5 depending on the complexity of the tasks. Therefore, we need to find ways to reduce the time cost in generating the training data by all means. Using mathematic calculations instead of full-wave numerical simulations to solve the response of optical systems is one solution, but it is not straightforward for two reasons: First, this approach can only be applied to simple optical systems, like transmittance of multilayers and scattering cross-section of spherical particles [102,

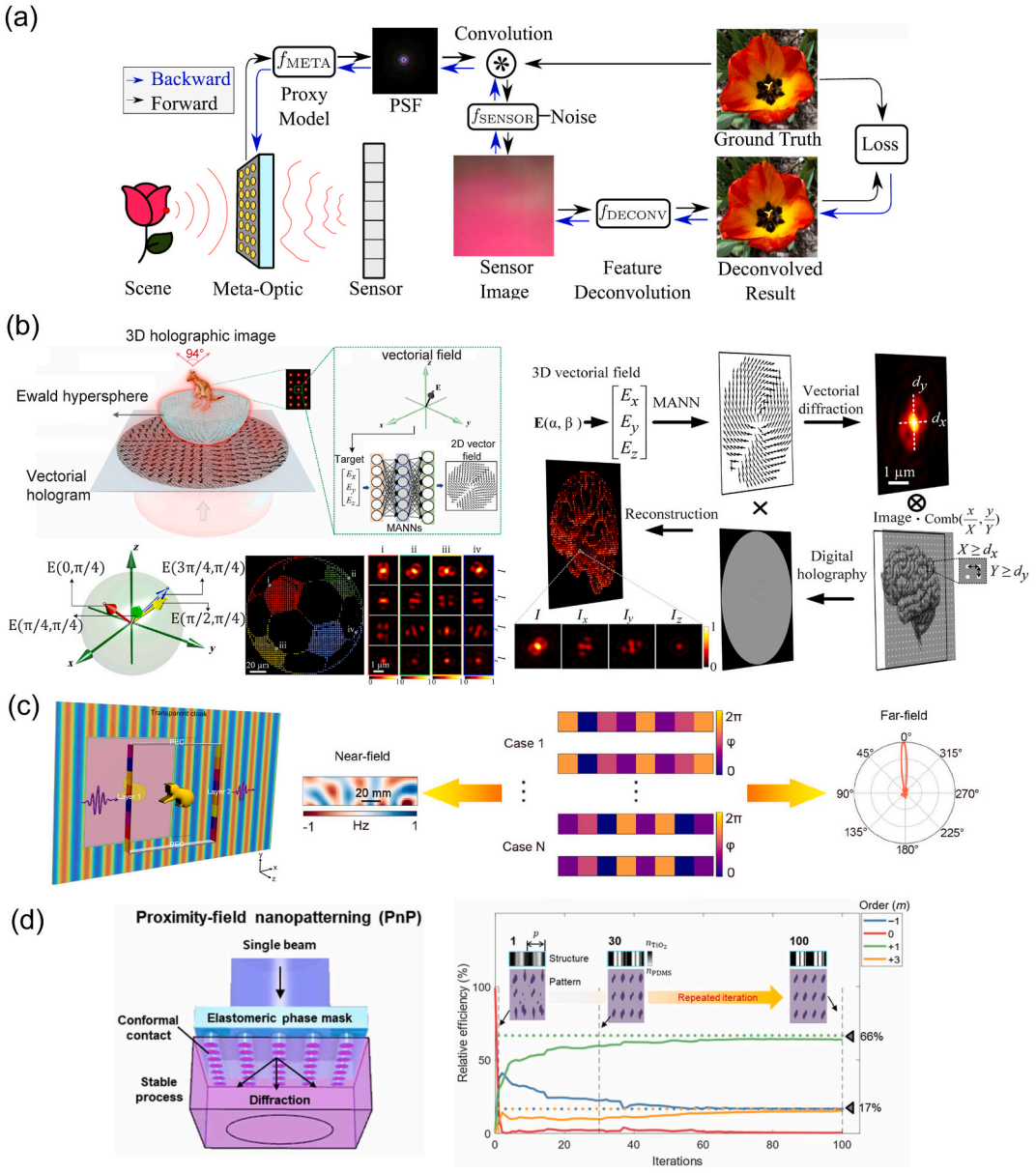

Fig. 4. (a) Training pipeline of the neural nano-optics model. Reproduced with permission from Ref. [105], copyright 2021 Nature Publishing Group. (b) Top left: Illustration of the multilayer perceptron ANNs used for reconstruction of 3D vectorial field. Bottom left and Right: Experimental approach and characterizations of 3D vectorial holography. Reproduced with permission from Ref. [106], copyright 2020 American Association for the Advancement of Science. (c) Left: Schematic of the transmission-type metasurface cloak. Right: Both the near-field and far-field properties of the cloak design are considered for designing the cloak, and the one-to-many mapping issue occurs in the inverse design process. Reproduced with permission from Ref. [107], copyright 2021 Optical Society of America. (d) Left: Schematic of a 3D holographic lithography with proximity-field nanopatterning. Right: Relative efficiencies of the diffraction orders over the optimizations. Reproduced with permission from Ref. [108], copyright 2022 American Association for the Advancement of Science.

103]. Second, if we can easily calculate the response of the system of interest with acceptable accuracy, there is no need to train an additional neural network for response prediction. Therefore, it is more realistic and significant to reduce the required number of data instead of reducing the simulation time in complicated design tasks. Under this circumstance, transfer learning serves as a very helpful method, as discussed in the work of Zhu and co-workers in 2021 [104]. The authors aimed to transfer the network and its weight from a well-trained image-based forward model (Inception V3, the third generation of GoogLeNet) to the metasurface platform. The original network can work very well for image classification that distinguishes different objects like fish and birds. As illustrated in Fig. 3(f), the network is based on a CNN, which extracts the features of the input images and performs classification based on the features. The process is also similar to the prediction of the phase response of a meta-atom (denoted as a 16×16 binary image). In the transfer process, the weight and bias in the convolutional layers and pooling layers are frozen, and only the parameters in the fully connected neural networks (FCNNs) are updated during the training process using the meta-atom data. To convert the regression problem to a classification problem, the phase response is discretized to 360 classes, each with 1° separation. In the end, the transferred network can show around 90% accuracy after training with a small number (20000) of data. Based on the forward model, all meta-atoms with phases from 1° to 360° can be generated. Using the generated meta-atom library, the authors have built different meta-devices, including the focusing metasurface and abnormal beam reflector at the working frequency of 10 GHz. The experimental results show excellent agreement with the expectation.

2.3. Design for high-quality imaging systems, invisibility cloaks and others

Although metasurface optics provides a route to miniaturized imagers, current techniques have produced images with quality significantly inferior to bulky refractive alternatives, which are fundamentally constrained by aberrations at large apertures and low f-numbers. A neural nano-optics imager was discussed in the paper by Tseng et al. to close this performance gap. The authors proposed a fully differentiable learning framework to learn the physical structure of a metasurface together with a neural feature-based image reconstruction technique [105]. Contrary to the design of a metalens, where the phase is computed directly and the meta-atoms are chosen to fit a preset phase, the polynomial coefficients that determine the phase of a metasurface serve as the parameters to be optimized in this work. To be specific, the phase function is expressed as $\varphi(r) = \sum_{i=0}^{n} a_i \left(\frac{r}{R}\right)^{2i}$, where $[a_0, \ldots, a_n]$ are the optimizable coefficients, and r and R are the distance from one point on the metasurface with respect to the optical axis and the phase mask radius, respectively. A neural network-based deconvolution method is used to evaluate the sensor image and reconstruct the image of the scene instead of simply showing it directly on the sensor. In addition to the phase of the metasurface, such a deconvolution network is also trainable and incorporates real-world noise into the sensor image. As depicted in Fig. 4(a), in the training phase, the scenes first interact with the metasurface, which is calculated by convolving the image of the scene with the point spread function of the metasurface. The outcomes match the sensor image, after adding the experimentally calibrated Gaussian and Poisson noise. The deconvolution network is then used to reconstruct the scenes using the sensor image and point spread function as the inputs. To simultaneously optimize the phase coefficients of the metasurface and the deconvolution network, the loss between the real-world and the reconstructed scenes is determined and backpropagated. In experiments, the authors have validated high-quality, full-color picture reconstructions employing such neural nano-optics. This work would inspire other meta-optic systems with high image quality, large aperture size, low f-number, wide fractional bandwidth, wide field of view, and polarization insensitivity.

According to a recent study by Ren et al., holographic images can be manipulated using artificial neural networks (ANNs) to provide a three-dimensional (3D) vectorial field with a wide viewing angle [106]. They used multilayer perceptron ANNs consisting of an input layer that can take input from any 3D vectorial fields, four hidden layers with one thousand neurons located in each layer, and an output layer that can create two-dimensional (2D) vector fields. First, the authors showed how arbitrary 3D vectorial field can be generated from the anticipated 2D vector field of a well-trained model. Subsequently, a 2D Dirac comb function was applied to sample the desired image. The required image was then used to generate a digital hologram, which was combined with a 2D vector field. This process is shown in the right panel of Fig. 4(b). Any required 2D vector beam can be produced using a split-screen spatial light modulator to individually adjust the amplitude and phase of orthogonal CP light. The experimentally measured holographic image can display four distinct 3D vectorial fields in various places, as shown in the left panel of Fig. 4(b). A high diffraction efficiency of 78% and an ultrawide viewing angle of 94° were experimentally achieved by the authors. The 3D vectorial holography opens a new door to holographic displays, multidimensional data storage, machine learning microscopy, as well as intelligent imaging systems.

Becoming invisible has long been a dream, as evidenced by numerous tales and works of science fiction. The development of optical metamaterials and metasurfaces has made it happen. The key is to alter the material properties in space so that light beams do not suffer from any scattering in the presence of an object. In the research by Z. Zhen et al. [107], a tandem neural network was proposed to generate a transmission-type metasurface cloak. Such transmitted metasurface cloak, which may conceal an object like a cat inside, was composed of two planar metasurfaces, labeled as layer 1 and layer 2, as shown in Fig. 4(c). Eight subwavelength metasurface elements were used to construct the metasurfaces, and each element could offer a locally transmitted spectrum shift. Two perfect electric conductor blocks were put together to make a closed rectangle to stop electromagnetic waves from dispersing in other directions. In this work, the authors quantified the cloaking performance by considering both the near-field distribution and the far-field radar cross-section. After passing through the two-layer metasurfaces, the incident wave should exhibit negligible forward and backward scattering, effectively rendering the rectangular box transparent. The goal is to generate an ideal metasurface arrangement S such that the near-field and far-field patterns F are identical to what they would be if there were no objects inside the hidden region. However, due to the prevalence of the one-to-many mapping problem, training a map straight from $F \rightarrow S$ may be problematic since very different metasurface designs, such as S_A and S_B, may have almost identical field distributions, but a FCNN is always deterministic

(one-to-one mapping). A tandem network, which compares the target field and the field generated from the retrieved metasurface design instead of directly comparing the retrieved metasurface designs and the ground-truth design in the dataset, can be employed to address this nonunique issue. A forward neural network must be pretrained to predict the near-field and far-field pattern from the metasurface design in order to construct the tandem network. The forward model exhibits 89% and 85.7% test accuracy for near-field and far-field pattern prediction after being trained with 200 epochs, respectively, enabling to evaluate new metasurface designs. After that, an inverse model is developed and coupled to the forward model for training. For the retrieved designs, the tandem network builds the loss between the target field and the predicted field, and it only utilizes backpropagation to update the parameters in the inverse model. After training, the inverse model can achieve test accuracy for target near-field and far-field patterns of 92.4% and 93.2%, respectively. The authors have further constructed the cloak using the inverse model by providing a zero scattering input. As a result, the wavefront is not strongly perturbed after passing through the cloaking device, which is very different from the situation when the cloak is absent.

Using interference photolithography to fabricate 3D structures is usually very challenging, since multiple beams need to be manipulated to form a desired interference pattern. An alternate way is to use proximity-field nanopatterning, which can generate multiple beams from a single coherent beam, as illustrated in the left panel of Fig. 4(d). A phase mask is essential in this process. Aiming to efficiently design phase masks for specific 3D nanostructures, Nam et al. proposed an inverse design platform using the adjoint method [108]. The 3D structure is highly related to the efficiencies of each diffraction order when light passes through the phase mask. Therefore, using the efficiencies at each diffraction order as an objective function, the phase mask can be gradually optimized as shown in the right panel of Fig. 4(d). The new inverse design method enables the fabrication of a 2D rectangular array of nanochannels, which is not a trivial task with conventional proximity-field nanopatterning. Furthermore, a recent study conducted by Chihun et al. reported the use of PSO to optimize a phase mask, which significantly enhanced the quality of the phase mask with an improved figure of merit for maximizing the electric field intensity contrast [109].

3. Nanophotonic spectrometers and polarimeters

Spectrometers [26,110–112] and polarimeters [40,113–115] at the micro and nano-scale have emerged as crucial components for nanophotonics [116,117], sensors [118,119] and information areas [120,121]. The research can be divided into two parts: the optimal design of optical devices, and signal reconstructions with high precision. Traditionally, efforts in these two parts have primarily focused on forward design and some classical iteration optimization methods, which are incapable of exploring the entire design space, resulting in large volume size and slow signal processing speed. In this section, we will review recent papers that demonstrate how machine learning methods can overcome these drawbacks and improve the performance of nanophotonic spectrometers and polarimeters.

3.1. *Nanophotonic spectrometers designed by machine learning*

People have explored a variety of platforms, such as disordered photonic chips [122], quantum dots [123,124], silicon photonic crystals [125,126], black phosphorus [127], pearl [128], and even single semiconductor nanowires [129], to implement nanophotonic spectrometers. The typical configuration and workflow of nanophotonic spectrometers are shown in Fig. 5 [125]. First, we need specially designed filters, such as PC slabs with varied geometries, to encode the input spectra by employing distinct filter functions that can provide diverse resonant features (Fig. 5(a)). The input spectra are then recovered using reconstruction algorithms from the raw data acquired by the detectors, often with a smaller number of detectors than the needed frequency points (Fig. 5(b)). In this case,

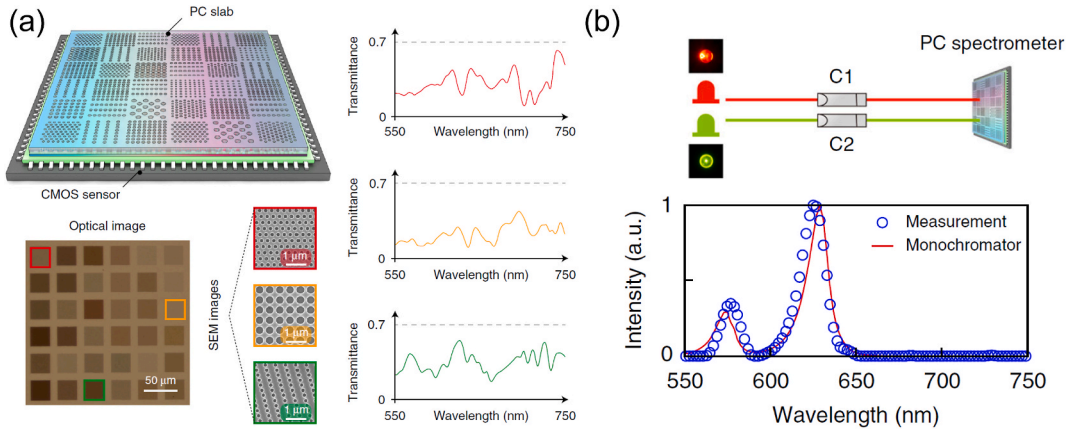

Fig. 5. (a) Schematic of a nanophotonic spectrometer, which consists of an array of PC slabs with distinct geometries to produce different transmission spectra. (b) Recovery setup and process of broadband spectra. Reproduced with permission from Ref. [125], copyright 2019 Nature Publishing Group.

the spectrum reconstruction process is typically an underdetermined problem that is ill-posed with associated measurement noise. As a result, regularization techniques and constrained optimization methods, such as Tikhonov regularization [130] and sparse recovery algorithm [131–133], are required to overcome these limitations and solve the inverse problem properly for nanophotonic spectrometers. However, successful application for spectrum reconstruction requires careful algorithm operation selection as well as a priori calibration of filter response functions, making the working process iterative and time-consuming [110,112].

Machine learning algorithms [19,22,134,135], as one subset of artificial intelligence, can improve the structure design and spectrum reconstruction process for computational spectrometers [110,111,136]. Since machine learning relies on data-driven processes, reconstructing the spectra is possible without prior knowledge of the filter response functions. They have the ability to directly trace the link between spectra and measured signals with high precision, thanks to the large number of hyper parameters in the neural network that can be optimized during the training process. As shown in Fig. 6(a), Zhang et al. utilized machine learning to reconstruct optical spectra through training a multilayer perceptron. The DNN is a common architecture that consists of an input layer (the raw measurement), several hidden layers, and an output layer (the true spectrum). To realize a better reconstruction performance, Bao et al. trained a DNN to learn a map from the derived features to the true spectrum by extracting spectral characteristics from the raw measurements [137], as shown in Fig. 6(b). According to experimental results, the DNN exhibits superior performance with an average reconstruction error reduction of over 80% in comparison with regularized non-negative least squares, demonstrating its ability to efficiently handle noise in real measurements and reconstruct spectra with higher accuracy and robustness. Another example can be seen in Fig. 6(c), where the lens-free diffraction images are utilized to rebuild the unknown input spectra in a feed-forward manner [138]. With a peak localization error of 0.19 nm, the deep-learning-based spectrometer can identify 96.86% of the spectral peaks after the training phase. In comparison to a linear regression model trained on the same data set, the trained neural network can reduce the average MSE from 3.85×10^{-4} to 7.77×10^{-5}. In addition to these notable improvements, the data-driven DNN method can also suppress background spectral noise and incorrect peaks. As a result, it has the potential as a useful software-defined calibration tool for data-driven nanophotonic spectrometers.

Another substantial benefit of DNN is that various architectures can be explored to modulate the specific incident spectrum more efficiently and accurately. As discussed above, encoding filters in nanophotonic spectrometers are usually built on a conventional design to realize a low correlation coefficient. The inverse-design capability of deep learning tools can realize better intelligent filters. Fig. 7(a) depicts a novel DNN-designed nanophotonic filters in nanophotonic spectrometers [139]. The innovative algorithm allows metasurfaces to form an encoding network. By adding a decoder after it, the whole network can capture and reconstruct the input spectrum. The comparison shows that the co-designed DNN framework outperforms the decomposed sequential-design method in terms of effective spectral responsivity for each random spectral filter. Spectral cameras that use such design have higher reconstruction accuracy with up to 30 times enhancement and are more immune to fabrication errors.

As previously mentioned, metasurfaces are able to manipulate the phase, amplitude, polarization, and spectrum of light, making them an ideal candidate for encoding filters. However, conventionally designed meta-atoms of metasurfaces use regular shapes, limiting the performance improvement. As shown in Fig. 7(b), Yang et al. reported the use of freeform metasurfaces for ultra-spectral imaging, where the freeform patterns were generated with specific feature sizes and boundary curvatures [140]. The freeform patterns enrich spectral response of metasurface with complicated Bloch modes, enhancing spectrum reconstruction precision for various spectra. The snapshot on-chip ultra-spectral imaging is demonstrated experimentally, where spectral resolution is as small as 0.5 nm and the mean fidelity of spectral reconstruction reaches 98.78%. The method for generating freeform patterns has advantages for forward and inverse designs in the field of intelligent perception.

3.2. *Nanophotonic polarimeters empowered by machine learning*

Polarization is another property of light that can carry information [141,142]. Imaging polarimetry refers to the technique of capturing and analyzing the polarization state of light across a wide scene [111,114,115,143–149]. Among different designs for

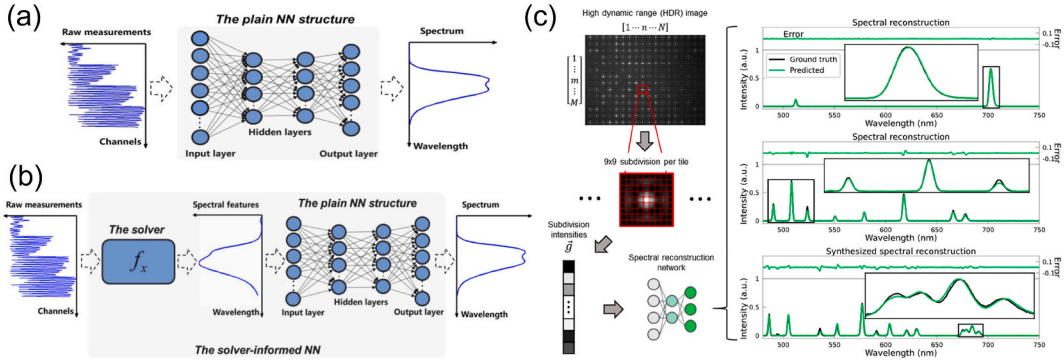

Fig. 6. (a) Architecture of the normal neural network. (b) Architecture of the solver-informed neural network which first extracts spectral features from the raw measurements. Reproduced with permission from Ref. [137], copyright 2021 Optical Society of America; (c) Workflow of spectral reconstructions using diffraction images. Reproduced with permission from Ref. [138], copyright 2021 American Chemical Society.

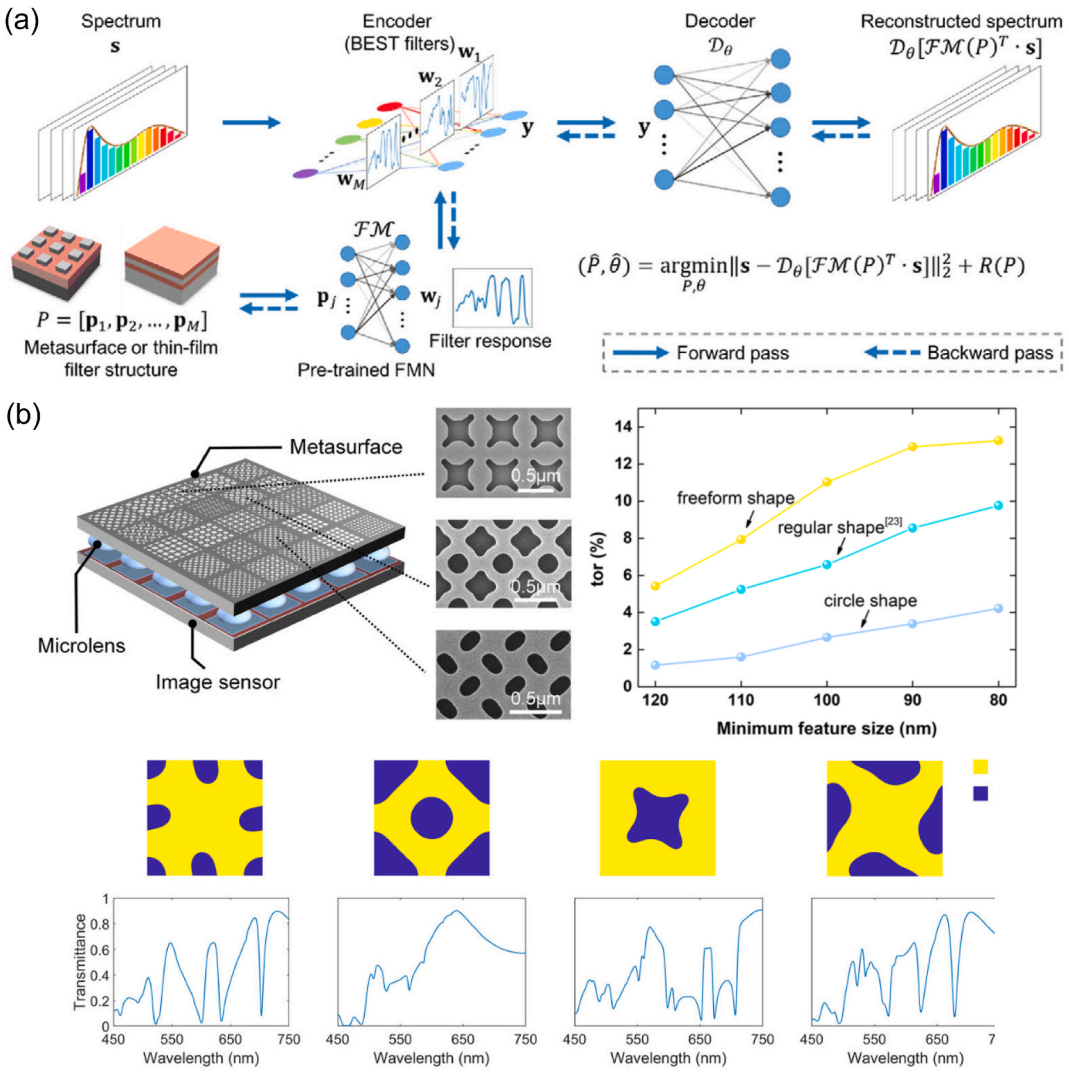

Fig. 7. (a) Schematic of the spectral encoder and decoder design framework. The encoding filters function as an encoder, whose connection weights are constrained by the structure parameters. Reproduced with permission from Ref. [139], copyright 2021 WILEY-VCH Verlag GmbH & Co. KGaA, Weinheim. (b) Ultra-spectral imager consisting of freeform meta-atoms with distinctive transmission spectra. Reproduced with permission from Ref. [140], copyright 2022 WILEY-VCH Verlag GmbH & Co. KGaA, Weinheim.

imaging polarimetry, division of focal plane polarization cameras (DoFP-PCs) are more compact and less complicated [40,150–155]. Fig. 8(a) shows a typical DoFP-PCs based on dielectric metasurfaces with polarization and phase control. Instead of polarization filtering, the proposed meta-device divides and focuses light into three distinct polarization bases, enabling full Stokes characterization and overcoming the 50% theoretical efficiency limit in olarization-filter-based DoFP-PCs [40]. Fig. 8(b) shows another typical example, where metasurface gratings can realize arbitrary, parallel polarization analysis [141]. The metasurface polarization camera, which operates without any moving components, has the potential to enable widespread adoption of polarization imaging in machine vision applications.

As the demand for increased precision and faster speeds rises, there is growing interest in applying deep learning to nanophotonic polarimeters [156–161]. For instance, Yang et al. achieved colorimetric polarization detection with all-dielectric metasurfaces using a ResNets-based polarization detection network [160]. The concept is illustrated in Fig. 9(a). The precision of the incident polarization variation was correctly identified by the polarization detection network to assess the color patterns of an arrayed color palette. The measured accuracy reaches 99.5% within a 1.4° error. The device can detect extremely subtle color variations, allowing for colorimetric polarization-angle detection with high precision. The polarization angle can be obtained in about 1 s after the network has been trained, which is faster than traditional polarimeter design.

Aside from the colorimetric design, holographic microscopy technology can also be used to detect polarization. Liu et al. demonstrated a deep-learning-based holographic polarization microscope capable of extracting birefringence retardance and specimen orientation information from a phase-recovered hologram [161]. As shown in Fig. 9(b), a trained DNN can extract birefringence

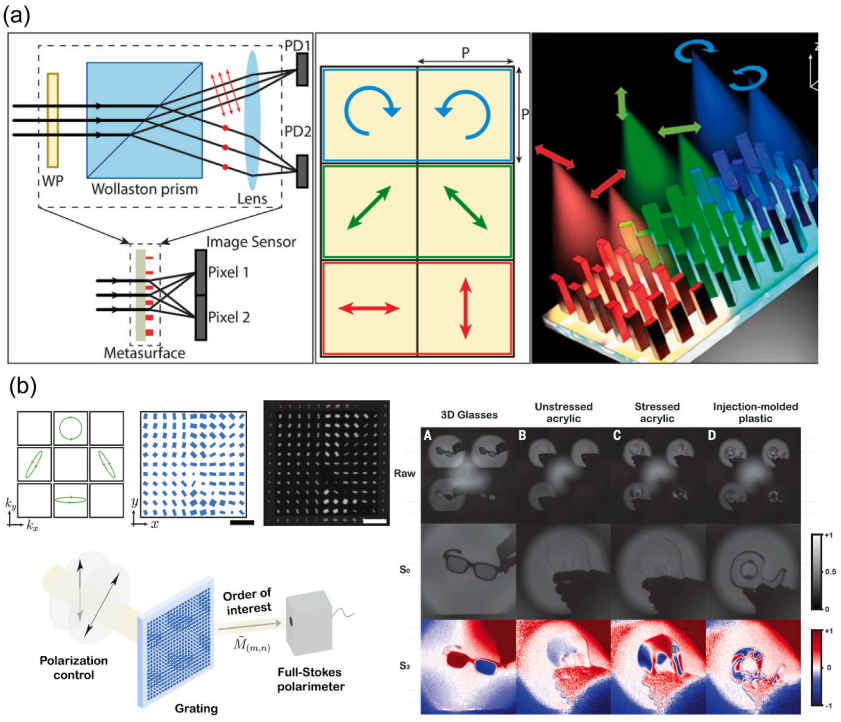

Fig. 8. (a) Schematic of a conventional setup used for polarimetry and 3D illustration of a superpixel that focuses light with different polarizations to different spots. Reproduced with permission from Ref. [40], copyright 2018 American Chemical Society. (b) Left: A 2D metasurface designed to analyze four different polarization states. Right: Example imagery from the camera. Reproduced with permission from Ref. [141], copyright 2019 American Association for the Advancement of Science.

information from holographic amplitude and phase distributions as well as sample-specific morphological features. This approach is useful because it can reconstruct the specimen's quantitative birefringent retardance and orientation information with high accuracy, and only requires the measurement of a single polarization state, which can be produced using a simple optical setup.

The preceding discussion of the polarimeter only focuses on nanostructures in regular shapes, which may limit its performance improvement. Liu et al. instead resorted to freeform complex structures, as shown in Fig. 10, which were designed by utilizing the full power of TO Ref. [159]. The authors demonstrated noise sensitivity and compactness significantly superior to either an optics-only or a computation-only approach by co-designing the end-to-end architecture. This method involves $\gtrsim 10^4$ degrees of freedom in a single large-scale optimization. The resulting structures have the ability to scatter light in distinct ways than either a typical lens or a random microstructure, and they greatly reduce the inverse-scattering computation's susceptibility to noise by orders of magnitude.

4. Silicon photonics and integrated photonics

Integrated photonics aims to miniaturize optical components and fabricate them in a single microchip in the same way as integrated electronic circuits. Compared with discrete optical components, integrated optics offers the advantages of greatly reduced footprint, more robust optical alignment and lower loss. Among all the integrated photonic platforms, silicon is usually considered as the most promising material due to its low loss in the near infrared region, high refractive index, and potential for achieving high integration density. More importantly, silicon photonics is compatible with modern complementary metal–oxide–semiconductor (CMOS) fabrication process, which makes it easy to scale up with the aid of mature integrated circuit (IC) fabrication techniques [162]. With decades of development of IC industry, the design of IC has now been deeply bonded with electronic design automation tools, where electronic components and modules are automatically designed, arranged and interconnected with algorithmic interfaces to significantly facilitate very large-scale IC design. Similarly, for integrated photonics and silicon photonics design, various automatic design algorithms have been investigated to produce devices with ultra-compact footprint or supreme performance.

4.1. *Miniaturization of conventional silicon photonic devices*

One seminal work on the inverse design of silicon photonic devices is applying adjoint-method-based TO in a wavelength demultiplexer by the researchers from Stanford University in 2015 [41]. Adjoint method calculates the derivatives of the target function with respect to shape parameters at all points in space, but requires only two simulations, namely a forward simulation to calculate current value of target function and an adjoint simulation with source defined by the derivatives of the target function [45].

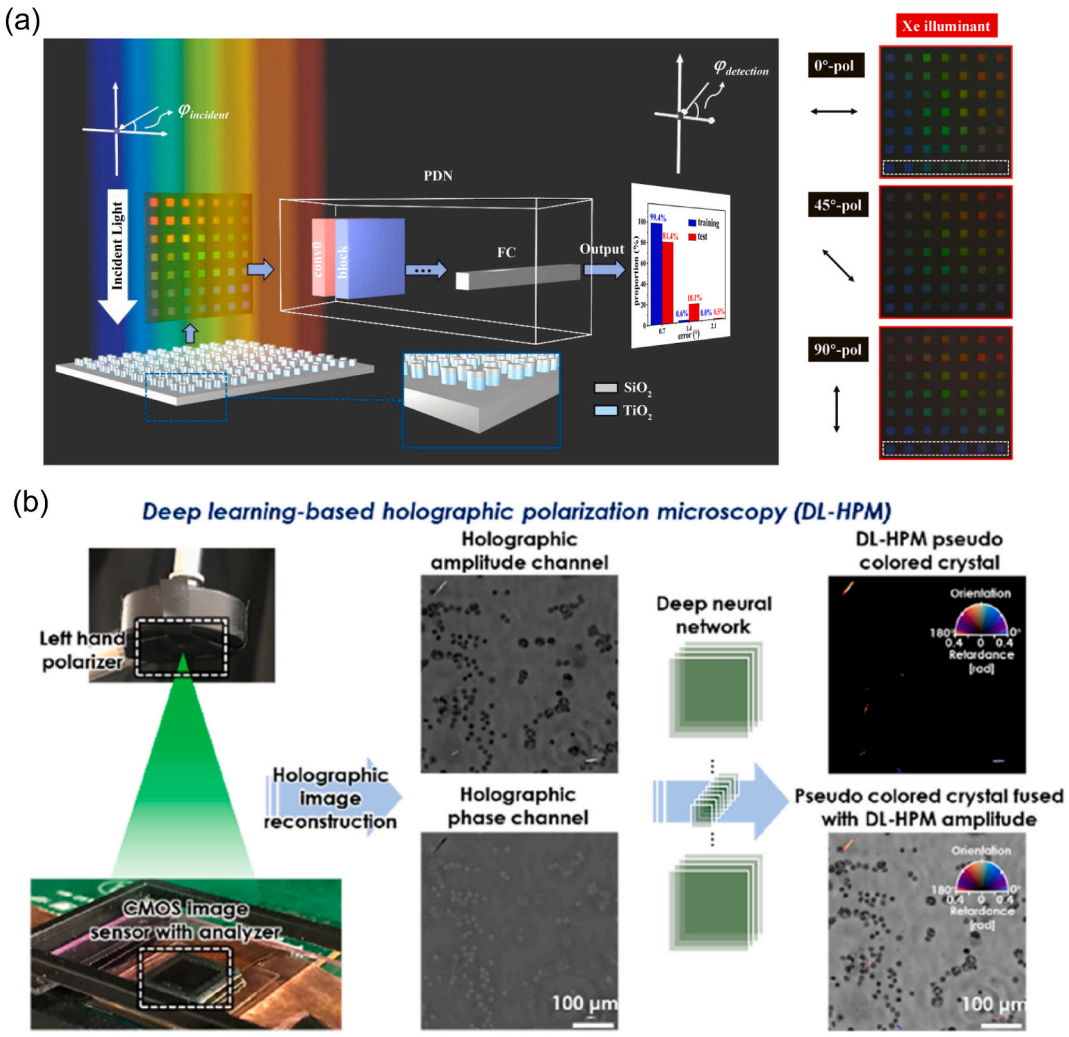

Fig. 9. (a) Schematic of colorimetric polarization-angle detection. A polarization detection network is used to detect incident polarization by altering the arrayed color palette of metasurfaces. Reproduced with permission from Ref. [160], copyright 2022 Optical Society of America. (b) Deep-learning-based holographic polarization microscope. Reproduced with permission from Ref. [161], copyright 2020 American Chemical Society.

As shown in Fig. 11, the device comprises one input waveguide, two output waveguides and a 2.8 × 2.8 μm^2 design region. The design region is initialized uniformly or randomly with continuous permittivity. In the first linear parameterization stage, the structure is optimized while allowing the permittivity to vary continuously. In the next step, the design region is converted to boundary parameterization and the device is optimized for operation at only two discrete center wavelengths of 1300 nm and 1550 nm. In the final step, broadband optimization is performed to generate a robust device by specifying the device performance at ten different wavelengths, with five frequencies equally spaced about each center frequencies. In the design process, the authors developed a set of frequency domain solvers for the objective first optimization, where the electric fields were constrained to satisfy the design requirement while the Maxwell's equations were allowed to be violated in the intermediate steps. As the optimization finally converges, the violation of physical equations was eliminated and the device was completely binary with two different materials.

Another contemporary work resorts to a completely different approach to design such ultra-compact integrated photonic devices, namely direct binary search algorithm [46]. As shown in Fig. 12, the device is composed of 20 × 20 square pixels with sides of 120 nm, giving an overall device footprint of only 2.4 × 2.4 μm^2. The binary state of each pixel stands for two different materials. After the design region is initialized, a randomly chosen pixel is first perturbed so as to switch its state in each optimization step, then the figure of merit (FOM) is calculated. The pixel state is retained if the FOM is improved, otherwise it is reversed and the algorithm proceeds to the next pixel. Such inspection is performed for all pixels in a single iteration, which continues until the FOM does not improve further. Clearly, this direct binary search approach does not rely on gradient information to guide the optimization process, but follows a stochastic search routine to find optimal solution in a global scope. However, the drawback is also obvious. Since each evaluation of the FOM requires a full wave simulation, the overall optimization is computationally intensive, which limits the number of optimizable

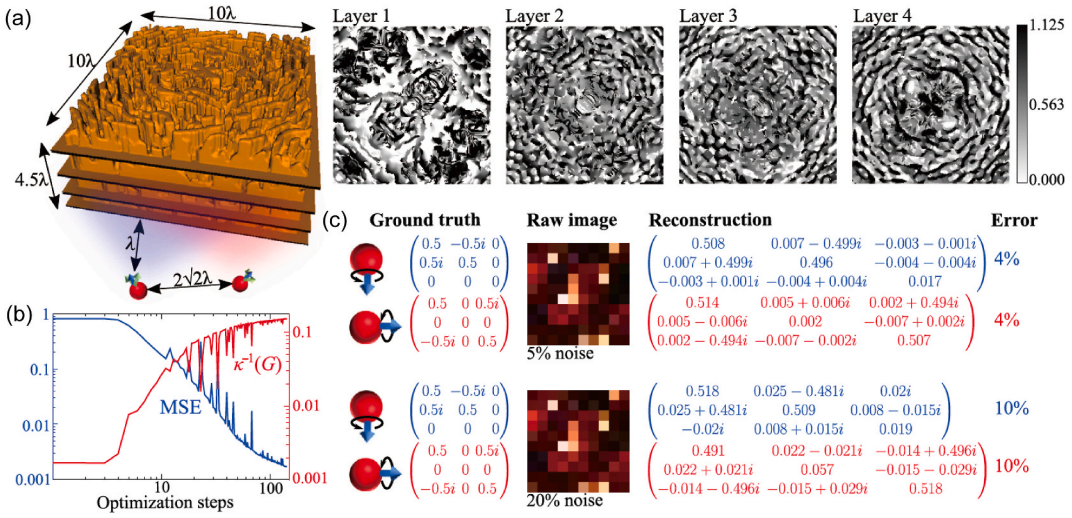

Fig. 10. (a) Topology-optimized nanophotonic probe for extracting the spatial, spectral and polarization information with freeform structures. (b) Mean square error (MSE, blue line) and inverse condition number κ^{-1} (redline) of the PSF kernel. (c) Two dipoles with two different polarization states and emission wavelengths of λ (blue) and 1.1 λ (red) are reconstructed under different noise levels. Reproduced with permission from Ref. [159], copyright 2021 Nanophotonics.

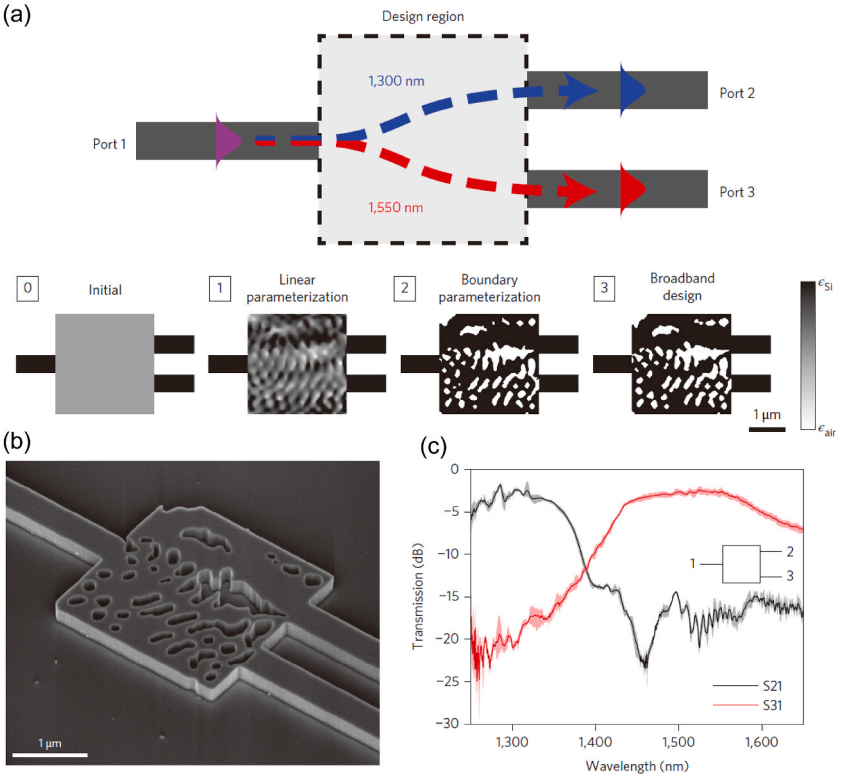

Fig. 11. (a) Design process of a wavelength demultiplexer using adjoint method. (b) Scanning electron micrograph of the fabricated device. (c) Measured transmission spectra of the device. Reproduced with permission from Ref. [41], copyright 2015 Nature Publishing Group.

parameters to 20 × 20 binary numbers in contrast to the physically continuous optimizable parameters restricted by simulation mesh in the adjoint method.

Following these two pioneering works, automatic inverse design algorithms have been vastly applied in integrated photonic devices, such as the grating coupler [163–167], polarization splitter [168], wavelength demultiplexer [169–171], polarization rotator

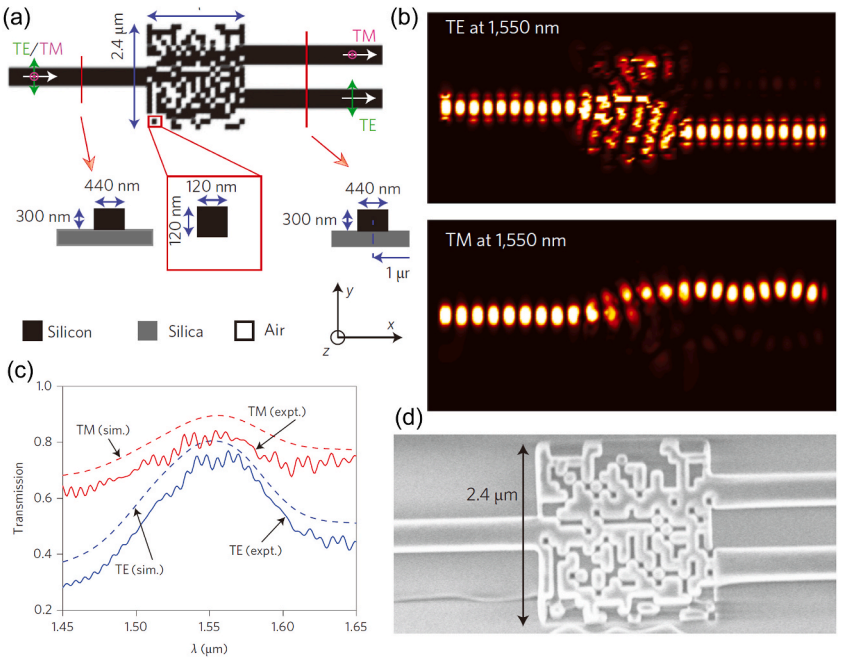

Fig. 12. (a) Structure and parameterization of a polarization splitter using direct binary search algorithm. (b) Simulated field distribution of the polarization splitter. (c) Simulated and measured transmission spectra for TE and TM polarization. (d) Scanning electron micrograph of the fabricated device. Reproduced with permission from Ref. [46], copyright 2015 Nature Publishing Group.

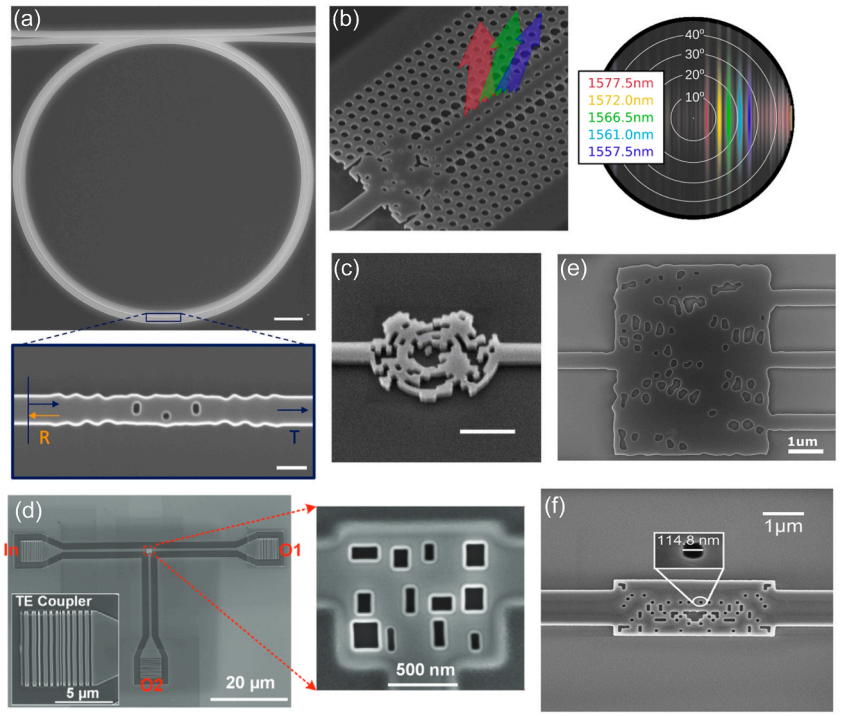

Fig. 13. Design of integrated photonic devices using intelligent algorithms. (a) Micro-resonator. Reproduced with permission from Ref. [181], copyright 2022 American Chemical Society. (b) Beam steering device. Reproduced with permission from Ref. [182], copyright 2021 American Chemical Society. (c) Spin Hall element. Reproduced with permission from Ref. [187], copyright 2020 Optical Society of America. (d) Polarization router. Reproduced with permission from Ref. [168], copyright 2020 Wiley-VCH. (e) Three-channel wavelength demultiplexer. Reproduced with permission from Ref. [171], copyright 2018 American Chemical Society. (f) Mode exchange device. Reproduced with permission from Ref. [178], copyright 2018 American Chemical Society.

[172,173], polarization splitter-rotator [174], mode sorter [175], mode converter [176–179], multimode cavity coupler [180], micro-resonator [181], optical beam steerer [182], multimode waveguide bend [183], and so on. Compared with their conventional counterparts, these inversely designed integrated photonic devices usually have much smaller footprint and comparable performance.

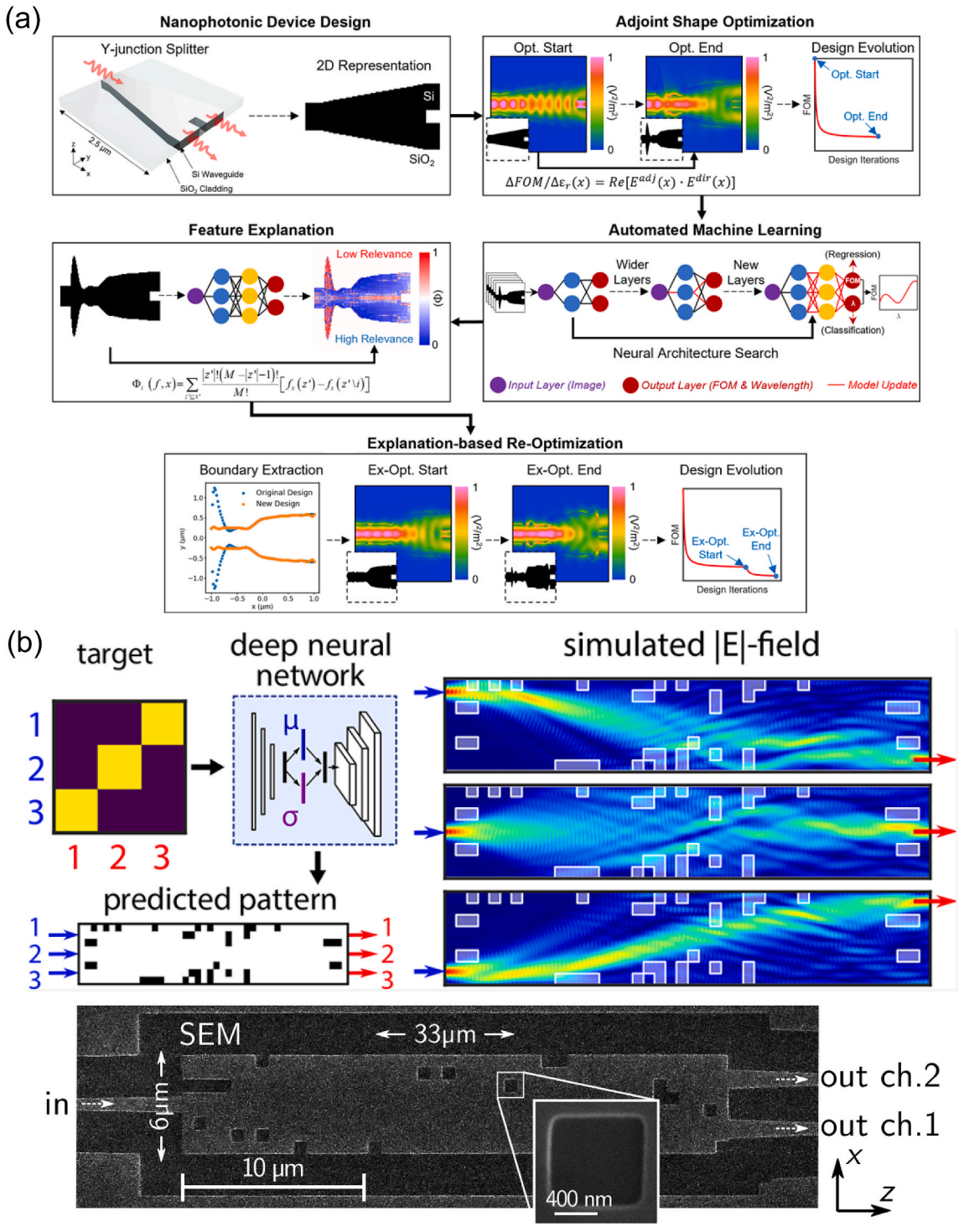

Fig. 14. (a) Design flowchart of a silicon-on-insulator Y-junction splitter for telecom applications using a hybrid model combining adjoint optimization and explainable machine learning. Reproduced with permission from Ref. [191], copyright 2022 American Chemical Society. (b) Deep-learning-aided design of universal integrated photonic devices for complex transmission matrices calculation. Reproduced with permission from Ref. [192], copyright 2021 American Chemical Society.

Moreover, by adjusting the optimization target function, optical logic devices [184], Smith-Purcell radiation devices [185,186], photonic spin Hall element [187], twisted light emitter [188], nonlinear nanophotonic devices [189] and other versatile integrated photonic devices can be constructed. As shown in Fig. 13, the software-defined scheme with flexible inverse design algorithms allows an objective-driven design process to realize extreme functionalities or device configurations on integrated photonic platforms that can be hardly designed by manual labor. Some design algorithms have been integrated and wrapped-up as user-friendly software for less experienced designers to design photonic devices and systems according to their demands [190].

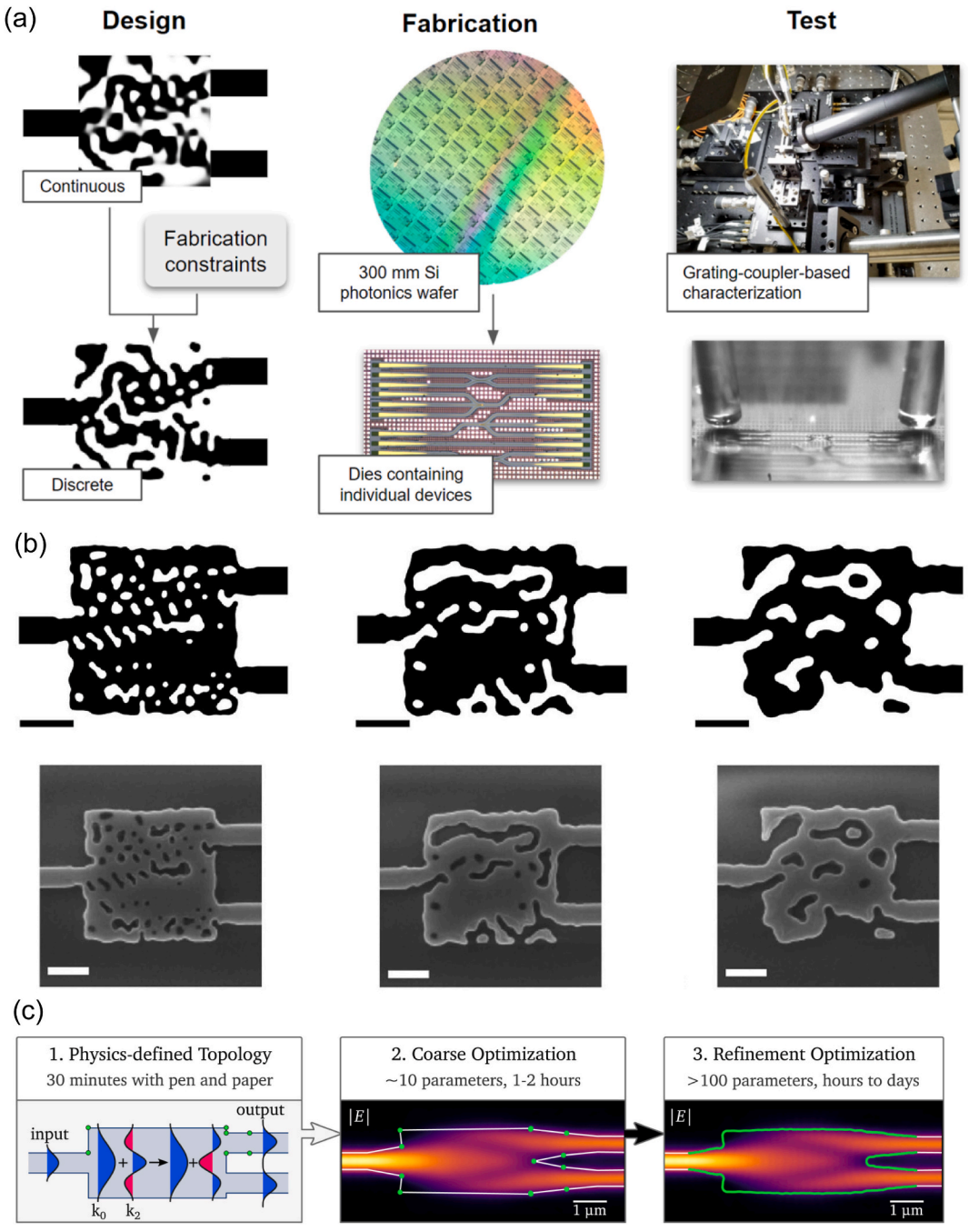

Fig. 15. (a) Workflow of photonics inverse design for commercial silicon photonics foundries. Reproduced with permission from Ref. [193], copyright 2020 American Chemical Society. (b) Design and fabrication results of a wavelength demultiplexer using a minimum feature size constraint of 80, 120 and 160 nm, respectively. Reproduced with permission from Ref. [194], copyright 2019 Nature Publishing Group. (c) A hierarchical shape optimization approach to design a 3 dB coupler. Reproduced with permission from Ref. [195], copyright 2019 IEEE.

4.2. Algorithm-enabled design for versatile functionalities and mass production

Apart from conventional adjoint-method and heuristic algorithms, deep learning and other data-driven models also find their applications in integrated photonic design. The data-driven models, benefitting from large amount of pre-collected training data, can provide very fast evaluation of the design and are often utilized in conjunction with other optimization algorithms. To reveal the relationships between device performance and nanoscale structuring, C. Yeung et al. proposed an inverse design framework by combining adjoint optimization method and machine learning [191]. As shown in Fig. 14(a), they used Shapley Additive explanations (SHAP) on the model to extract the structure−performance relationships as feature heatmaps, making a clear visualization of the structure-dependent device performance and thus helping to overcome local minima.

Another advantage of data-driven models is that the models, once trained, are easily generalized to other similar design tasks with little additional workload. Therefore, a deep learning inverse network has been proposed by N. J. Dinsdale and co-workers to design arbitrary transmission matrices using patterns of weakly scattering perturbations [192]. As shown in Fig. 14 (b), with the design region discretized into binary bins, the researchers train a forward predicting network and an inverse generating network that map bidirectionally between input signals and output signals. The deep learning model allows control over both the intensity and the phase in a multiport device with the footprint reduced by four orders of magnitude compared to conventional technologies, which can achieve arbitrary transmission matrices design.

In order to accommodate mass manufacture techniques in a standard foundry environment for large-scale integrated photonic systems, fabrication constraint must be carefully considered in the design process. Researchers have successfully demonstrated the inverse design in a commercial silicon photonics process as shown in Fig. 15(a) [193]. Fabrication constraints were applied in the discrete optimizations. The designs were fabricated as part of the AIM Photonics 300 mm wafer multi-project wafer (MPW) foundry via water-immersion deep UV photolithography. All devices were fabricated using a single fully etched layer of 220 nm thick silicon, surrounded by silicon dioxide cladding on all sides. These devices have footprints of only several micrometers across, and exhibit comparable performance and reproducibility to prior inversely designed devices fabricated by electron beam lithography.

To introduce fabrication constraint in the automatic design process, a level-set representation of the design region in the discrete optimization phase is often required. A level-set function is a continuous function that defines material where the function is positive, and defines etching where the function is negative, thereby setting the boundary to be the zero-crossing. Level-set representation is very convenient to model complex topology and the evolution of topology like merging and splitting during the optimization process. A common approach to set fabrication constraint is introducing minimum feature size to avoid very small lines or gaps, and minimum curvature radius to avoid very sharp corners. These constraints can be converted analytically to requirements of the level-set function [194,196]. By incorporating the analytical penalty function that limits both the gap size and boundary curvature of a device, the devices are optimized in a fully automated optical design flow using a quasi-Newton optimization method. As shown in Fig. 15(b), the

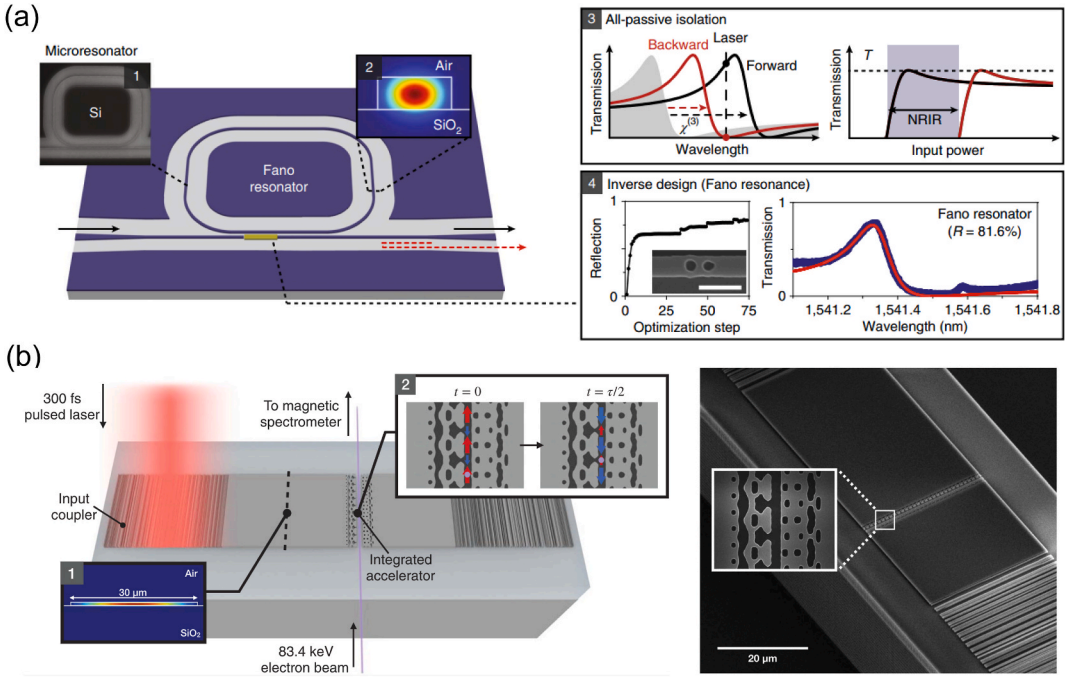

Fig. 16. (a) Inversely designed on-chip non-reciprocal pulse router for optical ranging applications. Reproduced with permission from Ref. [197], copyright 2020 Nature Publishing Group. (b) Inversely designed on-chip integrated laser-driven particle accelerator. Reproduced with permission from Ref. [198], copyright 2020 American Association for the Advancement of Science.

performance of such fabrication-constrained design method is evaluated by designing a series of waveguide demultiplexers with the feature size of 80, 120 and 160 nm, respectively.

Besides level-set representation of highly complex topological structures, another approach is the so-called shape optimization where only the outer boundaries of the device are optimized. This approach requires an empirical structure as the initial design. Fig. 15 (c) demonstrates a design flow using a hierarchical shape optimization algorithm [195]. This approach uses an explicit parameterization of the boundary curves and employs carefully chosen geometrical constraints, aiming to consistently produce robust, high-performance devices that can satisfy practical fabrication constraints of deep UV lithography. The optimized 3 dB coupler achieves better than 0.04 dB excess loss over the O-band. The authors also demonstrated the optimization of a four port 3-dB coupler and a fabrication-tolerant waveguide crossing. These automatic optimization approaches pave the way for high efficiency silicon photonic component libraries.

With the aid of algorithm-driven design, people can realize many versatile integrated photonic systems that can are difficult to implement by traditional methods. For example, an inversely designed nonlinear resonator can be used to achieve all-passive, low-loss, and bias-free non-reciprocal transmission, which relies on a combination of geometrical asymmetry and electromagnetic nonlinearity as shown in Fig. 16(a) [197]. The $\chi^{(3)}$ nonlinearity inside an asymmetric two-port resonator will lead to a different cavity frequency shift for the same input power. Therefore, using a demand-driven design of an asymmetric Fano resonator with complex topological shape, the authors successfully demonstrated an on-chip frequency comb-based optical ranging microsystem. Benefiting from powerful inverse design algorithms, the miniaturization of a dielectric laser accelerators was demonstrated [198]. As illustrated in Fig. 16(b), unlike conventional implementations relying on free-space lasers directly incident on the accelerating structures that limits the scalability and integrability, researchers present an experimental demonstration of a waveguide-integrated dielectric laser accelerators enabled by photonic inverse-design. In the optimization process, the target function is set to the acceleration gradient, which is defined

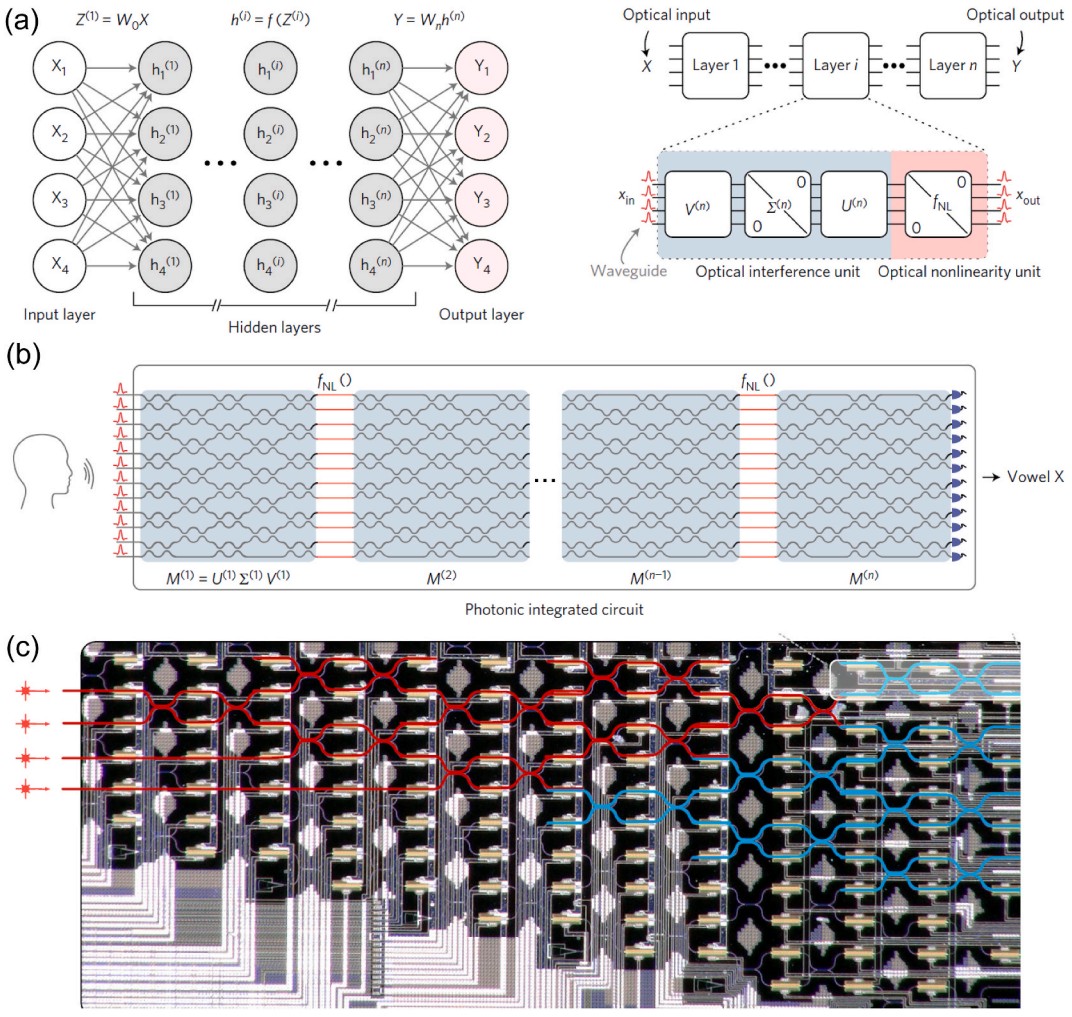

Fig. 17. (a) General architecture of artificial neural network. (b) Schematic of an all-optical neural network. (c) An optical micrograph of the chip used in the experiment that successfully demonstrated both matrix multiplication (red) and attenuation (blue). Reproduced with permission from Ref. [205], copyright 2017 American Association for the Advancement of Science.

by the integration of electric field along the acceleration path. A maximum energy gain of 0.915 kilo–electron volts over 30 μm is inferred based on the comparison between measured electron energy spectra and particle-tracking simulations, It corresponds to an acceleration gradient of 30.5 mega–electron volts per meter. The software-defined design scheme offers powerful tools to realize highly integrated on-chip systems for a variety of applications.

5. Optical neural networks and optical computing

ANNs are computational network models inspired by brain signal processing [8,22,199–204]. Many machine learning and deep learning tasks, including image recognition and high-speed sensing, have substantially benefited from these models. However, since a large portion of modern computing gear is made for von Neumann computing architectures, it is ineffective for using neural networks [205,206]. Significant efforts have been devoted to developing architectures that can be used to implement ANNs with increased computational speed and accuracy. One of the most promising candidates is the optical neural network (ONN) [207–211], which originates from the real number matrix operation to the complex number logical computing, and even results in the neural network in AI chips, reaching a more efficient computing speed and lower energy consumption. Based on the working conditions, we divide this section into two parts: integrated optical computing chips and diffractive neural networks.

5.1. Integrated optical computing chips

As one important work of integrated optical computing chips [212–217], in 2017, Shen et al. proposed a new architecture for a fully ONN as shown in Fig. 17(a), which could offer an enhancement in computational speed and power efficiency over electronic

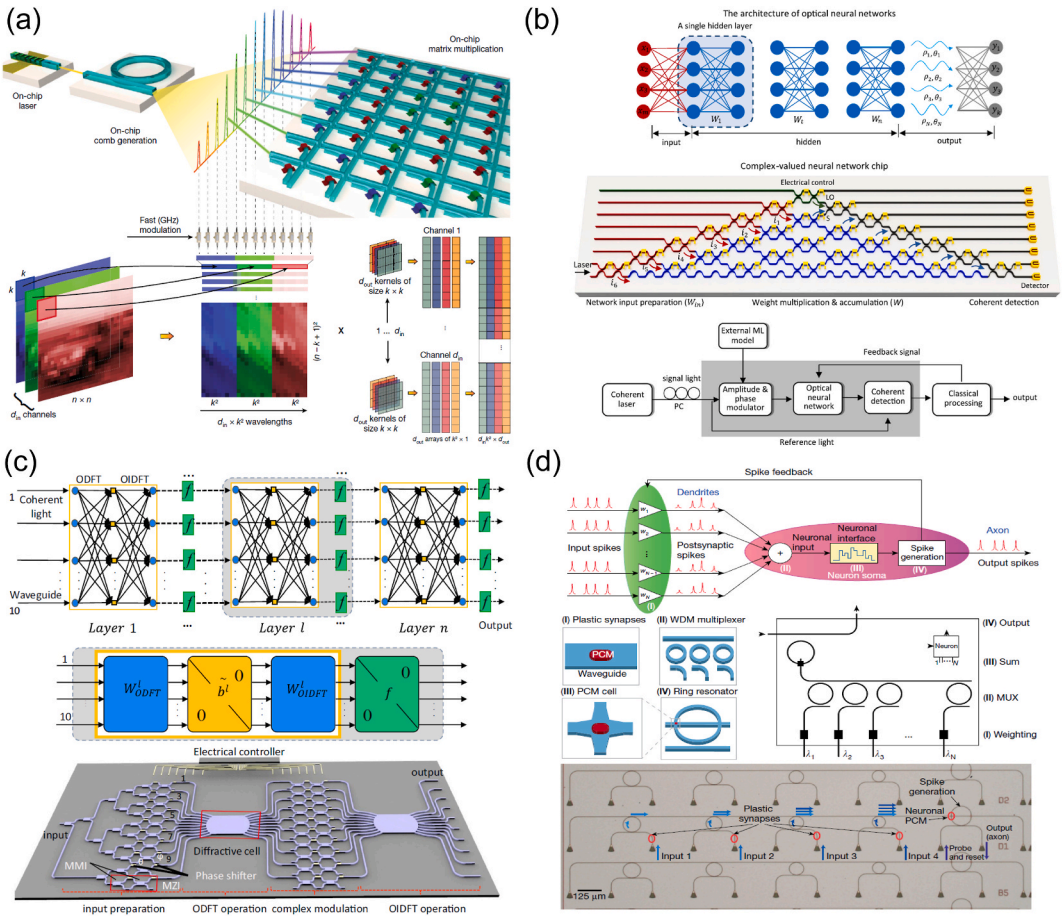

Fig. 18. (a) Schematic of a fully integrated photonic architecture for convolutional operations. Reproduced with permission from Ref. [219], copyright 2019 Nature Publishing Group. (b) Illustration of complex-valued coherent optical neural network. Reproduced with permission from Ref. [220], copyright 2019 Nature Publishing Group. (c) Schematic of the optical integrated diffractive neural networks. Reproduced with permission from Ref. [43], copyright 2019 Nature Publishing Group. (d) Schematic and optical image of the all-optical spiking neuronal circuits, consisting of several pre-synaptic input neurons and one post-synaptic output neuron connected via PCM synapses. Reproduced with permission from Ref. [221], copyright 2019 Nature Publishing Group.

computing chips for conventional inference tasks [205]. The authors demonstrated the concept experimentally using a programmable nanophotonic processor with a cascaded array of 56 programmable Mach-Zehnder interferometers (MZIs) (Fig. 17(b)), and applied it for vowel recognition. The measured correctness of 138/180 cases (76.7%) is compared to the computed correctness of 165/180 (91.7%) using a conventional 64-bit digital computer (Fig. 17(c)). More importantly, an optical computing system operating at 100 GHz has the potential to be over two orders of magnitude faster than electronic neural networks, which are limited to a clock rate in the GHz range. Forward propagation computing is conducted optically on a passive system after all parameters on the nanophotonic processor have been trained and programmed. In this architecture, the average power needed to maintain the phase modulator settings is just about 10 mW per modulator.

The emergence of ultra-high-speed mobile networks (5G and even 6G) has led to an exponential increase in the volume of data being generated globally [26,218]. As a result, highly parallelized, fast, and scalable hardware becomes crucial. J. Feldmann et al. demonstrated a specific integrated photonic hardware accelerator capable of trillions of multiply-accumulate operations per second, as shown in Fig. 18(a) [219]. The tensor core is the optical equivalent of an application-specific IC. It uses phase-change-material memory arrays and photonic chip-based optical frequency combs to achieve parallelized photonic in-memory computing. The computation can operate at a bandwidth exceeding 14 GHz, paving the way for full CMOS wafer-scale integration of the photonic tensor core.

As discussed above, optical computing offers advantages such as low power consumption, high computational speed, and inherent parallelism, far beyond the reach of the electronic counterpart. The neural network algorithms in these works are real-valued, which negates the advantages of complex-valued neural networks even if they are based on light interference. Zhang et al. proposed an optical neural chip (ONC), as shown in Fig. 18(b), which implements truly complex-valued neural networks [220]. The authors evaluated the complex-valued ONC's performance in different scenarios, including species classification of an Iris dataset and handwriting recognition. In terms of learning abilities, the complex-valued ONC performed better than its real-valued equivalent, including high accuracy, quick convergence, and the capacity to create nonlinear decision boundaries.

It should be pointed out that, traditional experimental implementations of ONNs require N^2 units, resulting in limited scalability and high-power consumption. Zhu et al. demonstrated an integrated diffractive optical network (Fig. 18(c)) for implementing parallel application-specific optical computing using two ultracompact diffractive cells and only N MZIs [43]. The footprint and energy use scale linearly with the input data dimension as opposed to the quadratic scaling of the conventional ONN approach. In experiments, recognition on the MNIST and Fashion-MNIST datasets resulted in a 10-fold reduction in footprint and energy use, as well as accuracy on par with earlier MZI-based ONNs.

Traditional computing architecture also has the drawback of physically separated memory and processing, which makes it challenging to produce quick, effective, and low-energy computing. To overcome such constraints, one appealing idea is to create hardware that mimics neurons and synapses. J. Feldmann and co-workers reported an all-optical neurosynaptic system capable of supervised and unsupervised learning, as shown in Fig. 18(d) [221]. They created a scalable circuit architecture for photonic neural networks using

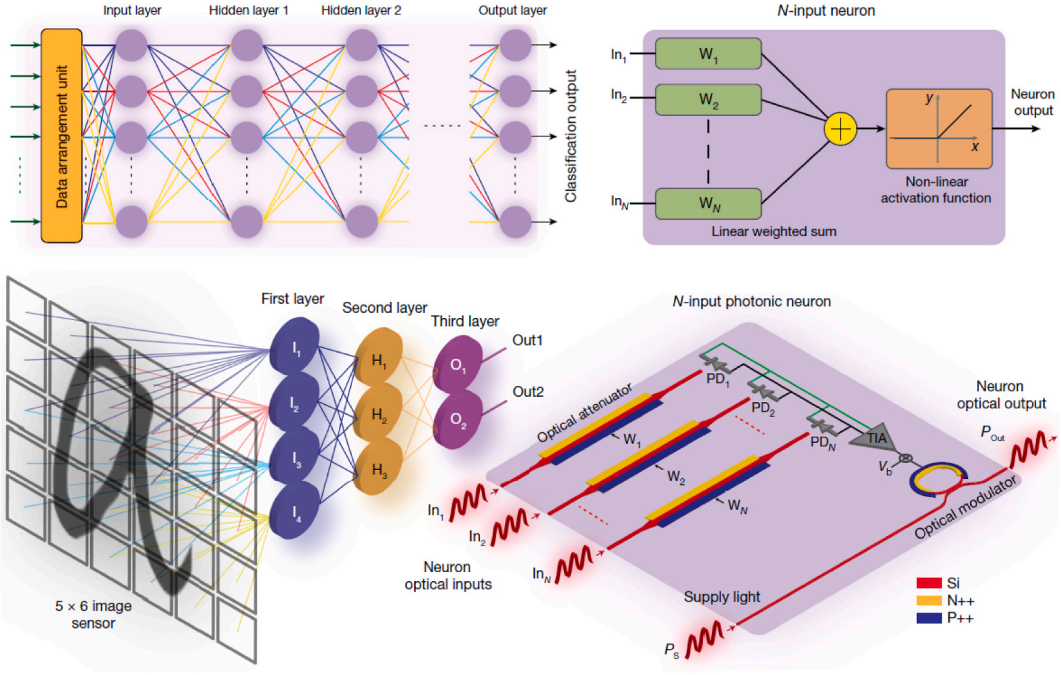

Fig. 19. The Schematic of the neuron network used in the work, in which the linear weighted sum of the inputs is passed through a nonlinear activation function to generate the neuron output. The optical MRM that realizes the ReLU nonlinear activation function is driven by the TIA output, and the neuron optical output is produced by manipulating the supply light. Reproduced with permission from Ref. [222], copyright 2022 Nature Publishing Group.

wavelength division multiplexing techniques, and they successfully showed pattern recognition in the optical domain. This type of photonic neurosynaptic network promises direct access to the high speed and bandwidth present in optical systems, enabling the processing of optical communications and visual data directly.

The lack of scalable on-chip optical nonlinearity restricts the scalability of optical deep networks despite the substantial advancements in photonic computation. In Fig. 19, Ashtiani et al. reported an integrated end-to-end photonic DNN accomplishes sub-nanosecond picture categorization by processing optical waves directly as they pass through layers of neurons and impinge on the on-chip pixel array [222]. A classification time of less than 570 ps, which is comparable to one clock cycle of cutting-edge digital platforms, is achieved by each neuron doing linear computing optically and realizing the nonlinear activation function opto-electronically. The accuracy of the two-class and four-class handwritten letter classifications used by the authors is greater than 93.8% and 89.8%, respectively. Future generations of deep learning systems will be able to use quicker and more energy-efficient neural networks thanks to direct, clock-free processing of optical data, which eliminates the need for analogue-to-digital conversion and a bulky memory module.

5.2. *Diffractive neural networks*

In addition to on-chip neural networks, optical computing can also be realized in free space [223–237]. In 2018, Ozcan's group demonstrated an all-optical diffractive DNN (D^2NN) architecture (Fig. 20) that can implement various computation functions based on the deep learning-based passive diffractive layers [224]. Each point on each metasurface layer transmits the incoming wave, acting as an artificial neuron that is optically diffracted to and connected with other neurons in the subsequent layers. The underlying mechanism is based on the fact that each point on the metasurface acts as a secondary source of a wave, the amplitude and phase of which are defined by the product of the input wave and the complex-valued transmission coefficient at that location, in accordance with the Huygens-Fresnel principle. They developed 3D-printed D^2NNs that perform image classification of handwritten digits and fashion products at terahertz frequencies. The all-optical deep learning framework can perform complex functions that computer-based neural networks can perform at the speed of light. This study has sparked the research and applications in all-optical image analysis using D^2NNs.

Although DNN is particularly appealing due to its inherent parallelism and low energy consumption, they rely heavily on linear optical transformations, and implementing a nonlinear activation function via diffraction is very challenging. Y. Zuo et al. demonstrated a fully functional all-optical neural network (AONN) as shown in Fig. 21(a), in which linear operations were programmed by spatial light modulators and Fourier lenses, and nonlinear optical activation functions were realized in laser-cooled atoms with electromagnetically induced transparency [238]. Because all errors from different optical neurons are independent, such an AONN is scalable. Furthermore, the hardware system can be reconfigured for different applications without requiring any changes to the physical structure. The architecture's capability and feasibility are demonstrated in a machine-learning application that can successfully classify order and disorder phases of a statistical Ising model.

Aside from neural networks, optical logic operations also enable a wide range of applications in optical computing such as ultrahigh speed data processing. However, traditional optical logic gates heavily rely on precise control of input light signals, such as phase difference, polarization, intensity, and incident beam size, resulting in complexity and difficulty during the miniaturization of optical

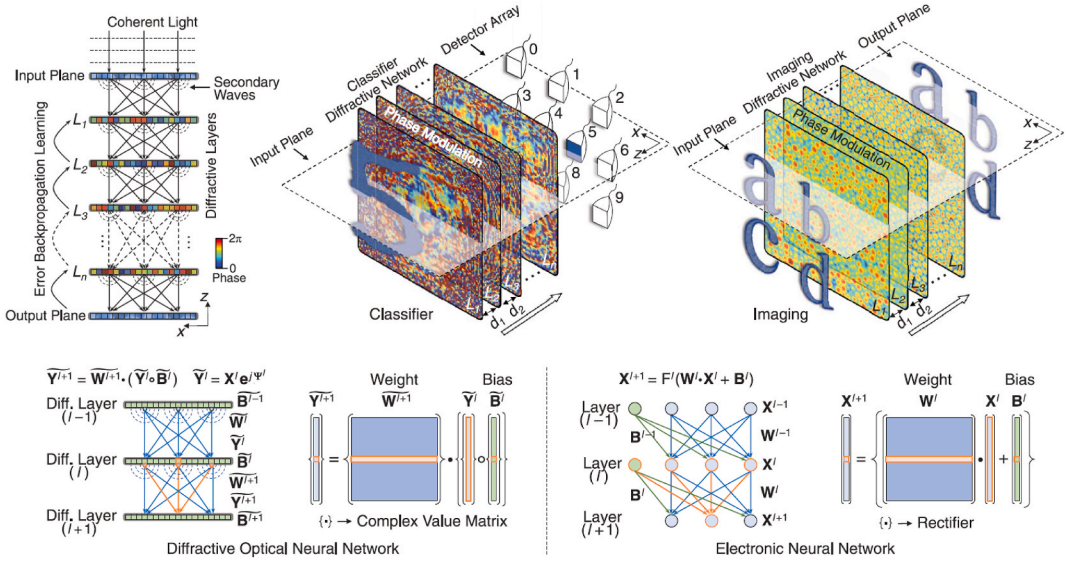

Fig. 20. Diagram of a diffractive deep neural network with many transmissive layers, where each point on a given layer acts as a neuron and exhibits a complex-valued transmission coefficient. Reproduced with permission from Ref. [224], copyright 2018 American Association for the Advancement of Science.

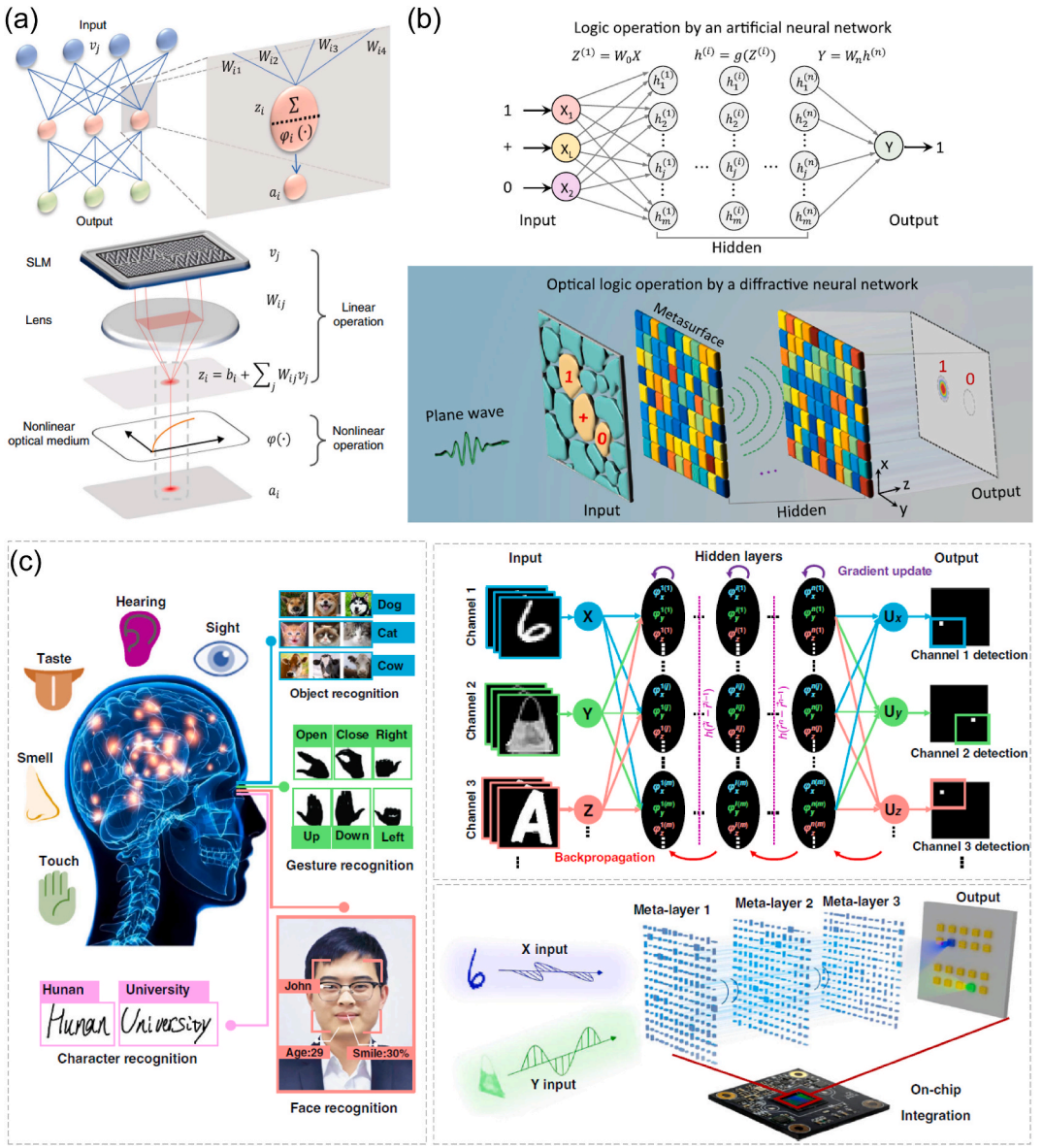

Fig. 21. (a) Schematic of an optical neuron including linear and nonlinear operations. The linear operations are implemented using Fourier lenses and spatial light modulators. The electromagnetically induced transparency is used to realize the nonlinear optical activation functions. Reproduced with permission from Ref. [238], copyright 2019 Optical Society of America. (b) Illustration of optical logic operations by a diffractive neural network. Reproduced with permission from Ref. [239], copyright 2020 Nature Publishing Group. (c) Schematic of multiplexed metasurface-based diffractive neural networks integrated on an imaging sensor chip. Reproduced with permission from Ref. [240], copyright 2022 Nature Publishing Group.

logic gates. As illustrated in Fig. 21(b) and C. Qian et al. proposed a novel design strategy for performing optical logic operations using a diffractive neural network [239]. Physically, the input layer's unique logic operation spatially encodes the incident plane wave, which is subsequently decoded through the hidden layers, namely a compound Huygens' metasurface. In order to convey information about the states of the output circuitry, the well-designed metasurface scatters the encoded light into one of two discrete tiny patches at the output layer. Significantly, the same metasurface can conduct all seven fundamental types of optical logic operations after the diffractive neural network is trained. As a proof-of-principle demonstration, three logic operations—NOT, OR, and AND—have been empirically performed at microwave frequencies.

To further enhance the speed and capacity of optical computing, X. Luo et al. demonstrated in a multiskilled diffractive neural network, as shown in Fig. 21(c), which can perform on-chip multi-channel sensing and multitasking in the visible region [240]. A multi-channel classifier framework for simultaneous recognition of digital and fashionable items is built using the polarization multiplexing scheme of subwavelength nanostructures. The artificial neurons' areal density can reach 6.25×10^6 mm^{-2} multiplied by the

number of channels. An advanced CMOS imaging sensor is integrated with the metasurface to create a chip-scale architecture that directly processes data at physical layers for extremely quick and energy-efficient image processing.

Even though DNNs have advanced significantly, there has been a persistent problem preventing their widespread use: the current processor architectures are not reconfigurable and have low experimental performance and limited model complexity due to restrictions on design flexibility and the buildup of system errors. To overcome these limitations, Zhou and co-workers proposed a programmable diffractive processing unit (Fig. 22), realizing an optoelectronic fused computing system that can support multiple neural networks with millions of neurons [241]. Using the newly devised adaptive training strategy to prevent system mistakes, they were able to achieve good experimental accuracies for high-speed image and video recognition over benchmark datasets as well as computation performance superior to cutting-edge electronic computing platforms. The experimental action accuracy of the work for categorizing the Weizmann and KTH databases even outperforms the electronic computing approaches, which have reported accuracies of 100% and 96.0%, respectively.

Finally, we would like to discuss the potential development for the next-generation optical computing platform. As illustrated in Fig. 23(a), in contrast to the separate design of physical layers (such as the lens or metasurface) and digital layers (such as the neural networks), we believe that it is advantageous to achieve an end-to-end design of imaging and perception systems for specific applications with machine learning models [26,242]. A deep computational camera can be trained offline to improve the performance of a high-level loss function, such as object detection or image classification. The advantage of the encoder-decoder interpretation is that it enables the error of a high-level loss function to be backpropagated all the way down to the physical parameters of the camera and the digital parameters of the neural network. Once it is optimized, the novel optical computing system can classify collected images more reliably, quickly, or efficiently than traditional digital layers.

As a recent effort, Mennel et al. demonstrated that an image sensor can itself constitute an ANN (Fig. 23(b)), capable of simultaneously sensing and processing optical images without latency [243]. The network's synaptic weights were stored in a continuously programmable photoresponsivity matrix, and the device was built on a reconfigurable 2D semiconductor. The sensor was trained to categorize and encode images that were optically projected onto the chip at a rate of 20 million bins per second by the authors. They also demonstrated supervised and unsupervised learning. The extensive amount of data was efficiently processed through the complete signal chain at high frame rates and low power consumption in contrast to conventional machine vision systems.

6. Quantum optics and materials physics

6.1. *Inverse design for aerospace and quantum physics*

The utilization of neural networks is not limited to the applications related to our daily technology, but has been extended to the field of aerospace and quantum physics. In 2022, Kudyshev et al. proposed the inverse design approach for nanocraft, an ultralight spacecraft to travel in outer space with a relativistic velocity of $\sim 6 \times 10^7$ m/s [38]. The nanocraft contains periodically aligned structures that can be accelerated via a high-power laser array located on the earth. To achieve a high acceleration, the design of the

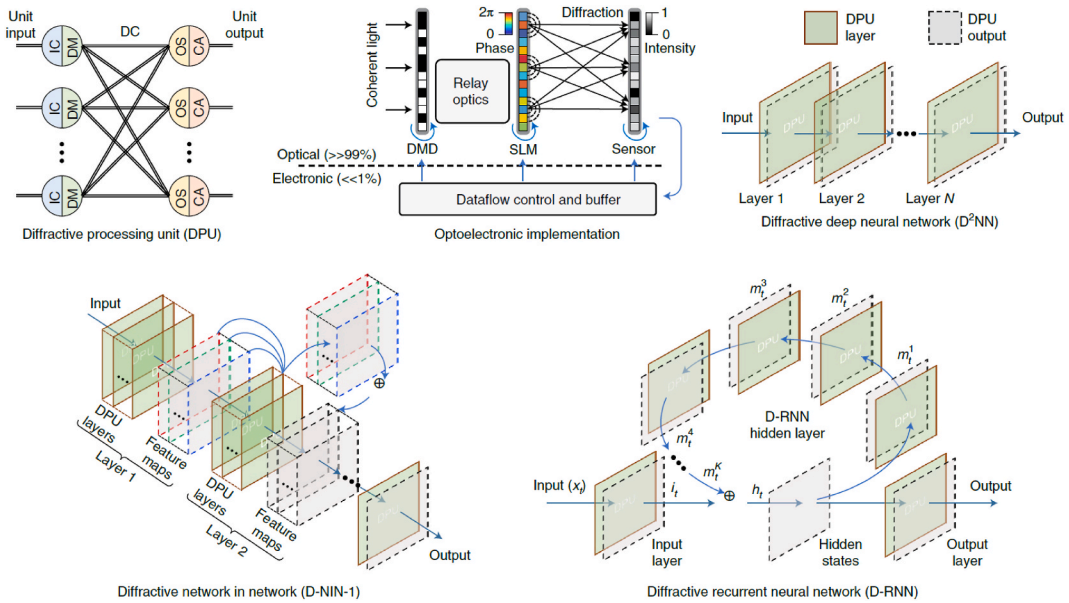

Fig. 22. The reconfigurable diffractive optoelectronic processor can be programmed to construct different DNNs. As an example, three types of neural network architectures were experimentally demonstrated. Reproduced with permission from Ref. [241], copyright 2021 Nature Publishing Group.

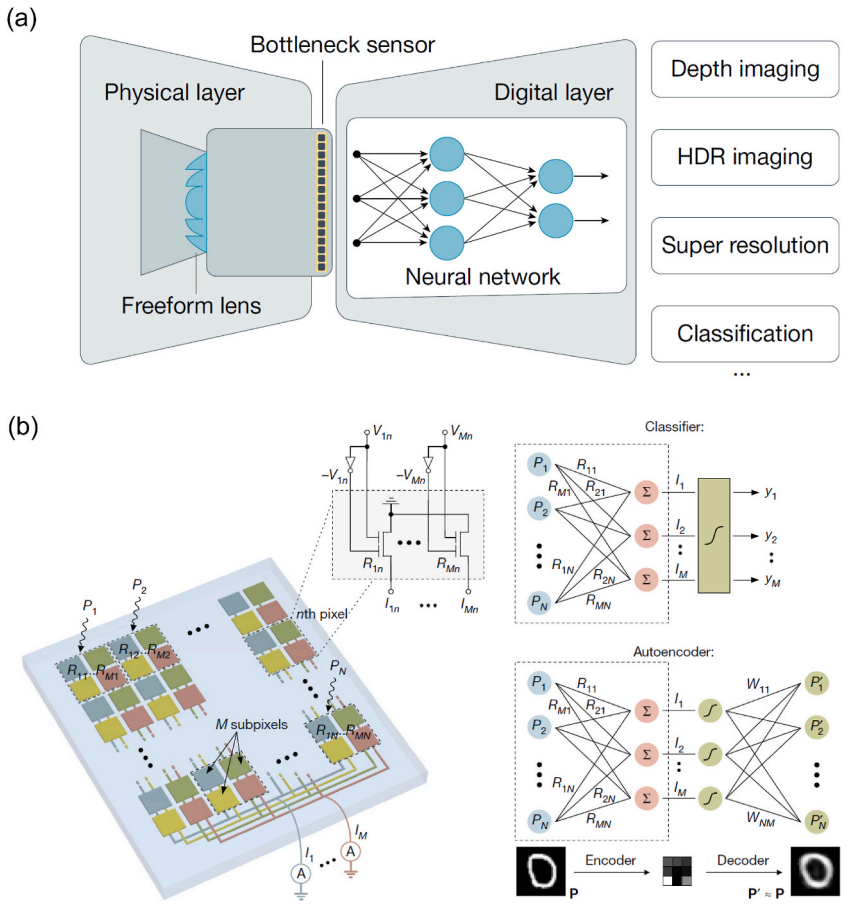

Fig. 23. (a) Illustration of an optical encoder–electronic decoder system. For a particular purpose, freeform lenses and customized sensor electronics can be combined for optimum performance. Reproduced with permission from Ref. [26], copyright 2020 Nature Publishing Group. (b) Illustration of the ANN photodiode array for encoding/decoding of a 28 × 28 pixels letter from the MNIST handwritten digit database. Reproduced with permission from Ref. [243], copyright 2020 Nature Publishing Group.

structures requires a minimized acceleration distance, which is the total distance required by the nanocraft to reach the desired velocity. It involves a tradeoff between the reflectivity of the design and the weight of the nanocraft. The entire optimization process is based on VAE and TO. As illustrated in Fig. 24(a), first, a dataset of initial designs is generated with TO. Then, a VAE is trained to encode the dataset to a 30-dimensional latent space, and decode the designs from a randomly sampled latent variable. After training, the VAE can learn the hidden features of these pre-optimized designs and try to produce more based on random latent variables. These new designs are set as the initial designs for further TO. Finally, the best design is produced which can reduce the acceleration distance by 50% (from 4×10^9 to 1.9×10^9 m).

Quantum physics has also benefited from the use of inverse design techniques. Quantum state analysis involves measuring a quantum system, obtaining readouts, and reconstructing the quantum states using the readouts, either directly or after processing. Each of these steps is crucial in the study of quantum states. In general, this process can be described by $\vec{c} = A(\rho) + \vec{\varepsilon}$, where $\vec{c}$ is expectation values obtained from the measurements specified by sensing function A, ρ is the quantum state (usually described as density matrix), and $\vec{\varepsilon}$ is the noise in the measurement. The quantum forward problem (QFP) is the technique by which we can derive $\vec{c}$ from observations represented by A if we already know the quantum state. The quantum inverse problem (QIP), on the other hand, is the procedure for retrieving the quantum state of the observed data. One specific type of QIP is quantum state tomography (QST), in which the function A directly maps ρ to complete measurements $\vec{c}$. Since the measurements can directly provide us with the expectation values, the QFP is often a rather simple problem to solve. The QIP or QST, however, is not trivial due to the size of the potential quantum state space. The conventional QST methods usually only work with specific kinds of quantum states and may not succeed in other circumstances. To address such an issue, DNNs were used by Cao et al. to develop a solution for QIPs that was motivated by the recent advances in deep learning [246]. First, the training data for the QIP is generated using the QFP, which is based on quantum physics and predicts a fixed set of observables. The dataset consists of pairs of density matrices and their accompanying measurement expectation values. The density matrices are bijectively parameterized to a vector $\vec{a}$ prior to training, and the mapping is selected depending on the set of density matrices. Inverse mapping is learned using a full connected neural network, where a prediction

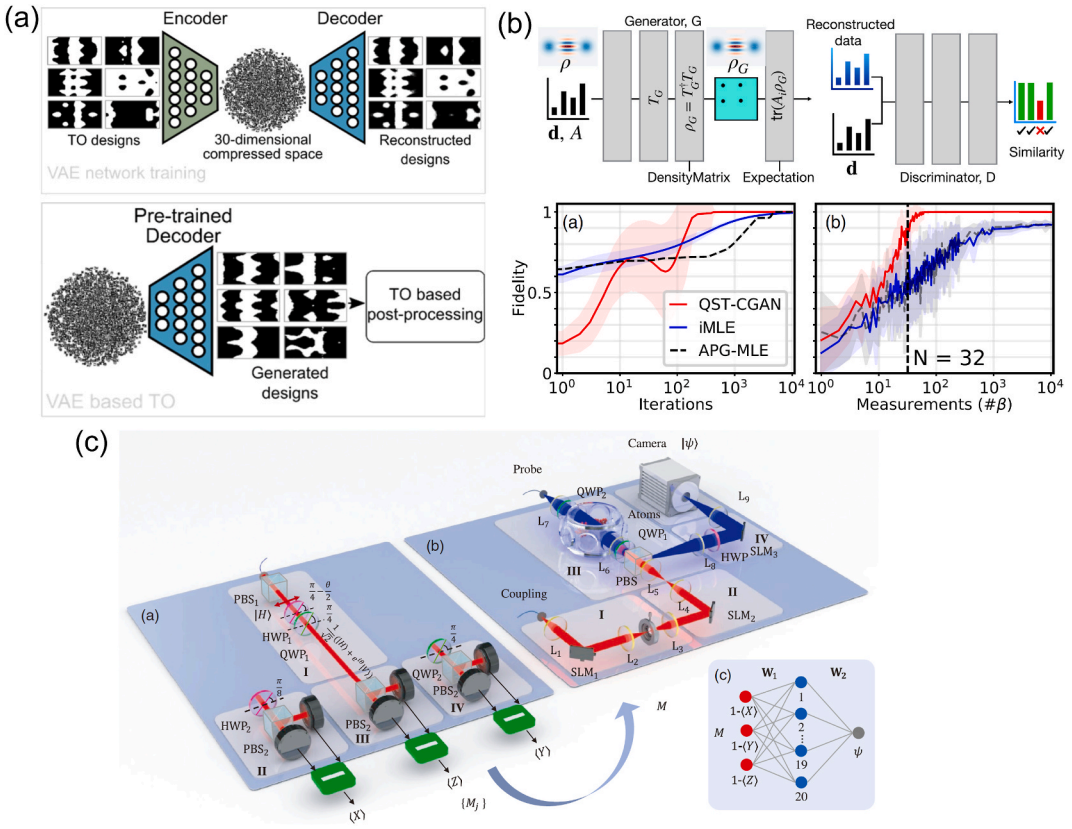

Fig. 24. (a) Top: Training of the VAE on topology-optimized lightsail designs. Bottom: VAE-based topology optimization. Reproduced with permission from Ref. [38], copyright 2021 American Chemical Society. (b) Illustration of the cGAN architecture for QST. Reproduced with permission from Ref. [244], copyright 2021 American Physical Society. (c) Schematic of the implementation of QST with optical neural networks. Reproduced with permission from Ref. [245], copyright 2022 SPIE.

of $\vec{a}$ is obtained from the input $\vec{c}$. The loss function in the training process can be changed depending on the target of QIP. For instance, if the magnitudes of the vector $\vec{a}$ need to be approximated exactly, the loss function can be the mean square error. A loss function that minimizes angle, such as cosine similarity, will be a preferable choice if the mapping focuses more on the direction of $\vec{a}$. The neural networks used by the authors in their studies can both display a fidelity of >97% for the predicted density matrices in two cases with varying input dimensions of $\vec{c}$. Furthermore, the authors have developed a qutrit photonic setup that is capable of creating various qutrit states and measuring arbitrary operators in order to further demonstrate the effectiveness of the well-trained neural network in processing real-world experimental data and its robustness against experimental noise. The average errors of the various operators range from 0.79% to 2.43%, which show extraordinarily good processing efficiency for the experimental data.

In parallel, Ahmed et al. demonstrated QST based on conditional generative adversarial networks (cGANs) [244]. For a given quantum state, the density matrix ρ is unique, which is the property to be reconstructed. As depicted in Fig. 24(b), in each measurement, the authors interact with the quantum state and an outcome d can be obtained. Taking use of these data, the generator in cGAN receives the input of d and A, and generates a guess of the density matrix ρ_G. Then ρ_G is evaluated to generate the measurement statistics $\widehat{d}$. The discriminator in cGAN, on the other hand, tries to distinguish such 'fake' measurement statistics from the true data. After training both networks, the generator can generate an optimal density matrix that can produce almost identical statistics with the ground-truth, which corresponds to an optical reconstruction of the quantum states. The authors benchmarked the cGANs in multiple QST tasks and prove a high fidelity as well as a low amount of measurement required. In parallel, the same group also demonstrated the quantum state classification based on neural networks in the same year [247].

Very recently, Zuo et al. have proposed one remarkable work that perform QST based on an ONN system [245]. In the experiment, the quantum state is defined using the polarization of light. Specifically, a polarization state with a phase shift between horizontal and vertical polarizations is generated, i.e., $|\psi\rangle = \frac{1}{\sqrt{2}}(|H\rangle + e^{i\theta}|V\rangle)$. The schematic of the implementation of the ONN is illustrated in Fig. 24 (c). To determine the state, three measurements are performed to obtain the response data M. The dataset consists of different $\theta \in [0, \pi/2]$ and M are generated and used to train a single-hidden-layer neural network. After optimizing all the weights based on backpropagation, the authors have designed a physics system to realize the identical operation: First, the input (M) is represented by a coupling laser beam generated by a spatial light modulator (SLM_1). Then, another spatial light modulator (SLM_2) diffracts each beam

to 20 diffraction directions with a designed weights based on W_1 in the neural network. The results from three beams in each diffraction order are summed based on a Fourier lens L_4, and 20 spots are focused on the focal plane. The nonlinearity (or activation) arises from the electromagnetically induced transparency in cold atoms: A probe beam comes from the opposite direction whose spatial transmission is nonlinearly dependent on the beam spots intensity. Finally, SLM_3 and Fourier lens L_9 perform the linear matrix operation according to W_2 and summation, and the output is recorded by a camera. Utilizing such a technique, the phase angle and thus the density matrix can be retrieved efficiently.

6.2. Physical neural networks using other platforms

It is worth noting the concept of ONN can be expanded to other wave-physics-based platforms, for instance, the mechanical vibration system, electronic circuit, acoustic system, and magnonic system [225,248,249]. In a more general definition, they can be called physical neural networks (PNNs). PNNs can be applied to mimic neural networks like FCNNs, CNNs, and even RNNs. As one representative work, Hughes et al. studied the analogy between an acoustic system and a RNN [225]. The main feature of a RNN is the introduction of an additional variable, i.e., the hidden state of the system. Each time when the RNN is mapping the input to an output, the state variable needs to be involved in the mapping as well, and at the same time, the state variable is also updated for the next input. In an acoustic system (or other wave-based systems), the field at each location depends on both the external excitation at this moment and the field residual in the systems from previous excitation, making it ideal to mimic a RNN. Similar to other neural networks, RNNs also require a certain amount of nonlinearity to learn complicated mappings. Therefore, the authors used two kinds of materials in the acoustic system. One of the materials shows a constant sound speed, while the other has an additional speed term proportional to the field intensity. Then, by updating the material distribution in such system via gradient-based backpropagation, it can work for different tasks just like neural networks. As an example, the authors demonstrated the classification of different vowels, i.e., ae, ei and iy, as shown in Fig. 25(a). By sending the waveforms of the vowel directly to the system as sound waves, the correct class can be read out from the probe location with the maximum intensity. As a result, an 86.3% classification accuracy is reported on the test dataset.

Papp et al. demonstrated a similar application using spin waves, also known as magnons [248]. Although a few hints have been provided for the realistic implementation of such a nonlinear system, it is still challenging to realize in experiments. This is because nonlinearity usually demands high field intensity, and it is often implemented separately from the linear scatterer in these systems, which hinders the advantage of high interconnections. To adjust the tradeoff between nonlinearity and interconnectivity, the authors proposed the potential superiority of spin-wave-based devices, which is proved to possess both properties [250]. As illustrated in Fig. 25(b), to build a computational system based on spin waves, a punchcard-like pattern of nanomagnets are placed on top of a YIG substrate, which acts as the spin-wave scatterer due to their strong perpendicular magnetic anisotropy. The spin wave is generated by a microwave coplanar waveguide and scattered by the nanomagnets, and the output signals are detected at three locations where the one corresponding to the correct class is expected to show maximum intensity. It is worth noting that the micromagnetic solver used in this work fully accounts for the change in magnetic field due to the magnetization precession, which is the stem of nonlinearity. Therefore, the trained system with optimized nanomagnets distribution can address the nonlinear effect correctly. Based on this platform, the frequency separation and vowel classification (in linear and nonlinear regimes with different excitation strength) have been successfully demonstrated.

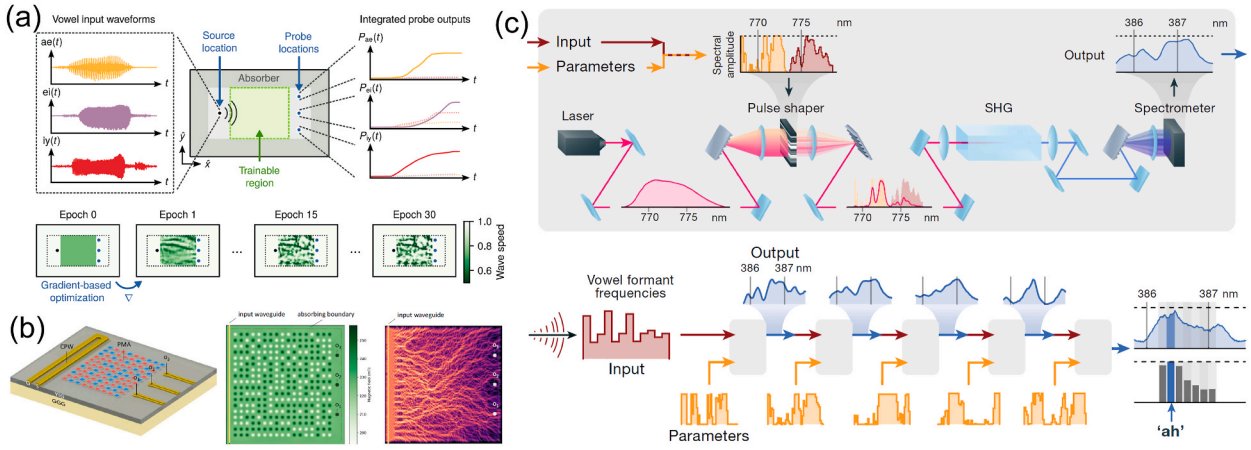

Fig. 25. (a) Schematic of the vowel recognition setup and the training procedure on an acoustic platform. Reproduced with permission from Ref. [225], copyright 2019 American Association for the Advancement of Science. (b) Nanomagnet-based spin-wave scatterer. Reproduced with permission from Ref. [248], copyright 2021 Nature Publishing Group (c) Top: A laser pulse's spectrum contains input data that have been encoded. A portion of the pulse's spectrum is used as trainable parameters (orange) to regulate the changes conducted by the broadband SHG process. The spectrum of a blue pulse produced in a nonlinear medium yields the physical computation result. Bottom: The outputs of the SHG transformations are fed into other SHG transformations with independent trainable parameters to construct a deep PNN. Reproduced with permission from Ref. [249], copyright 2022 Nature Publishing Group.

A similar design platform using magnons can also be optimized with direct binary search algorithm [251,252], a traditional optimization method, as demonstrated by Wang and co-workers [252]. In this work, the air-YIG material distribution is designed to scatter the spin wave to a desired direction under an external magnetic field. During the optimization, the material at a random grid (100 nm × 100 nm region) is switched and the objective function is evaluated via micromagnetic simulation. If the objective function is improved, the switching takes effect. The iteration ends when the switching at any location reduces the objective function for the current configuration. Based on this optimizer, the functionalities like magnonic (de)multiplexer, nonlinear magnonic switch and nonreciprocal magnonic circulator are demonstrated.

In the previous examples of ONNs and PNNs, the neural network parameters are often corresponding to the material or structure distributions in the system. However, this is not the only approach to building a PNN. In 2022, Wright et al. utilizing an alternative way to train all kinds of PNNs [249]. In this work, the parameters of the neural networks are also represented by an external signal, just as the input signal. To be more specific, in the example of a vowel classification problem, the input is represented by a pulse that covers a certain wavelength range, while the trainable parameters are also input as a pulse but at distinct wavelength range. The interaction between the input and the parameters can be achieved by nonlinear effects like frequency mixing. Finally, the true class can be read out by looking at the wavelength range with maximum intensity. The entire process is plotted in Fig. 25(c). Such a technique can be utilized to build a deep PNN where different parameters are input at different stages, corresponding to the weight in different layers in a neural network. The superiority of such parameters conversion is clear: On one hand, only the external signal needs to be modified, while the system itself is fixed and does not need any modification (even when the task changes). This is not achievable in systems where the weights are represented by the material distribution. On the other hand, the parameters can be directly updated based on the response in the experimental system to achieve a better classification performance. Three PNN systems, including mechanical, electrical and optical systems, are experimentally demonstrated in this paper to show more than 90% classification accuracy for handwritten digits classification problem.

7. Summary and perspectives

In this review, we have examined the concept of the software-defined platform that has recently been developed. This platform is useful for consolidating and advancing interdisciplinary research by interfacing nanophotonics with intelligent algorithms, particularly machine learning algorithms, in device design, measurement, and system setup. In general, the software-defined nanophotonic platform offers the following benefits.

1. Manageability: The software-defined framework has distinct levels that are very easy to manage. On the one hand, the functionality and knowledge requirements of each layer are segregated and isolated. More specifically, the knowledge of full-wave simulations or experimental measurements is only necessary for the data layer for data generation, while understanding the inverse design algorithm is necessary for the control layer, as skills in machine learning and multi-objective optimization. Interestingly, the application layer, which is the most significant layer directly related to the design task, calls for the least amount of expertise. The only thing left to undertake is to determine the design objective and have the ability to obtain the design from the interface that connects to the control layer. On the other hand, it is effective to make use of the complete expertise of the engineers who work for a single layer with such a compartmentalized structure of capabilities and knowledge base. This includes tweaks and error fixes for each layer, enabling a high degree of manageability across the entire software-based architecture.
2. Flexibility: The three layers in the software-defined framework can be adaptably changed without affecting the other two layers. First, the application layer can be switched while using the existing dataset and a fixed inverse design technique, allowing the user to continue inversely designing distinct devices like metalens, meta-holograms, beam deflectors, etc. Second, when the dataset and application are both fixed, the control layer can be altered to support the use of several algorithms, each with benefits and drawbacks. Lastly, the data layer can be improved/replaced later to make the models better/more general. On the one hand, the algorithm, particularly the machine learning models, can be retrained as more data are generated to achieve better performance; this is referred to as active learning notation. On the other hand, we can swap out the present dataset for an alternative but analogous dataset (e.g., meta-atoms with different periods, materials, and geometries). In this case, the overall framework does not need significant changes; only the control layer may require a minor adjustment to accommodate the new data structure.
3. Extensibility: Inverse design tasks are widespread in science and technology fields. However, the expertise and design approach in a particular field are typically unique and task-specific. It is challenging, if not impossible, to transfer the methodology and knowledge from one field to another. The software-defined framework is a general idea that can be used to solve practical problems in a variety of fields. This methodology offers a wide range of possibilities for extending its application to various fields. For instance, regardless of their physical significance, machine learning and deep learning algorithms connect input and output data structures. In other words, if the interfaces to the software and hardware sides are consistent in different tasks and domains (for instance, the inputs are all binary images or parameters, and the outputs are class labels or continuous values), the same models may be applied directly and easily to various tasks.

All of these benefits outweigh the drawbacks of traditional approaches. While the software-defined platform holds great promise, it is still in its nascent stages, and requires further development in several areas, including applications, interfaces, and integrations. To unleash the full potential of the software-defined platform, it is important to enhance and advance these areas considering the following aspects.

1. It is crucial to create a high-level architecture for the software-defined framework. This should cover the relationships between the three levels and the framework's general structure. Based on results from testing and actual usage, we must develop and improve programming languages, data libraries, and user-friendly interfaces. This effort could entail introducing fresh features, enhancing current ones, and resolving any detected flaws or problems.
2. We need to realize dynamic control of every layer and even every pixel within the framework that produces an optoelectronic computing network with the ability for self-learning and self-correction. The success of this task can offer significantly improved computing performance and thereby accelerate the development of optical AI processors as a vital part of contemporary computing. However, it is equally important to enable intelligent model selection so that the best model may always be chosen for the specific issue and target specified by the user, considering the applicability, capability, and generality of the model. Such a dynamic system is applicable in many fields, including microscopic imaging and free-space optical communication.
3. It is highly beneficial to implement the transfer of knowledge or techniques between tasks in various domains. We can, for example, create a database of nanophotonic designs and devices that go beyond empirical structures. The software-defined system enables the sharing of knowledge among tasks in several domains. With the shared data layer, design process experience will grow across experts. A set of standard devices will develop as the database keeps expanding and may eventually be directly invoked upon request. Moreover, well-organized device data can be analyzed using data mining and machine learning techniques to reveal valuable design insights that cannot be obtained through any other means. The primary objective is to establish a standardized data structure that simplifies the creation of inverse design models in subsequent stages. Devices with unconventional architectures, flexible capabilities, and extreme performance are anticipated to be developed with the use of data-driven models and a large number of empirical designs.
4. We need to unify the software and hardware optimization as much as possible. The virtualization of the hardware frontend, which enables the automatic design of photonic devices and automatic results processing directly driven by the need of end users, is the core of a software-defined nanophotonic system. A key step of this process is enhancing and merging the control layer interfaces to establish a seamless connection between the software and hardware sides. These interfaces should be adaptable, simple to use, and reliable. Therefore, the future promotion of such a methodology should concentrate on how well the three basic layers interact with one another. To enable a fully end-to-end architecture, demand with a higher abstract level should be supported for the application layer. For instance, a user-end need, such as the accuracy of detection, might be sent directly to the software-defined scheme in the construction of a nanophotonic object detection system with the use of spectral and polarization information. The control layer offers methods to identify relevant optical information to extract and automatically find potential hardware solutions rather than requiring users to manually find appropriate spectrum bands and polarization states. It is possible to tune the entire system, including the frontend nanophotonic hardware and the backend processing algorithms simultaneously and systematically.

To conclude, the photonics community should collaborate to build a comprehensive dataset of photonic concepts, architectures, components, materials and measurements to support all types of inverse design algorithms that could create devices with the highest possible efficiency, in order to explore and advance new possibilities in this software-defined inverse design platform. The development of all-optical and optoelectronic systems that can execute machine learning and other computing algorithms at the speed of light is crucial for ushering in a new era of even more sophisticated and successful inverse design algorithms. We think the discipline will rapidly grows as more researchers with diverse backgrounds participate in this endeavor.

Declaration of competing interest

The authors declare that they have no known competing financial interests or personal relationships that could have appeared to influence the work reported in this paper.

Acknowledgment

Y.L. acknowledges the financial support of the National Science Foundation, United States (ECCS-1916839, CBET-1931777, and DMR-2202268).

References

[1] L. Novotny, B. Hecht, Principles of Nano-Optics, Cambridge university press, 2012.
[2] S.-y. Lin, J. Fleming, D. Hetherington, B. Smith, R. Biswas, K. Ho, M. Sigalas, W. Zubrzycki, S. Kurtz, J. Bur, A three-dimensional photonic crystal operating at infrared wavelengths, Nature 394 (6690) (1998) 251–253.
[3] W.L. Barnes, A. Dereux, T.W. Ebbesen, Surface plasmon subwavelength optics, Nature 424 (6950) (2003) 824–830.
[4] N. Yu, F. Capasso, Flat optics with designer metasurfaces, Nat. Mater. 13 (2) (2014) 139–150.
[5] A.V. Kildishev, A. Boltasseva, V.M. Shalaev, Planar photonics with metasurfaces, Science 339 (6125) (2013), 1232009.
[6] V.R. Almeida, C.A. Barrios, R.R. Panepucci, M. Lipson, All-optical control of light on a silicon chip, Nature 431 (7012) (2004) 1081–1084.
[7] G.T. Reed, G. Mashanovich, F.Y. Gardes, D. Thomson, Silicon optical modulators, Nat. Photonics 4 (8) (2010) 518–526.
[8] B.J. Shastri, A.N. Tait, T. Ferreira de Lima, W.H. Pernice, H. Bhaskaran, C.D. Wright, P.R. Prucnal, Photonics for artificial intelligence and neuromorphic computing, Nat. Photonics 15 (2) (2021) 102–114.
[9] S. Wang, P.C. Wu, V.C. Su, Y.C. Lai, M.K. Chen, H.Y. Kuo, B.H. Chen, Y.H. Chen, T.T. Huang, J.H. Wang, R.M. Lin, C.H. Kuan, T. Li, Z. Wang, S. Zhu, D.P. Tsai, A broadband achromatic metalens in the visible, Nat. Nanotechnol. 13 (3) (2018) 227–232.
[10] D. Pérez, I. Gasulla, L. Crudgington, D.J. Thomson, A.Z. Khokhar, K. Li, W. Cao, G.Z. Mashanovich, J. Capmany, Multipurpose silicon photonics signal processor core, Nat. Commun. 8 (1) (2017) 1–9.

[11] H. Altug, S.-H. Oh, S.A. Maier, J. Homola, Advances and applications of nanophotonic biosensors, Nat. Nanotechnol. 17 (1) (2022) 5–16.
[12] J. Wang, F. Sciarrino, A. Laing, M.G. Thompson, Integrated photonic quantum technologies, Nat. Photonics 14 (5) (2020) 273–284.
[13] T.-J. Yen, W. Padilla, N. Fang, D. Vier, D. Smith, J. Pendry, D. Basov, X. Zhang, Terahertz magnetic response from artificial materials, Science 303 (5663) (2004) 1494–1496.
[14] X. Liu, T. Tyler, T. Starr, A.F. Starr, N.M. Jokerst, W.J. Padilla, Taming the blackbody with infrared metamaterials as selective thermal emitters, Phys. Rev. Lett. 107 (4) (2011), 045901.
[15] D. Kreutz, F.M. Ramos, P.E. Verissimo, C.E. Rothenberg, S. Azodolmolky, S. Uhlig, Software-defined networking: a comprehensive survey, Proc. IEEE 103 (1) (2014) 14–76.
[16] H. Farhady, H. Lee, A. Nakao, Software-defined networking: a survey, Comput. Network. 81 (2015) 79–95.
[17] L. Deng, Y. Xu, Y. Liu, Hybrid inverse design of photonic structures by combining optimization methods with neural networks, Photon. Nanostruct: Fundam. Appl. 52 (2022), 101073.
[18] S.D. Campbell, D. Sell, R.P. Jenkins, E.B. Whiting, J.A. Fan, D.H. Werner, Review of numerical optimization techniques for meta-device design, Opt. Mater. Express 9 (4) (2019) 1842–1863.
[19] W. Ma, Z. Liu, Z.A. Kudyshev, A. Boltasseva, W. Cai, Y. Liu, Deep learning for the design of photonic structures, Nat. Photonics 15 (2) (2021) 77–90.
[20] J. Chen, S. Hu, S. Zhu, T. Li, Metamaterials: from fundamental physics to intelligent design, Interdisciplinary Mater. (2022).
[21] M.K. Chen, X. Liu, Y. Sun, D.P. Tsai, Artificial intelligence in meta-optics, Chem. Rev. (2022).
[22] J. Jiang, M. Chen, J.A. Fan, Deep neural networks for the evaluation and design of photonic devices, Nat. Rev. Mater. 6 (8) (2021) 679–700.
[23] O. Khatib, S. Ren, J. Malof, W.J. Padilla, Deep learning the electromagnetic properties of metamaterials—a comprehensive review, Adv. Funct. Mater. 31 (31) (2021), 2101748.
[24] J. Park, S. Kim, D.W. Nam, H. Chung, C.Y. Park, M.S. Jang, Free-form optimization of nanophotonic devices: from classical methods to deep learning, Nanophotonics (2022).
[25] N. Wang, W. Yan, Y. Qu, S. Ma, S.Z. Li, M. Qiu, Intelligent designs in nanophotonics: from optimization towards inverse creation, PhotoniX 2 (1) (2021) 1–35.
[26] G. Wetzstein, A. Ozcan, S. Gigan, S. Fan, D. Englund, M. Soljačić, C. Denz, D.A. Miller, D. Psaltis, Inference in artificial intelligence with deep optics and photonics, Nature 588 (7836) (2020) 39–47.
[27] P.R. Wiecha, A. Arbouet, C. Girard, O.L. Muskens, Deep learning in nano-photonics: inverse design and beyond, Photon. Res. 9 (5) (2021) B182–B200.
[28] K. Yao, R. Unni, Y. Zheng, Intelligent nanophotonics: merging photonics and artificial intelligence at the nanoscale, Nanophotonics 8 (3) (2019) 339–366.
[29] C. Zuo, J. Qian, S. Feng, W. Yin, Y. Li, P. Fan, J. Han, K. Qian, Q. Chen, Deep learning in optical metrology: a review, Light Sci. Appl. 11 (1) (2022) 1–54.
[30] S. So, T. Badloe, J. Noh, J. Bravo-Abad, J. Rho, Deep learning enabled inverse design in nanophotonics, Nanophotonics 9 (5) (2020) 1041–1057.
[31] Z. Liu, D. Zhu, L. Raju, W. Cai, Tackling photonic inverse design with machine learning, Adv. Sci. 8 (5) (2021), 2002923.
[32] J. Valentine, S. Zhang, T. Zentgraf, E. Ulin-Avila, D.A. Genov, G. Bartal, X. Zhang, Three-dimensional optical metamaterial with a negative refractive index, Nature 455 (7211) (2008) 376–379.
[33] P.G. Nanfang Yu, Mikhail A. Kats, Francesco Aieta, Jean-Philippe Tetienne, Federico Capasso, Zeno Gaburro, Light propagation with phase discontinuities generalized laws of reflection and refraction, Science 334 (6054) (2011) 333–337.
[34] J. Fleming, S. Lin, I. El-Kady, R. Biswas, K. Ho, All-metallic three-dimensional photonic crystals with a large infrared bandgap, Nature 417 (6884) (2002) 52–55.
[35] S.J. Tan, M.J. Campolongo, D. Luo, W. Cheng, Building plasmonic nanostructures with DNA, Nat. Nanotechnol. 6 (5) (2011) 268–276.
[36] W. Ma, Y. Xu, B. Xiong, L. Deng, R.W. Peng, M. Wang, Y. Liu, Pushing the limits of functionality-multiplexing capability in metasurface design based on statistical machine learning, Adv. Mater. 34 (16) (2022), e2110022.
[37] J. Zhang, C. Qian, Z. Fan, J. Chen, E. Li, J. Jin, H. Chen, Heterogeneous transfer-learning-enabled diverse metasurface design, Adv. Opt. Mater. 10 (17) (2022), 2200748.
[38] Z.A. Kudyshev, A.V. Kildishev, V.M. Shalaev, A. Boltasseva, Optimizing Startshot lightsail design: a generative network-based approach, ACS Photonics 9 (1) (2021) 190–196.
[39] S. Van der Jeught, J.J. Dirckx, Deep neural networks for single shot structured light profilometry, Opt Express 27 (12) (2019) 17091–17101.
[40] E. Arbabi, S.M. Kamali, A. Arbabi, A. Faraon, Full-Stokes imaging polarimetry using dielectric metasurfaces, ACS Photonics 5 (8) (2018) 3132–3140.
[41] A.Y. Piggott, J. Lu, K.G. Lagoudakis, J. Petykiewicz, T.M. Babinec, J. Vučković, Inverse design and demonstration of a compact and broadband on-chip wavelength demultiplexer, Nat. Photonics 9 (6) (2015) 374–377.
[42] B. Xiong, Y. Liu, Y. Xu, L. Deng, C.-W. Chen, J.-N. Wang, R. Peng, Y. Lai, Y. Liu, M. Wang, Breaking the limitation of polarization multiplexing in optical metasurfaces with engineered noise, Science 379 (6629) (2023) 294–299.
[43] H. Zhu, J. Zou, H. Zhang, Y. Shi, S. Luo, N. Wang, H. Cai, L. Wan, B. Wang, X. Jiang, Space-efficient optical computing with an integrated chip diffractive neural network, Nat. Commun. 13 (1) (2022) 1–9.
[44] S. Molesky, Z. Lin, A.Y. Piggott, W. Jin, J. Vucković, A.W. Rodriguez, Inverse design in nanophotonics, Nat. Photonics 12 (11) (2018) 659–670.
[45] C.M. Lalau-Keraly, S. Bhargava, O.D. Miller, E. Yablonovitch, Adjoint shape optimization applied to electromagnetic design, Opt Express 21 (18) (2013) 21693–21701.
[46] B. Shen, P. Wang, R. Polson, R. Menon, An integrated-nanophotonics polarization beamsplitter with 2.4× 2.4 μm 2 footprint, Nat. Photonics 9 (6) (2015) 378–382.
[47] C. Liu, S.A. Maier, G. Li, Genetic-algorithm-aided meta-atom multiplication for improved absorption and coloration in nanophotonics, ACS Photonics 7 (7) (2020) 1716–1722.
[48] N. Bonod, S. Bidault, G.W. Burr, M. Mivelle, Evolutionary optimization of all-dielectric magnetic nanoantennas, Adv. Opt. Mater. 7 (10) (2019), 1900121.
[49] C. Forestiere, M. Donelli, G.F. Walsh, E. Zeni, G. Miano, L. Dal Negro, Particle-swarm optimization of broadband nanoplasmonic arrays, Opt Lett. 35 (2) (2010) 133–135.
[50] P.R. Wiecha, A. Lecestre, N. Mallet, G. Larrieu, Pushing the limits of optical information storage using deep learning, Nat. Nanotechnol. 14 (3) (2019) 237–244.
[51] K. Kulkarni, P. Turaga, Reconstruction-free action inference from compressive imagers, IEEE Trans. Pattern Anal. Mach. Intell. 38 (4) (2015) 772–784.
[52] D. Rodrigo, A. Tittl, N. Ait-Bouziad, A. John-Herpin, O. Limaj, C. Kelly, D. Yoo, N.J. Wittenberg, S.-H. Oh, H.A. Lashuel, Resolving molecule-specific information in dynamic lipid membrane processes with multi-resonant infrared metasurfaces, Nat. Commun. 9 (1) (2018) 1–9.
[53] S. Colburn, A. Zhan, A. Majumdar, Metasurface optics for full-color computational imaging, Sci. Adv. 4 (2) (2018) eaar2114.
[54] V.G. Veselago, The Electrodynamics of Substances with Simultaneously Negative Values of and μ.Pdf, 1968.
[55] J. Pendry, Extremely Low Frequency Plasmons in Metallic Microstructures, 1996.
[56] C.M. Soukoulis, M. Wegener, Past achievements and future challenges in the development of three-dimensional photonic metamaterials, Nat. Photonics (2011).
[57] D.R. Smith, B.P. J, 2M.C.K. Wiltshire3, Metamaterials and Negative Refractive Index, 2004.
[58] Y. Liu, X. Zhang, Metamaterials: a new frontier of science and technology, Chem. Soc. Rev. 40 (5) (2011) 2494–2507.
[59] M. Kim, K. Yao, G. Yoon, I. Kim, Y. Liu, J. Rho, A broadband optical diode for linearly polarized light using symmetry-breaking metamaterials, Adv. Opt. Mater. 5 (19) (2017), 1700600.
[60] D. Lin, P. Fan, E. Hasman, M.L. Brongersma, Dielectric gradient metasurface optical elements, Science 345 (6194) (2014) 298–302.
[61] N. Yu, F. Capasso, Flat optics with designer metasurfaces, Nat. Mater. 13 (2) (2014) 139–150.
[62] A.A. High, R.C. Devlin, A. Dibos, M. Polking, D.S. Wild, J. Perczel, N.P. de Leon, M.D. Lukin, H. Park, Visible-frequency hyperbolic metasurface, Nature 522 (7555) (2015) 192–196.
[63] B. Xiong, L. Deng, R. Peng, Y. Liu, Controlling the degrees of freedom in metasurface designs for multi-functional optical devices, Nanoscale Adv. 1 (10) (2019) 3786–3806.

[64] L. Li, K. Yao, Z. Wang, Y. Liu, Harnessing evanescent waves by bianisotropic metasurfaces, Laser Photon. Rev. 14 (12) (2020), 1900244.
[65] Z. Wang, K. Yao, M. Chen, H. Chen, Y. Liu, Manipulating smith-purcell emission with babinet metasurfaces, Phys. Rev. Lett. 117 (15) (2016), 157401.
[66] J. Valentine, S. Zhang, T. Zentgraf, E. Ulin-Avila, D.A. Genov, G. Bartal, X. Zhang, Three-dimensional optical metamaterial with a negative refractive index, Nature 455 (7211) (2008) 376–379.
[67] R.A. Shelby, D.R. Smith, S. Schultz, Experimental verification of a negative index of refraction, Science 292 (5514) (2001) 77–79.
[68] J.B. Pendry, D. Schurig, D.R. Smith, Controlling electromagnetic fields, Science 312 (5781) (2006) 1780–1782.
[69] D. Schurig, J.J. Mock, B.J. Justice, S.A. Cummer, J.B. Pendry, A.F. Starr, D.R. Smith, Metamaterial electromagnetic cloak at microwave frequencies, Science 314 (5801) (2006) 977–980.
[70] J. Valentine, J. Li, T. Zentgraf, G. Bartal, X. Zhang, An optical cloak made of dielectrics, Nat. Mater. 8 (7) (2009) 568–571.
[71] M. Khorasaninejad, F. Capasso, Metalenses: versatile multifunctional photonic components, Science 358 (6367) (2017).
[72] M. Khorasaninejad, W.T. Chen, R.C. Devlin, J. Oh, A.Y. Zhu, F. Capasso, Metalenses at visible wavelengths: diffraction-limited focusing and subwavelength resolution imaging, Science 352 (6290) (2016) 1190–1194.
[73] R. Jin, L. Tang, J. Li, J. Wang, Q. Wang, Y. Liu, Z.-G. Dong, Experimental demonstration of multidimensional and multifunctional metalenses based on photonic spin hall effect, ACS Photonics 7 (2) (2020) 512–518.
[74] W. Ma, F. Cheng, Y. Liu, Deep-learning-enabled on-demand design of chiral metamaterials, ACS Nano 12 (6) (2018) 6326–6334.
[75] Z. Wang, H. Jia, K. Yao, W. Cai, H. Chen, Y. Liu, Circular dichroism metamirrors with near-perfect extinction, ACS Photonics 3 (11) (2016) 2096–2101.
[76] S. Zhang, Y.-S. Park, J. Li, X. Lu, W. Zhang, X. Zhang, Negative refractive index in chiral metamaterials, Phys. Rev. Lett. 102 (2) (2009), 023901.
[77] L. Kang, S. Lan, Y. Cui, S.P. Rodrigues, Y. Liu, D.H. Werner, W. Cai, An active metamaterial platform for chiral responsive optoelectronics, Adv. Mater. 27 (29) (2015) 4377–4383.
[78] B. Wang, J. Zhou, T. Koschny, M. Kafesaki, C.M. Soukoulis, Chiral metamaterials: simulations and experiments, J. Opt. Pure Appl. Opt. 11 (11) (2009), 114003.
[79] L. Kang, S.P. Rodrigues, M. Taghinejad, S. Lan, K.-T. Lee, Y. Liu, D.H. Werner, A. Urbas, W. Cai, Preserving spin states upon reflection: linear and nonlinear responses of a chiral meta-mirror, Nano Lett. 17 (11) (2017) 7102–7109.
[80] X. Zou, Y. Zhang, R. Lin, G. Gong, S. Wang, S. Zhu, Z. Wang, Pixel-level Bayer-type colour router based on metasurfaces, Nat. Commun. 13 (1) (2022) 3288.
[81] G. Roberts, C. Ballew, T. Zheng, J.C. Garcia, S. Camayd-Muñoz, P.W. Hon, A. Faraon, 3D-Patterned Inverse-Designed Mid-infrared Metaoptics, 2022 *arXiv preprint arXiv:2209.07553*.
[82] J. Li, Q. Zhang, H. Yang, T. Lei, L. Du, X. Wang, J. Bu, Q. Chen, Y. Liu, Z. Xie, Single-layer bayer metasurface via inverse design, ACS Photonics 9 (8) (2022) 2607–2613.
[83] M. Miyata, N. Nemoto, K. Shikama, F. Kobayashi, T. Hashimoto, Full-color-sorting metalenses for high-sensitivity image sensors, Optica 8 (12) (2021) 1596–1604.
[84] J. Burch, A. Di Falco, Surface topology specific metasurface holograms, ACS Photonics 5 (5) (2018) 1762–1766.
[85] G. Zheng, H. Muhlenbernd, M. Kenney, G. Li, T. Zentgraf, S. Zhang, Metasurface holograms reaching 80% efficiency, Nat. Nanotechnol. 10 (4) (2015) 308–312.
[86] B. Xiong, Y. Xu, J. Wang, L. Li, L. Deng, F. Cheng, R.W. Peng, M. Wang, Y. Liu, Realizing colorful holographic mimicry by metasurfaces, Adv. Mater. 33 (21) (2021), e2005864.
[87] W. Hadibrata, H. Wei, S. Krishnaswamy, K. Aydin, Inverse design and 3D printing of a metalens on an optical fiber tip for direct laser lithography, Nano Lett. 21 (6) (2021) 2422–2428.
[88] Z. Li, R. Pestourie, J.-S. Park, Y.-W. Huang, S.G. Johnson, F. Capasso, Inverse design enables large-scale high-performance meta-optics reshaping virtual reality, Nat. Commun. 13 (1) (2022) 1–11.
[89] H. Cai, S. Srinivasan, D.A. Czaplewski, A.B. Martinson, D.J. Gosztola, L. Stan, T. Loeffler, S.K. Sankaranarayanan, D. López, Inverse design of metasurfaces with non-local interactions, npj Comput. Mater. 6 (1) (2020) 1–8.
[90] Z. Wang, C. Dai, Z. Li, Z. Li, Free-space optical merging via meta-grating inverse-design, Nano Lett. 22 (5) (2022) 2059–2064.
[91] H. Chung, O.D. Miller, Tunable metasurface inverse design for 80% switching efficiencies and 144 angular deflection, ACS Photonics 7 (8) (2020) 2236–2243.
[92] N. Jin, Y. Rahmat-Samii, Parallel particle swarm optimization and finite-difference time-domain (PSO/FDTD) algorithm for multiband and wide-band patch antenna designs, IEEE Trans. Antenn. Propag. 53 (11) (2005) 3459–3468.
[93] L. Raju, K.-T. Lee, Z. Liu, D. Zhu, M. Zhu, E. Poutrina, A. Urbas, W. Cai, Maximized frequency doubling through the inverse design of nonlinear metamaterials, ACS Nano 16 (3) (2022) 3926–3933.
[94] D. Zhu, Z. Liu, L. Raju, A.S. Kim, W. Cai, Building multifunctional metasystems via algorithmic construction, ACS Nano 15 (2) (2021) 2318–2326.
[95] W. Ma, F. Cheng, Y. Xu, Q. Wen, Y. Liu, Probabilistic representation and inverse design of metamaterials based on a deep generative model with semi-supervised learning strategy, Adv. Mater. 31 (35) (2019), 1901111.
[96] W. Ma, Y. Liu, A data-efficient self-supervised deep learning model for design and characterization of nanophotonic structures, Sci. China Phys. Mech. Astron. 63 (8) (2020) 1–8.
[97] Z. Liu, L. Raju, D. Zhu, W. Cai, A hybrid strategy for the discovery and design of photonic structures, IEEE J. Emerging Selected Topics Circuits Sys. 10 (1) (2020) 126–135.
[98] S. An, B. Zheng, H. Tang, M.Y. Shalaginov, L. Zhou, H. Li, M. Kang, K.A. Richardson, T. Gu, J. Hu, Multifunctional metasurface design with a generative adversarial network, Adv. Opt. Mater. 9 (5) (2021), 2001433.
[99] P. Kidger, J. Foster, X. Li, T.J. Lyons, In Neural sdes as infinite-dimensional gans, in: International Conference on Machine Learning, PMLR, 2021, pp. 5453–5463.
[100] I. Gulrajani, F. Ahmed, M. Arjovsky, V. Dumoulin, A.C. Courville, Improved training of wasserstein gans, Adv. Neural Inf. Process. Syst. 30 (2017).
[101] W. Ma, Y. Xu, B. Xiong, L. Deng, R.-W. Peng, M. Wang, Y. Liu, Pushing the limits of functionality-multiplexing capability in metasurface design based on statistical machine learning, Adv. Mater. 34 (16) (2022), e2110022.
[102] D. Liu, Y. Tan, E. Khoram, Z. Yu, Training deep neural networks for the inverse design of nanophotonic structures, ACS Photonics 5 (4) (2018) 1365–1369.
[103] J. Peurifoy, Y. Shen, L. Jing, Y. Yang, F. Cano-Renteria, B.G. DeLacy, J.D. Joannopoulos, M. Tegmark, M. Soljačić, Nanophotonic particle simulation and inverse design using artificial neural networks, Sci. Adv. 4 (6) (2018) eaar4206.
[104] R. Zhu, T. Qiu, J. Wang, S. Sui, C. Hao, T. Liu, Y. Li, M. Feng, A. Zhang, C.-W. Qiu, Phase-to-pattern inverse design paradigm for fast realization of functional metasurfaces via transfer learning, Nat. Commun. 12 (1) (2021) 1–10.
[105] E. Tseng, S. Colburn, J. Whitehead, L. Huang, S.H. Baek, A. Majumdar, F. Heide, Neural nano-optics for high-quality thin lens imaging, Nat. Commun. 12 (1) (2021) 6493.
[106] H. Ren, W. Shao, Y. Li, F. Salim, M. Gu, Three-dimensional vectorial holography based on machine learning inverse design, Sci. Adv. 6 (16) (2020) eaaz4261.
[107] Z. Zhen, C. Qian, Y. Jia, Z. Fan, R. Hao, T. Cai, B. Zheng, H. Chen, E. Li, Realizing transmitted metasurface cloak by a tandem neural network, Photon. Res. 9 (5) (2021) B229–B235.
[108] S.-H. Nam, M. Kim, N. Kim, D. Cho, M. Choi, J.H. Park, J. Shin, S. Jeon, Photolithographic realization of target nanostructures in 3D space by inverse design of phase modulation, Sci. Adv. 8 (21) (2022), eabm6310.
[109] C. Lee, G. Chang, J. Kim, G. Hyun, G. Bae, S. So, J. Yun, J. Seong, Y. Yang, D.Y. Park, S. Jeon, J. Rho, Concurrent optimization of diffraction fields from binary phase mask for three-dimensional nanopatterning, ACS Photonics (2022).
[110] L. Gao, Y. Qu, L. Wang, Z. Yu, Computational spectrometers enabled by nanophotonics and deep learning, Nanophotonics 11 (11) (2022) 2507–2529.
[111] Z. Ballard, C. Brown, A.M. Madni, A. Ozcan, Machine learning and computation-enabled intelligent sensor design, Nat. Mach. Intell. 3 (7) (2021) 556–565.
[112] Z. Yang, T. Albrow-Owen, W. Cai, T. Hasan, Miniaturization of optical spectrometers, Science 371 (6528) (2021), eabe0722.
[113] J.S. Tyo, D.L. Goldstein, D.B. Chenault, J.A. Shaw, Review of passive imaging polarimetry for remote sensing applications, Appl. Opt. 45 (22) (2006) 5453–5469.
[114] J.B. Mueller, K. Leosson, F. Capasso, Ultracompact metasurface in-line polarimeter, Optica 3 (1) (2016) 42–47.

[115] M. Garcia, C. Edmiston, R. Marinov, A. Vail, V. Gruev, Bio-inspired color-polarization imager for real-time in situ imaging, Optica 4 (10) (2017) 1263–1271.
[116] M. Faraji-Dana, E. Arbabi, A. Arbabi, S.M. Kamali, H. Kwon, A. Faraon, Compact folded metasurface spectrometer, Nat. Commun. 9 (1) (2018) 1–8.
[117] Y. Chen, H. Lin, J. Hu, M. Li, Heterogeneously integrated silicon photonics for the mid-infrared and spectroscopic sensing, ACS Nano 8 (7) (2014) 6955–6961.
[118] A. Tittl, A. Leitis, M. Liu, F. Yesilkoy, D.-Y. Choi, D.N. Neshev, Y.S. Kivshar, H. Altug, Imaging-based molecular barcoding with pixelated dielectric metasurfaces, Science 360 (6393) (2018) 1105–1109.
[119] Ž. Zobenica, R.W. van der Heijden, M. Petruzzella, F. Pagliano, R. Leijssen, T. Xia, L. Midolo, M. Cotrufo, Y. Cho, F.W. Van Otten, Integrated nano-opto-electro-mechanical sensor for spectrometry and nanometrology, Nat. Commun. 8 (1) (2017) 1–8.
[120] G. Barbastathis, A. Ozcan, G. Situ, On the use of deep learning for computational imaging, Optica 6 (8) (2019) 921–943.
[121] S.N. Zheng, J. Zou, H. Cai, J. Song, L. Chin, P. Liu, Z. Lin, D. Kwong, A. Liu, Microring resonator-assisted Fourier transform spectrometer with enhanced resolution and large bandwidth in single chip solution, Nat. Commun. 10 (1) (2019) 1–8.
[122] B. Redding, S.F. Liew, R. Sarma, H. Cao, Compact spectrometer based on a disordered photonic chip, Nat. Photonics 7 (9) (2013) 746–751.
[123] J. Bao, M.G. Bawendi, A colloidal quantum dot spectrometer, Nature 523 (7558) (2015) 67–70.
[124] X. Zhu, L. Bian, H. Fu, L. Wang, B. Zou, Q. Dai, J. Zhang, H. Zhong, Broadband perovskite quantum dot spectrometer beyond human visual resolution, Light Sci. Appl. 9 (1) (2020) 1–9.
[125] Z. Wang, S. Yi, A. Chen, M. Zhou, T.S. Luk, A. James, J. Nogan, W. Ross, G. Joe, A. Shahsafi, Single-shot on-chip spectral sensors based on photonic crystal slabs, Nat. Commun. 10 (1) (2019) 1–6.
[126] Y. Zhu, X. Lei, K.X. Wang, Z. Yu, Compact CMOS spectral sensor for the visible spectrum, Photon. Res. 7 (9) (2019) 961–966.
[127] S. Yuan, D. Naveh, K. Watanabe, T. Taniguchi, F. Xia, A wavelength-scale black phosphorus spectrometer, Nat. Photonics 15 (8) (2021) 601–607.
[128] Y. Kwak, S.M. Park, Z. Ku, A. Urbas, Y.L. Kim, A pearl spectrometer, Nano Lett. 21 (2) (2020) 921–930.
[129] Z. Yang, T. Albrow-Owen, H. Cui, J. Alexander-Webber, F. Gu, X. Wang, T.-C. Wu, M. Zhuge, C. Williams, P. Wang, Single-nanowire spectrometers, Science 365 (6457) (2019) 1017–1020.
[130] U. Kurokawa, B.I. Choi, C.-C. Chang, Filter-based miniature spectrometers: spectrum reconstruction using adaptive regularization, IEEE Sensor. J. 11 (7) (2010) 1556–1563.
[131] E.J. Candes, T. Tao, Decoding by linear programming, IEEE Trans. Inf. Theor. 51 (12) (2005) 4203–4215.
[132] D.L. Donoho, Compressed sensing, IEEE Trans. Inf. Theor. 52 (4) (2006) 1289–1306.
[133] E. Candes, J. Romberg, Sparsity and incoherence in compressive sampling, Inverse Probl. 23 (3) (2007) 969.
[134] Y. Xu, X. Zhang, Y. Fu, Y. Liu, Interfacing photonics with artificial intelligence: an innovative design strategy for photonic structures and devices based on artificial neural networks, Photon. Res. 9 (4) (2021) B135–B152.
[135] G. Genty, L. Salmela, J.M. Dudley, D. Brunner, A. Kokhanovskiy, S. Kobtsev, S.K. Turitsyn, Machine learning and applications in ultrafast photonics, Nat. Photonics 15 (2) (2021) 91–101.
[136] C. Saigre-Tardif, R. Faqiri, H. Zhao, L. Li, P. del Hougne, Intelligent Meta-Imagers: from Compressed to Learned Sensing, 2021 *arXiv preprint arXiv:2110.14022*.
[137] J. Zhang, X. Zhu, J. Bao, Solver-informed neural networks for spectrum reconstruction of colloidal quantum dot spectrometers, Opt Express 28 (22) (2020) 33656–33672.
[138] C. Brown, A. Goncharov, Z.S. Ballard, M. Fordham, A. Clemens, Y. Qiu, Y. Rivenson, A. Ozcan, Neural network-based on-chip spectroscopy using a scalable plasmonic encoder, ACS Nano 15 (4) (2021) 6305–6315.
[139] H. Song, Y. Ma, Y. Han, W. Shen, W. Zhang, Y. Li, X. Liu, Y. Peng, X. Hao, Deep-learned broadband encoding stochastic filters for computational spectroscopic instruments, Adv. Theory Simul. 4 (3) (2021), 2000299.
[140] J. Yang, K. Cui, X. Cai, J. Xiong, H. Zhu, S. Rao, S. Xu, Y. Huang, F. Liu, X. Feng, Ultraspectral Imaging Based on Metasurfaces with Freeform Shaped Meta-Atoms, Laser & Photonics Reviews, 2022, 2100663.
[141] N.A. Rubin, G. D'Aversa, P. Chevalier, Z. Shi, W.T. Chen, F. Capasso, Matrix Fourier optics enables a compact full-Stokes polarization camera, Science 365 (6448) (2019), eaax1839.
[142] F.Z. Shu, J.N. Wang, R.W. Peng, B. Xiong, R.H. Fan, Y.J. Gao, Y. Liu, D.X. Qi, M. Wang, Electrically driven tunable broadband polarization states via active metasurfaces based on joule-heat-induced phase transition of vanadium dioxide, Laser Photon. Rev. 15 (10) (2021), 2100155.
[143] W.-L. Hsu, G. Myhre, K. Balakrishnan, N. Brock, M. Ibn-Elhaj, S. Pau, Full-Stokes imaging polarimeter using an array of elliptical polarizer, Opt Express 22 (3) (2014) 3063–3074.
[144] F. Liu, S. Zheng, X. He, A. Chaturvedi, J. He, W.L. Chow, T.R. Mion, X. Wang, J. Zhou, Q. Fu, Highly sensitive detection of polarized light using anisotropic 2D ReS2, Adv. Funct. Mater. 26 (8) (2016) 1169–1177.
[145] G. Myhre, W.-L. Hsu, A. Peinado, C. LaCasse, N. Brock, R.A. Chipman, S. Pau, Liquid crystal polymer full-Stokes division of focal plane polarimeter, Opt Express 20 (25) (2012) 27393–27409.
[146] P. Camayd-Muñoz, C. Ballew, G. Roberts, A. Faraon, Multifunctional volumetric meta-optics for color and polarization image sensors, Optica 7 (4) (2020) 280–283.
[147] B. Cheng, Y. Zou, H. Shao, T. Li, G. Song, Full-Stokes imaging polarimetry based on a metallic metasurface, Opt Express 28 (19) (2020) 27324–27336.
[148] Y. Intaravanne, X. Chen, Recent advances in optical metasurfaces for polarization detection and engineered polarization profiles, Nanophotonics 9 (5) (2020) 1003–1014.
[149] T. Sun, J. Hu, X. Zhu, F. Xu, C. Wang, Broadband single-chip full Stokes polarization-spectral imaging based on all-dielectric spatial multiplexing metalens, Laser Photon. Rev. (2022), 2100650.
[150] Z. Yang, Z. Wang, Y. Wang, X. Feng, M. Zhao, Z. Wan, L. Zhu, J. Liu, Y. Huang, J. Xia, Generalized Hartmann-Shack array of dielectric metalens sub-arrays for polarimetric beam profiling, Nat. Commun. 9 (1) (2018) 1–7.
[151] Y. Zhang, J. Jin, M. Pu, Q. He, Y. Guo, X. Li, X. Ma, X. Luo, Full Stokes polarimetry for wide-angle incident light, Phys. Status Solidi Rapid Res. Lett. 14 (5) (2020), 2000044.
[152] T.S. Nowack, Y.D. Shah, I. Escorcia, J.P. Grant, M. Kenney, V. Pusino, D. Faccio, E. Wasige, D.R. Cumming, Terahertz polarimetry with a monolithic metasurface, Opt Lett. 47 (16) (2022) 4199–4202.
[153] C. Yan, X. Li, M. Pu, X. Ma, F. Zhang, P. Gao, K. Liu, X. Luo, Midinfrared real-time polarization imaging with all-dielectric metasurfaces, Appl. Phys. Lett. 114 (16) (2019), 161904.
[154] C. Zhang, J. Hu, Y. Dong, A. Zeng, H. Huang, C. Wang, High efficiency all-dielectric pixelated metasurface for near-infrared full-Stokes polarization detection, Photon. Res. 9 (4) (2021) 583–589.
[155] Y. Ren, S. Guo, W. Zhu, P. Huo, S. Liu, S. Zhang, P. Chen, L. Chen, H.J. Lezec, A. Agrawal, Full-Stokes polarimetry for visible light enabled by an all-dielectric metasurface, Adv. Photonics Res. (2022), 2100373.
[156] M. Juhl, K. Leosson, Polarimetry with disordered photonic structures, ACS Photonics 7 (1) (2019) 203–211.
[157] J. Li, L. Bao, S. Jiang, Q. Guo, D. Xu, B. Xiong, G. Zhang, F. Yi, Inverse design of multifunctional plasmonic metamaterial absorbers for infrared polarimetric imaging, Opt Express 27 (6) (2019) 8375–8386.
[158] C. Liu, Y. Bai, J. Zhou, Q. Zhao, Y. Yang, H. Chen, L. Qiao, High-performance bifunctional polarization switch chiral metamaterials by inverse design method, npj Comput. Mater. 5 (1) (2019) 1–8.
[159] Z. Lin, C. Roques-Carmes, R. Pestourie, M. Soljačić, A. Majumdar, S.G. Johnson, End-to-end nanophotonic inverse design for imaging and polarimetry, Nanophotonics 10 (3) (2021) 1177–1187.
[160] B. Yang, D. Ma, W. Liu, D.-Y. Choi, Z. Li, H. Cheng, J. Tian, S. Chen, Deep-learning-based colorimetric polarization-angle detection with metasurfaces, Optica 9 (2) (2022) 217–220.
[161] T. Liu, K. de Haan, B. Bai, Y. Rivenson, Y. Luo, H. Wang, D. Karalli, H. Fu, Y. Zhang, J. FitzGerald, Deep learning-based holographic polarization microscopy, ACS Photonics 7 (11) (2020) 3023–3034.

[162] N. Margalit, C. Xiang, S.M. Bowers, A. Bjorlin, R. Blum, J.E. Bowers, Perspective on the future of silicon photonics and electronics, Appl. Phys. Lett. 118 (22) (2021), 220501.
[163] A.Y. Piggott, J. Lu, T.M. Babinec, K.G. Lagoudakis, J. Petykiewicz, J. Vučković, Inverse design and implementation of a wavelength demultiplexing grating coupler, Sci. Rep. 4 (1) (2014) 1–5.
[164] A. Michaels, E. Yablonovitch, Inverse design of near unity efficiency perfectly vertical grating couplers, Opt Express 26 (4) (2018) 4766–4779.
[165] L. Su, R. Trivedi, N.V. Sapra, A.Y. Piggott, D. Vercruysse, J. Vučković, Fully-automated optimization of grating couplers, Opt Express 26 (4) (2018) 4023–4034.
[166] C. Sideris, A. Khachaturian, A.D. White, O.P. Bruno, A. Hajimiri, Foundry-fabricated grating coupler demultiplexer inverse-designed via fast integral methods, Commun. Phys. 5 (1) (2022) 1–8.
[167] N.V. Sapra, D. Vercruysse, L. Su, K.Y. Yang, J. Skarda, A.Y. Piggott, J. Vučković, Inverse design and demonstration of broadband grating couplers, IEEE J. Sel. Top. Quant. Electron. 25 (3) (2019) 1–7.
[168] C. Lu, Z. Liu, Y. Wu, Z. Xiao, D. Yu, H. Zhang, C. Wang, X. Hu, Y.C. Liu, X. Liu, Polarization routers: nanophotonic polarization routers based on an intelligent algorithm (advanced optical materials 10/2020), Adv. Opt. Mater. 8 (10) (2020), 2070039.
[169] J. Huang, J. Yang, D. Chen, W. Bai, J. Han, Z. Zhang, J. Zhang, X. He, Y. Han, L. Liang, Implementation of on-chip multi-channel focusing wavelength demultiplexer with regularized digital metamaterials, Nanophotonics 9 (1) (2020) 159–166.
[170] Z. Liu, X. Liu, Z. Xiao, C. Lu, H.-Q. Wang, Y. Wu, X. Hu, Y.-C. Liu, H. Zhang, X. Zhang, Integrated nanophotonic wavelength router based on an intelligent algorithm, Optica 6 (10) (2019) 1367–1373.
[171] L. Su, A.Y. Piggott, N.V. Sapra, J. Petykiewicz, J. Vuckovic, Inverse design and demonstration of a compact on-chip narrowband three-channel wavelength demultiplexer, ACS Photonics 5 (2) (2018) 301–305.
[172] W. Chang, S. Xu, M. Cheng, D. Liu, M. Zhang, Inverse design of a single-step-etched ultracompact silicon polarization rotator, Opt Express 28 (19) (2020) 28343–28351.
[173] A. Majumder, B. Shen, R. Polson, R. Menon, Ultra-compact polarization rotation in integrated silicon photonics using digital metamaterials, Opt Express 25 (17) (2017) 19721–19731.
[174] Y. Liu, S. Wang, Y. Wang, W. Liu, H. Xie, Y. Yao, Q. Song, X. Zhang, Y. Yu, K. Xu, Subwavelength polarization splitter–rotator with ultra-compact footprint, Opt Lett. 44 (18) (2019) 4495–4498.
[175] G. Di Domenico, D. Weisman, A. Panichella, D. Roitman, A. Arie, Large-scale inverse design of a planar on-chip mode sorter, ACS Photonics 9 (2) (2022) 378–382.
[176] H. Ma, J. Huang, K. Zhang, J. Yang, Ultra-compact and efficient 1×2 mode converters based on rotatable direct-binary-search algorithm, Opt Express 28 (11) (2020) 17010–17019.
[177] H. Jia, H. Chen, T. Wang, H. Xiao, G. Ren, A. Mitchell, J. Yang, Y. Tian, Multi-channel parallel silicon mode-order converter for multimode on-chip optical switching, IEEE J. Sel. Top. Quant. Electron. 26 (2) (2019) 1–6.
[178] H. Jia, T. Zhou, X. Fu, J. Ding, L. Yang, Inverse-design and demonstration of ultracompact silicon meta-structure mode exchange device, ACS Photonics 5 (5) (2018) 1833–1838.
[179] L. Deng, Y. Xu, R. Jin, Z. Cai, Y. Liu, On-demand mode conversion and wavefront shaping via on-chip metasurfaces, Adv. Opt. Mater. (2022), 2200910.
[180] W. Jin, S. Molesky, Z. Lin, K.-M.C. Fu, A.W. Rodriguez, Inverse design of compact multimode cavity couplers, Opt Express 26 (20) (2018) 26713–26721.
[181] G.H. Ahn, K.Y. Yang, R. Trivedi, A.D. White, L. Su, J. Skarda, J. Vučković, Photonic Inverse Design of On-Chip Microresonators, ACS Photonics, 2022.
[182] D. Vercruysse, N.V. Sapra, K.Y. Yang, J. Vuckovic, Inverse-designed photonic crystal circuits for optical beam steering, ACS Photonics 8 (10) (2021) 3085–3093.
[183] S. Sun, P. Dong, F. Zhang, J. Wang, N. Zhu, Y. Shi, Inverse design of ultra-compact multimode waveguide bends based on the free-form curves, Laser Photon. Rev. 15 (9) (2021), 2100162.
[184] L. He, F. Zhang, H. Zhang, L.-J. Kong, W. Zhang, X. Xu, X. Zhang, Topology-optimized ultracompact all-optical logic devices on silicon photonic platforms, ACS Photonics 9 (2) (2022) 597–604.
[185] U. Haeusler, M. Seidling, P. Yousefi, P. Hommelhoff, Boosting the efficiency of smith–purcell radiators using nanophotonic inverse design, ACS Photonics 9 (2) (2022) 664–671.
[186] Z. Su, B. Xiong, Y. Xu, Z. Cai, J. Yin, R. Peng, Y. Liu, Manipulating Cherenkov radiation and smith–purcell radiation by artificial structures, Adv. Opt. Mater. 7 (14) (2019), 1801666.
[187] Z. Xie, T. Lei, H. Qiu, Z. Zhang, H. Wang, X. Yuan, Broadband on-chip photonic spin Hall element via inverse design, Photon. Res. 8 (2) (2020) 121–126.
[188] Z. Xie, T. Lei, F. Li, H. Qiu, Z. Zhang, H. Wang, C. Min, L. Du, Z. Li, X. Yuan, Ultra-broadband on-chip twisted light emitter for optical communications, Light Sci. Appl. 7 (4) (2018) 18001, 18001.
[189] T.W. Hughes, M. Minkov, I.A. Williamson, S. Fan, Adjoint method and inverse design for nonlinear nanophotonic devices, ACS Photonics 5 (12) (2018) 4781–4787.
[190] L. Su, D. Vercruysse, J. Skarda, N.V. Sapra, J.A. Petykiewicz, J. Vučković, Nanophotonic inverse design with SPINS: software architecture and practical considerations, Appl. Phys. Rev. 7 (1) (2020), 011407.
[191] C. Yeung, D. Ho, B. Pham, K.T. Fountaine, Z. Zhang, K. Levy, A.P. Raman, Enhancing adjoint optimization-based photonic inverse design with explainable machine learning, ACS Photonics 9 (5) (2022) 1577–1585.
[192] N.J. Dinsdale, P.R. Wiecha, M. Delaney, J. Reynolds, M. Ebert, I. Zeimpekis, D.J. Thomson, G.T. Reed, P. Lalanne, K. Vynck, Deep learning enabled design of complex transmission matrices for universal optical components, ACS Photonics 8 (1) (2021) 283–295.
[193] A.Y. Piggott, E.Y. Ma, L. Su, G.H. Ahn, N.V. Sapra, D. Vercruysse, A.M. Netherton, A.S. Khope, J.E. Bowers, J. Vuckovic, Inverse-designed photonics for semiconductor foundries, ACS Photonics 7 (3) (2020) 569–575.
[194] D. Vercruysse, N.V. Sapra, L. Su, R. Trivedi, J. Vučković, Analytical level set fabrication constraints for inverse design, Sci. Rep. 9 (1) (2019) 1–7.
[195] A. Michaels, M.C. Wu, E. Yablonovitch, Hierarchical design and optimization of silicon photonics, IEEE J. Sel. Top. Quant. Electron. 26 (2) (2019) 1–12.
[196] A.Y. Piggott, J. Petykiewicz, L. Su, J. Vučković, Fabrication-constrained nanophotonic inverse design, Sci. Rep. 7 (1) (2017) 1–7.
[197] K.Y. Yang, J. Skarda, M. Cotrufo, A. Dutt, G.H. Ahn, M. Sawaby, D. Vercruysse, A. Arbabian, S. Fan, A. Alù, Inverse-designed non-reciprocal pulse router for chip-based LiDAR, Nat. Photonics 14 (6) (2020) 369–374.
[198] N.V. Sapra, K.Y. Yang, D. Vercruysse, K.J. Leedle, D.S. Black, R.J. England, L. Su, R. Trivedi, Y. Miao, O. Solgaard, On-chip integrated laser-driven particle accelerator, Science 367 (6473) (2020) 79–83.
[199] T.F. De Lima, B.J. Shastri, A.N. Tait, M.A. Nahmias, P.R. Prucnal, Progress in neuromorphic photonics, Nanophotonics 6 (3) (2017) 577–599.
[200] L. De Marinis, M. Cococcioni, P. Castoldi, N. Andriolli, Photonic neural networks: a survey, IEEE Access 7 (2019) 175827–175841.
[201] J. Li, D. Mengu, Y. Luo, Y. Rivenson, A. Ozcan, Class-specific differential detection in diffractive optical neural networks improves inference accuracy, Adv. Photonics 1 (4) (2019).
[202] D. Brunner, D. Psaltis, Competitive photonic neural networks, Nat. Photonics 15 (5) (2021) 323–324.
[203] Z. Chen, M. Segev, Highlighting photonics: looking into the next decade, ELight 1 (1) (2021) 1–12.
[204] J. Cheng, H. Zhou, J. Dong, Photonic matrix computing: from fundamentals to applications, Nanomaterials 11 (7) (2021) 1683.
[205] Y. Shen, N.C. Harris, S. Skirlo, M. Prabhu, T. Baehr-Jones, M. Hochberg, X. Sun, S. Zhao, H. Larochelle, D. Englund, Deep learning with coherent nanophotonic circuits, Nat. Photonics 11 (7) (2017) 441.
[206] D.R. Solli, B. Jalali, Analog optical computing, Nat. Photonics 9 (11) (2015) 704–706.
[207] A.A. Sawchuk, T.C. Strand, Digital optical computing, Proc. IEEE 72 (7) (1984) 758–779.
[208] M. Ferrera, Y. Park, L. Razzari, B.E. Little, S.T. Chu, R. Morandotti, D.J. Moss, J. Azaña, On-chip CMOS-compatible all-optical integrator, Nat. Commun. 1 (1) (2010) 1–5.
[209] H. Wei, Z. Wang, X. Tian, M. Käll, H. Xu, Cascaded logic gates in nanophotonic plasmon networks, Nat. Commun. 2 (1) (2011) 1–5.

[210] K. Vandoorne, P. Mechet, T. Van Vaerenbergh, M. Fiers, G. Morthier, D. Verstraeten, B. Schrauwen, J. Dambre, P. Bienstman, Experimental demonstration of reservoir computing on a silicon photonics chip, Nat. Commun. 5 (1) (2014) 1–6.
[211] N.M. Estakhri, B. Edwards, N. Engheta, Inverse-designed metastructures that solve equations, Science 363 (6433) (2019) 1333–1338.
[212] S.S. Kou, G. Yuan, Q. Wang, L. Du, E. Balaur, D. Zhang, D. Tang, B. Abbey, X.-C. Yuan, J. Lin, On-chip photonic Fourier transform with surface plasmon polaritons, Light Sci. Appl. 5 (2) (2016), e16034 e16034.
[213] T.W. Hughes, M. Minkov, Y. Shi, S. Fan, Training of photonic neural networks through in situ backpropagation and gradient measurement, Optica 5 (7) (2018) 864–871.
[214] J. Wang, Y. Long, On-chip silicon photonic signaling and processing: a review, Sci. Bull. 63 (19) (2018) 1267–1310.
[215] Z. Wang, T. Li, A. Soman, D. Mao, T. Kananen, T. Gu, On-chip wavefront shaping with dielectric metasurface, Nat. Commun. 10 (1) (2019) 1–7.
[216] Z. Ying, C. Feng, Z. Zhao, S. Dhar, H. Dalir, J. Gu, Y. Cheng, R. Soref, D.Z. Pan, R.T. Chen, Electronic-photonic arithmetic logic unit for high-speed computing, Nat. Commun. 11 (1) (2020) 1–9.
[217] E. Goi, X. Chen, Q. Zhang, B.P. Cumming, S. Schoenhardt, H. Luan, M. Gu, Nanoprinted high-neuron-density optical linear perceptrons performing near-infrared inference on a CMOS chip, Light Sci. Appl. 10 (1) (2021) 1–11.
[218] J. Wu, X. Lin, Y. Guo, J. Liu, L. Fang, S. Jiao, Q. Dai, Analog optical computing for artificial intelligence, Engineering (2021).
[219] J. Feldmann, N. Youngblood, M. Karpov, H. Gehring, X. Li, M. Stappers, M. Le Gallo, X. Fu, A. Lukashchuk, A.S. Raja, Parallel convolutional processing using an integrated photonic tensor core, Nature 589 (7840) (2021) 52–58.
[220] H. Zhang, M. Gu, X. Jiang, J. Thompson, H. Cai, S. Paesani, R. Santagati, A. Laing, Y. Zhang, M. Yung, An optical neural chip for implementing complex-valued neural network, Nat. Commun. 12 (1) (2021) 1–11.
[221] J. Feldmann, N. Youngblood, C.D. Wright, H. Bhaskaran, W.H. Pernice, All-optical spiking neurosynaptic networks with self-learning capabilities, Nature 569 (7755) (2019) 208–214.
[222] F. Ashtiani, A.J. Geers, F. Aflatouni, An on-chip photonic deep neural network for image classification, Nature 606 (7914) (2022) 501–506.
[223] J. Bueno, S. Maktoobi, L. Froehly, I. Fischer, M. Jacquot, L. Larger, D. Brunner, Reinforcement learning in a large-scale photonic recurrent neural network, Optica 5 (6) (2018) 756–760.
[224] X. Lin, Y. Rivenson, N.T. Yardimci, M. Veli, Y. Luo, M. Jarrahi, A. Ozcan, All-optical machine learning using diffractive deep neural networks, Science 361 (6406) (2018) 1004–1008.
[225] T.W. Hughes, I.A. Williamson, M. Minkov, S. Fan, Wave physics as an analog recurrent neural network, Sci. Adv. 5 (12) (2019), eaay6946.
[226] Y. Luo, D. Mengu, N.T. Yardimci, Y. Rivenson, M. Veli, M. Jarrahi, A. Ozcan, Design of task-specific optical systems using broadband diffractive neural networks, Light Sci. Appl. 8 (1) (2019) 1–14.
[227] T. Zhou, L. Fang, T. Yan, J. Wu, Y. Li, J. Fan, H. Wu, X. Lin, Q. Dai, In situ optical backpropagation training of diffractive optical neural networks, Photon. Res. 8 (6) (2020) 940–953.
[228] O. Kulce, D. Mengu, Y. Rivenson, A. Ozcan, All-optical information-processing capacity of diffractive surfaces, Light Sci. Appl. 10 (1) (2021) 1–17.
[229] O. Kulce, D. Mengu, Y. Rivenson, A. Ozcan, All-optical synthesis of an arbitrary linear transformation using diffractive surfaces, Light Sci. Appl. 10 (1) (2021) 1–21.
[230] M.S.S. Rahman, J. Li, D. Mengu, Y. Rivenson, A. Ozcan, Ensemble learning of diffractive optical networks, Light Sci. Appl. 10 (1) (2021) 1–13.
[231] A. Ryou, J. Whitehead, M. Zhelyeznyakov, P. Anderson, C. Keskin, M. Bajcsy, A. Majumdar, Free-space optical neural network based on thermal atomic nonlinearity, Photon. Res. 9 (4) (2021) B128–B134.
[232] M.S. Sakib Rahman, A. Ozcan, Computer-free, all-optical reconstruction of holograms using diffractive networks, ACS Photonics 8 (11) (2021) 3375–3384.
[233] J. Shi, L. Zhou, T. Liu, C. Hu, K. Liu, J. Luo, H. Wang, C. Xie, X. Zhang, Multiple-view D 2 NNs array: realizing robust 3D object recognition, Opt Lett. 46 (14) (2021) 3388–3391.
[234] M. Veli, D. Mengu, N.T. Yardimci, Y. Luo, J. Li, Y. Rivenson, M. Jarrahi, A. Ozcan, Terahertz pulse shaping using diffractive surfaces, Nat. Commun. 12 (1) (2021) 1–13.
[235] D. Mengu, Y. Rivenson, A. Ozcan, Scale-, shift-, and rotation-invariant diffractive optical networks, ACS Photonics 8 (1) (2020) 324–334.
[236] H. Chen, J. Feng, M. Jiang, Y. Wang, J. Lin, J. Tan, P. Jin, Diffractive deep neural networks at visible wavelengths, Engineering 7 (10) (2021) 1483–1491.
[237] J. Li, Y.-C. Hung, O. Kulce, D. Mengu, A. Ozcan, Polarization multiplexed diffractive computing: all-optical implementation of a group of linear transformations through a polarization-encoded diffractive network, Light Sci. Appl. 11 (1) (2022) 1–20.
[238] Y. Zuo, B. Li, Y. Zhao, Y. Jiang, Y.-C. Chen, P. Chen, G.-B. Jo, J. Liu, S. Du, All-optical neural network with nonlinear activation functions, Optica 6 (9) (2019) 1132–1137.
[239] C. Qian, X. Lin, X. Lin, J. Xu, Y. Sun, E. Li, B. Zhang, H. Chen, Performing optical logic operations by a diffractive neural network, Light Sci. Appl. 9 (1) (2020) 1–7.
[240] X. Luo, Y. Hu, X. Ou, X. Li, J. Lai, N. Liu, X. Cheng, A. Pan, H. Duan, Metasurface-enabled on-chip multiplexed diffractive neural networks in the visible, Light Sci. Appl. 11 (1) (2022) 1–11.
[241] T. Zhou, X. Lin, J. Wu, Y. Chen, H. Xie, Y. Li, J. Fan, H. Wu, L. Fang, Q. Dai, Large-scale neuromorphic optoelectronic computing with a reconfigurable diffractive processing unit, Nat. Photonics 15 (5) (2021) 367–373.
[242] J.N. Martel, L.K. Mueller, S.J. Carey, P. Dudek, G. Wetzstein, Neural sensors: learning pixel exposures for HDR imaging and video compressive sensing with programmable sensors, IEEE Trans. Pattern Anal. Mach. Intell. 42 (7) (2020) 1642–1653.
[243] L. Mennel, J. Symonowicz, S. Wachter, D.K. Polyushkin, A.J. Molina-Mendoza, T. Mueller, Ultrafast machine vision with 2D material neural network image sensors, Nature 579 (7797) (2020) 62–66.
[244] S. Ahmed, C.S. Muñoz, F. Nori, A.F. Kockum, Quantum state tomography with conditional generative adversarial networks, Phys. Rev. Lett. 127 (14) (2021), 140502.
[245] Y. Zuo, C. Cao, N. Cao, X. Lai, B. Zeng, S. Du, Optical neural network quantum state tomography, Adv. Photonics 4 (2) (2022), 026004.
[246] N. Cao, J. Xie, A. Zhang, S.-Y. Hou, L. Zhang, B. Zeng, Neural networks for quantum inverse problems, New J. Phys. (2022).
[247] S. Ahmed, C.S. Muñoz, F. Nori, A.F. Kockum, Classification and reconstruction of optical quantum states with deep neural networks, Phys. Rev. Res. 3 (3) (2021), 033278.
[248] Á. Papp, W. Porod, G. Csaba, Nanoscale neural network using non-linear spin-wave interference, Nat. Commun. 12 (1) (2021) 1–8.
[249] L.G. Wright, T. Onodera, M.M. Stein, T. Wang, D.T. Schachter, Z. Hu, P.L. McMahon, Deep physical neural networks trained with backpropagation, Nature 601 (7894) (2022) 549–555.
[250] J. Grollier, D. Querlioz, K. Camsari, K. Everschor-Sitte, S. Fukami, M.D. Stiles, Neuromorphic spintronics, Nat. electron. 3 (7) (2020) 360–370.
[251] Y. Sebbag, E. Talker, A. Naiman, Y. Barash, U. Levy, Demonstration of an integrated nanophotonic chip-scale alkali vapor magnetometer using inverse design, Light Sci. Appl. 10 (1) (2021) 1–8.
[252] Q. Wang, A.V. Chumak, P. Pirro, Inverse-design magnonic devices, Nat. Commun. 12 (1) (2021) 1–9.